A Numerical Investigation of Heat Transfer Coefficients for Indoor Window Insect Screens

by

Glen McIntyre

A thesis
presented to the University of Waterloo
in fulfillment of the
thesis requirement for the degree of
Master of Applied Science
in
Mechanical Engineering

Waterloo, Ontario, Canada, 2011

I hereby declare that I am the sole author of this thesis. This is a true copy of the thesis, including any required final revisions, as accepted by my examiners.

I understand that my thesis may be made electronically available to the public.

Abstract

Due to rising energy prices as well as supply and ecological concerns, there is a strong interest in reducing the energy used in buildings. As such, it is desirable to model the operation of a building and predict its future energy use. In predicting the energy use of a building, the heat gain/loss through windows is an important factor. In order to accurately model this heat gain/loss, the convective heat transfer coefficient of any insect screens mounted adjacent to the windows needs to be known. This thesis describes an investigation into the heat transfer from insect screens mounted towards the indoor side of a window.

The convective heat transfer coefficient of an insect screen varies based on several parameters. For implementation in building energy modelling software, it is desirable to be able to predict the convective heat transfer coefficient for an arbitrary insect screen. Due to the number of variables and the large dynamic range of the details required for modelling, direct simulation of a range of whole insect screens was not completed. Instead, a range of numerical models representing small sections of an insect screen were created. By comparing results from these to available correlations for simpler geometries, such as cylinders and flat plates, estimates for the heat transfer coefficient of a screen can be obtained.

The results were non-dimensionalized for analysis and different methodologies for the prediction of heat transfer from an indoor window insect screen are described.

Acknowledgements

Thanks are in order to Professors Michael Collins, Elizabeth Weckman and John Wright for their assistance in completing this work.

Contents

List of Figures

List of Tables

Notation

D	Cylinder diameter, m
D_{domain}	Diameter of cylindrical domain, m
d	Molecular diameter, m
$L_{cyl.}$	Cylinder Length, m
L_{domain}	Length of domain, m
L^*_{domain}	Length of domain side relative to cylinder diameter
L	Vertical height from bottom of screen or plate, m
L'	Length parameter $= L \cdot (\pi \cdot \gamma)$, m
ξ	Length parameter $= f(L)$, m
s	Cylinder centre-centre spacing, m
l	Screen height, m
w	Screen width, m
y	Height above heat source, m
A	Surface area transferring heat to fluid, m^2
x	Distance through porous media m
λ	Molecular mean free path, m

ι	Characteristic length dimension, m
ϕ	Screen porosity = Fraction of screen cross-section that is open
γ	Screen density = Solid fraction of screen cross-section $= 1 - \phi$
K	Permeability of a porous media, m^2
V_∞	Bulk flow velocity of forced convection, m/s
$V_{centreline}$	Fluid velocity measured at a point directly above a cylinder's centre m/s
T	Temperature, K
T_∞	Ambient temperature of fluid, K
T_s	Surface temperature, K
ΔT	Temperature difference between surface and ambient fluid, K
$T_{centreline}$	Fluid temperature measured at a point directly above a cylinder's centre K
P	Fluid pressure, Pa
k	Thermal Conductivity of a fluid $W/(m \cdot K)$
β	Fluid thermal expansion coefficient, K^{-1}
μ	Dynamic viscosity, $Pa \cdot s$
ν	Kinematic viscosity, m^2/s
n	Particle concentration, m^{-3}
N_A	Avogadro's number, mol^{-1}
m	Molecular mass, g/mol
g	Gravitational acceleration m/s^2
h_c	Convective heat transfer coefficient, $W/(m^2 \cdot K)$
h_c^*	'Engineering' convective heat transfer coefficient $= h_c \cdot (\pi \cdot \gamma)$, $W/(m^2 \cdot K)$
$\overline{h}_c$	Average heat transfer coefficient of a surface, $W/(m^2 \cdot K)$

i	Arbitrary length dimension, m
Ω	Number of different values a parameter is modelled for
H	Ostrach dimensionless temperature function
Pr	Prandtl number $= \nu/\alpha$, calculated for fluid at $T = T_\infty$
Pr_T	Prandtl number $= \nu/\alpha$, calculated for fluid at T
Nu_i	Nusselt number $= (h_c \cdot i)/k$
Nu_L	'Engineering' Nusselt number $= Nu_L \cdot (\pi \cdot \gamma)$
$\overline{Nu}_i$	Average Nusselt number for $0 < L < i \ = (\overline{h}_c \cdot i)/k$
Gr_i	Grashof number $= \frac{g\beta\Delta T i^3}{\nu^2}$
Ra_i	Rayleigh number $= Pr \cdot \left(\frac{g\beta\Delta T i^3}{\nu^2}\right)$
Re_i	Reynolds number $= \frac{V \cdot i}{\nu}$
Ri_i	Richardson number $= \frac{Gr_i}{Re_i^2}$
Pe_i	Peclet number $= V \cdot i/\alpha = Re_i \cdot Pr$
Kn	Knudson number $= \lambda/l$

Chapter 1

Introduction

At the present time the world is grappling with how to satisfy increasing demands for energy availability. Meeting these demands has a variety of drawbacks which vary based on the particular source of energy. Some of these issues include CO_2 emissions, impacts on land-use due to fossil fuel extraction, nuclear safety as well as adversely affected air and water quality. One way to mitigate these diverse negatives is to reduce energy use.

Buildings are a major user of energy. Currently in Canada, buildings are estimated to account for over 30% of total national energy consumption [Bruneau 2006]. As such, reductions of energy use in buildings can have a significant impact on national energy consumption.

Buildings are large and expensive structures which are typically designed for a long service lifespan. Frequently, choices that are made as part of the original design of a building will be difficult to undo or change through a retrofit. As such, the effects of the design of

a building can have a long-term impact on energy consumption. Due to this long-term impact, it is highly desirable to be able to accurately predict the energy performance of a building during its design stage. Unfortunately, current building modelling software packages have been found to have a large tolerance of error in their energy-use predictions [Turner 2008] & [Norford 1994]. Improvements in the accuracy of building energy models are therefore desired.

One major source of energy use in a building is compensating for heat gains and losses through windows. This component of building energy use will be the subject of the present work. This work will be further restricted to the sub-case of operable windows.

Operable windows are defined as windows that can be opened and closed by building occupants. The presence of operable windows may increase the energy consumption of a building's HVAC system [Daly 2002]. However if integrated as part of an appropriate design, operable windows also have the potential to decrease building energy consumption [Daly 2002]. Aside from their impact on the energy consumption of the building, operable windows may be desired for a number of other reasons. First of all, it has been found that building occupants prefer being able to control windows [Heerwagen 1998]. It has also been suggested that the presence of operable windows can reduce employee absenteeism [Hedge 1989]. Due to these and other reasons, the LEED 2009 rating system also encourages the use of operable windows [CAGBC 2010].

If operable windows are present, they typically will include insect screens to exclude insects from the indoor environment. Depending on the style of window, these screens may be placed on either side of the window glazing. The presence of an insect screen

adjacent to the window glazing can be expected to impact the heat transfer into the building in two ways. The first is that the screen will absorb a fraction of the incoming solar radiation. This effect has been shown to reduce the solar heat-gain coefficient of a window by 46% for a screen mounted on the outdoor side of the window and 15% for an indoor one [Brunger 1999]. The presence of the screen will also affect convective heat transfer at the glazing surface adjacent to the screen. This effect has been shown to increase the thermal resistance of a window by 7% and 14% for outdoor and indoor mounted screens respectively [Brunger 1999]. Thus it can be seen that the presence of an insect screen is significant in analysing fenestration heat transfer. While experiments have been completed for a limited number of screen/window cases by Brunger, it is desirable to be able to predict the effect that the presence of an insect screen will have on an arbitrary window and screen assembly [Brunger 1999].

One primary piece of information needed to predict the impact of an insect screen on fenestration heat transfer is the convective heat transfer coefficient of the screen itself. The development of a simple correlation for the convective heat transfer coefficient for an insect screen over the range of fluid velocities expected for an indoor screen is the primary objective of this investigation. This document summarizes the work completed towards the development of said correlation and is structured as follows:

- Chapter 1, the present chapter, outlines the motivation and scope of this investigation.

- Chapter 2 contains a review of previous literature which provide background and foundation for the present work.

- Chapter 3 describes the numerical models which were developed to simulate heat transfer from insect screens.

- Chapter 4 presents the results of the numerical models.

- Chapter 5 includes a discussion of the results, analysis of data and development of semi-empirical correlations.

- Chapter 6 provides a summary of the significant findings and recommendations for further research.

Chapter 2

Literature Review

Published research that was deemed relevant to the study of convective heat transfer from an insect screen is summarized in this chapter.

2.1 Work on Screens, Momentum Only

In the absence of previous research studying the heat transfer from an insect screen, studies of airflow interactions with an insect screen are somewhat useful in analyzing the convection process.

The momentum loss of fluid flow around an insect screen was studied by Miguel [Miguel 1997],[Miguel 1998]. Initially two insect screens were tested. Two significant parameters of these screens are the mesh filament spacing and porosity which are defined

as:

$$s = \text{screen filament centre to centre spacing} \tag{2.1}$$

$$\phi = \text{screen porosity} = \text{fraction of screen area that is open space} \tag{2.2}$$

The two screens investigated both had mesh spacings of $s = 0.11m$. The porosities of the screens were $\phi = 0.26$ and $\phi = 0.34$. These screens were tested for air velocities of up to $3m/s$ [Miguel 1997]. Several screening materials that were not designed for insect exclusion were also tested. It was found that the pressure drop through the screens corresponded to that predicted by the Darcy-Forchheimer equation [Miguel 1997]. This equation takes the form of:

$$\frac{\partial P}{\partial x} = \left(\frac{\mu}{K}\right) V + \left(\frac{\rho Y}{K^{1/2}}\right) |V| \cdot V \tag{2.3}$$

Where: P = fluid pressure

x = distance through porous media

μ = dynamic viscosity

ρ = fluid density

V = fluid velocity

K = screen permeability

Y = constant

In Miguel's work [Miguel 1998], experiments were completed to further characterize the effect of the presence of a screen on an airflow. A velocity ratio parameter of α was defined as $\alpha = (Velocity_{screen}/Velocity_{no\ screen})$. Using $Re_{\sqrt{K}} = Velocity * (\sqrt{K}/\nu)$ where K equals the permeability of the screen and ν is the kinematic viscosity of the fluid, it was found that for $Re_{\sqrt{K}} > 100$, α was independent of $Re_{\sqrt{K}}$. For $Re_{\sqrt{K}} < 100$, α increased with increasing $Re_{\sqrt{K}}$. Fourteen different screening materials were tested, some with rectangular meshes and some with irregular meshes [Miguel 1997]. One significant finding was that only the total porosity, or the fraction of open area of the screen, was significant. The geometry of the screen filaments was not. Thus it was suggested that the airflow through a screen, could be adequately predicted using only the pressure difference across the screen and the screen permeability [Miguel 1997].

Norris [Norris 2009] completed CFD models to simulate the effect that the presence of an insect screen had on the rate of heat transfer through the entire window/screen unit. The results of the numerical simulations were compared to those of an analytical solution for the special cases of a 0% and 100% porosity (i.e., closed and open cavity cases). In addition, flow visualization experiments were completed and compared to velocity vector plots generated from the numerical solutions [Norris 2009].

Norris [Norris 2009] used results from Miguel [Miguel 1997] for the pressure loss properties of the insect screens. Miguel [Miguel 1997] studied the momentum loss of fluid flow due to the presence of a screen. In his numerical models, Norris treated the screen as a finite volume of a porous media. The properties of the porous media were chosen based on the findings of Miguel [Miguel 1998] which were described above. The research of Miguel was entirely directed at an insect screen's effect on momentum; heat transfer from the

screen was not investigated [Miguel 1998]. The work of Norris similarly did not describe the heat transfer coefficient used in his models for the insect screen [Norris 2009].

2.2 Natural Convection

Clearly, a heated or cooled insect screen submerged in air at a different temperature is expected to transfer heat to the ambient air via natural convection. Natural convection has been studied for many common geometries. Prior research for geometries which share some similarities with an insect screen adjacent to a window glazing is summarized below.

2.2.1 Vertical Plane

An early solution to the problem of natural convection from a vertical plane was developed by Lorenz [Lorenz 1881]. To solve the problem analytically, Lorenz assumed a constant boundary layer thickness and flow parallel to the plane surface. By doing this, the problem was reduced to an ordinary differential equation with the following solution for

air[Lorenz 1881]:

$$\overline{Nu}_L = 0.548 \cdot (Ra_L)^{1/4}, \quad \text{for } 10^9 > Ra_L > 10^4 \tag{2.4}$$

Where: $\overline{Nu}_L = \overline{h}_c \cdot L/k$

$Ra_L = Pr \cdot (g\beta\Delta T L^3)/(\nu^2)$

$Pr = \nu/\alpha$

$\overline{h}_c$ = average convective heat transfer coefficient

k = thermal conductivity of fluid

L = vertical distance from bottom of plane

g = gravitational acceleration

β = fluid thermal expansion coefficient

ΔT = temperature difference between surface and bulk fluid

ν = fluid kinematic viscosity

α = fluid thermal diffusivity

A later correlation was found by Ostrach using a similarity solution method [Ostrach 1953]. The correlation is as follows;

$$Nu_L = -H'(0)\left(\frac{Gr_L}{4}\right)^{1/4}, \quad \text{for } 10^9 > Ra_L > 10^4 \tag{2.5}$$

$$\tag{2.6}$$

Where: H = Ostrach dimensionless temperature function

$$\overline{Nu}_L = \overline{h}_c \cdot L/k$$

$$Gr_L = \frac{g\beta\Delta T L^3}{\nu^2}$$

If $H'(0)$ is numerically calculated for air at $300K$ ($Pr = 0.71$), it has a value of $H'(0) = 0.50$. Using this value of $H'(0)$, Equation 2.6 becomes [Ostrach 1953]:

$$Nu_L = 0.50 \cdot \left(\frac{Pr_L}{4 \cdot 0.71}\right)^{1/4} = 0.38 \cdot Ra_L^{1/4}, \quad \text{for } 10^9 > Ra_L > 10^4 \tag{2.7}$$

Eckert solved the vertical flat plate problem using integrated energy and momentum equations and obtained the following relations [Eckert 1963]:

$$Nu_L = \frac{0.508 \cdot Pr^{1/2} Gr_L^{1/4}}{(0.952 + Pr)^{1/4}}, \quad \text{for } 10^9 > Ra_L > 10^4 \tag{2.8}$$

Which for air at $300K$ gives;

$$Nu_L = 0.41 \cdot Ra_L^{1/4}, \quad \text{for } 10^9 > Ra_L > 10^4 \tag{2.9}$$

Equation 2.9 can be integrated to give an average value of Nu_L over the plate.

$$\overline{Nu}_L = \frac{4}{3} \cdot Nu_L, \quad \text{for } 10^9 > Ra_L > 10^4 \tag{2.10}$$

Churchill and Chu suggested that correlations of the form $Nu_L = a * Ra_L^b$ are inherently restricted to limited ranges of Ra_L [Churchill & Chu 1975(2)]. For a wide range of Ra_L they suggested the correlation given below [Churchill & Chu 1975(2)].

$$Nu_L = \left[0.825 + \frac{0.387 \cdot Ra_L^{1/6}}{[1 + (0.492/Pr)^{9/16}]^{8/27}} \right]^2, \quad 0 < Ra_L < \infty \tag{2.11}$$

For air at 300K;

$$Nu_L = \left[0.825 + 0.324 \cdot Ra_L^{1/6} \right]^2, \quad 0 < Ra_L < \infty \tag{2.12}$$

2.2.2 Single Cylinder

For the geometry of a single cylinder, heat transfer from cylinders in vertical and horizontal positions are discussed separately below.

Vertical Cylinder

The case of an isothermal cylinder with a vertical axis is treated first. One method of solving for this case was described by Jaluria [Jaluria 1980]. This method involved using a

similarity method to adapt boundary layer solutions to the vertical cylinder geometry. The result is as follows [Jaluria 1980]:

$$Nu_D = \frac{4}{3}\left[\frac{7 \cdot Gr_L Pr^2}{5(20 + 21 \cdot Pr)}\right]^{1/4} + \frac{4}{35}\left[\frac{272 + 315 \cdot Pr}{64 + 63 \cdot Pr}\right]\left(\frac{L_{cyl}}{D}\right) \tag{2.13}$$

Where: L_{cyl} = cylinder length

$Nu_D = h_c \cdot D/k$

For air at $300K$ ($Pr = 0.71$) this correlation becomes:

$$Nu_D = \left(\frac{4}{3}\right)[0.020 \cdot Gr_L]^{1/4} + 0.52\left(\frac{L_{cyl}}{D}\right) \tag{2.14}$$

A vertical cylinder can also be treated as a planar surface if its L/D ratio is small enough. This is discussed further in the aspect ratio section below.

Horizontal Cylinder

Multiple correlations for the case of a single, horizontal, isothermal, infinite cylinder are available. Using an aggregate of empirical data available at the time (1975), Morgan recommended using a simple correlation of the form $Nu_D = a * (Ra_D)^b$ [Morgan 1975]. The values of a and b were chosen for ranges of Ra_D based on the available empirical data. The

correlations for the two lowest ranges of Ra_D are given here:

$$Nu_D = 0.675 \cdot Ra_D^{0.058}, \qquad 10^{-10} < Ra_D < 10^{-2} \qquad \text{[Morgan 1975]} \qquad (2.15)$$

$$Nu_D = 1.02 \cdot Ra_D^{0.148}, \qquad 10^{-2} < Ra_D < 10^{2} \qquad \text{[Morgan 1975]} \qquad (2.16)$$

Churchill and Chu used a more complex function to provide a correlation which closely fit the empirical data over a wide range of Ra_D [Churchill & Chu 1975(1)]. The following correlation is claimed by Churchill and Chu to be useful for any Ra_D [Churchill & Chu 1975(1)]:

$$Nu_D = \left\{ 0.6 + \frac{0.387 \cdot Ra_D^{1/6}}{[1 + (0.559/Pr)^{9/16}]^{8/27}} \right\}^2, \qquad 0 < Ra_D < \infty \qquad (2.17)$$

An analytical series solution for natural convection over a horizontal isothermal cylinder was developed by Saville and Churchill [Saville & Churchill 1967]. They found that the first term of the series solution provided good agreement with available experimental data. For $Pr \approx 0.7$ the following correlation was recommended [Saville & Churchill 1967]:

$$Nu_D = 0.545 \cdot Ra^{1/4} \qquad (2.18)$$

In comparison, for the extremum limits of Pr the following correlations were recommended by Churchill and Chu [Churchill & Chu 1975(1)]:

$$\lim_{Pr \to \infty} Nu_D = 0.518 \cdot Ra^{1/4} \qquad (2.19)$$

$$\lim_{Pr \to 0} Nu_D = 0.599 \cdot Ra^{1/4} \qquad (2.20)$$

Farouk and Guceri numerically studied natural convection for a 2-D horizontal isothermal cylinder [Farouk & Guceri 1981]. Their investigation involved Ra_D ranges of $10^4 < Ra_D < 10^8$ which gave results for Nu_D in the range of $6 < Nu_D < 50$ [Farouk & Guceri 1981].

As the Rayleigh number approaches zero, the Nusselt number is expected to approach zero as well [Ohman 1970]. Clearly this is the case for the correlations given above. However, correlations of the form $Nu_D = a + b * Ra_D^c$ have been proposed with $a \neq 0$ [Morgan 1975]. A theoretical treatment by Ohman [Ohman 1970] which ascribes these results to experimental limitations is described below in the edge effects section.

2.2.3 Multiple Horizontal Cylinders

Corcione numerically studied vertical arrays of horizontal isothermal cylinders [Corcione 2005]. Cylinder arrays of 2 to 6 cylinders with spacings ranging from 2-50 diameters apart were studied for Ra_D in the range of $500 < Ra_D < 50 * 10^5$ [Corcione 2005]. These values of Ra_D are several orders of magnitude larger than those for insect screen filaments. It was found that the bottom cylinder had an unchanged rate of heat transfer from that of a single cylinder. Upper cylinders had reduced heat transfer rates at closer cylinder spacings and increased heat transfer rates when the cylinders were more openly spaced. The explanation for these results was proposed as two concurrent and conflicting phenomena [Corcione 2005]. The first effect is an increase in the buoyancy-driven fluid flow due to greater numbers of cylinders. As the amount of heat transferred to the fluid increases due to an increased number of cylinders transferring heat, the magnitude of the buoyancy driven flow will increase. The correspondingly increased fluid velocities will increase the heat

transfer rates. The second effect is due to the finite thermal mass of the fluid. A greater number of heated cylinders will naturally increase the total amount of heat transferred to the surrounding fluid and consequently increase the temperature of the fluid. As a result, cylinders higher up in the array will be transferring heat to a fluid that is hotter than the ambient temperature. For a fixed cylinder temperature, this increase in fluid temperature will reduce the temperature gradient surrounding the cylinder and reduce the rate of heat transfer and the value of h_c as defined as $h_c = q * A^{-1}(T_{wall} - T_\infty)^{-1}$ [Corcione 2005]. Over the range of Ra_D studied, the ratio $Nu_{D_{i^{th}cylinder}}$ / $Nu_{D_{bottom\_cylinder}}$ was found to be dependent on the spacing of the cylinders and not on Ra_D [Corcione 2005].

Lieberman and Gebhart experimentally looked at natural convection in air from arrays of cylinders [Lieberman & Gebhart 1969]. In their experiments, each $0.13mm$ cylinder had a constant heat flux applied to it that resulted in a surface temperature less than 60^oC above ambient. It was found that the average Nu_D for the array was higher than Nu_D for a single cylinder if the spacing between the cylinders was large enough and lower for closer spacings. The reason for this was hypothesized as the existence of both velocity and heat capacity effects as also noted by Corcione [Corcione 2005] and described above. The relative strengths of these effects are predicted by boundary layer theory to be [Lieberman & Gebhart 1969]:

$$T_{centreline} \quad \alpha \quad y^{-\frac{3}{5}} \tag{2.21}$$

$$V_{centreline} \quad \alpha \quad y^{5} \tag{2.22}$$

Where: $y =$ height above the heat source

$V_{centreline} =$ fluid velocity measured at a point directly above a cylinder's centre

$T_{centreline} =$ fluid temperature measured at a point directly above a cylinder's centre

It was found that at the closest cylinder spacing tested of $37.5 * D$, the array's average Nu_D was less than that for a single cylinder [Lieberman & Gebhart 1969]. At this spacing, the value for Nu_D decreased for wires higher in the array. In contrast, Nu_D increased for wires higher in the array at a cylinder spacing of $75 * D$, $113 * D$ and $150 * D$ [Lieberman & Gebhart 1969]. The highest value of Nu_D occurred for a spacing of $113 * D$. These trends and obvious theory predict that the value of Nu_D will converge to the value of Nu_D for a single wire as the spacing between the wires goes to ∞ [Lieberman & Gebhart 1969].

D'Orazio and Fontana completed physical experiments on arrays of 5 horizontal cylinders [D'Orazio & Fontana 2010]. Arrays with five cylinders of $1.5mm$ diameter were used with vertical spacings ranging from 4 to 12 diameters. A constant heat input rather than temperature condition on the cylinders was used and the Ra_D of their setup ranged from

2 to 12. It was noted that the level of heat transfer decreased for higher (downstream) cylinders in the array except for the top cylinder. The top cylinder consistently had a larger degree of heat transfer than the one below it [D'Orazio & Fontana 2010]. This finding was attributed to the absence of flow blockage due to a higher cylinder.

2.2.4 Edge Effects

The geometries discussed thus far all assume infinite or semi-infinite cylinder length. The experimental data was collected with the goal of approaching values found for the infinite limit. However the probability of edge effects causing noticeable effects on the heat transfer from an insect screen must be considered and this is done below.

Horizontal Cylinder

It was noted by Morgan [Morgan 1975] as well as Collis and Williams [Collis & Williams 1959] that axial conduction can be neglected for aspect ratios of $L_{cyl.}/D > 10^4$. For screening filaments with diameters in the $0.1 - 1.0mm$ range, an aspect ratio of 10^4 corresponds to an overall screen width of $1 - 10m$. Thus axial conduction towards the edges of a window screen could distort results from those predicted from models neglecting edge effects.

As noted in the horizontal single cylinder section above, Ohman [Ohman 1970] predicted that $\lim_{Ra_D \to 0} Nu_D = 0$. However, it was also shown by Ohman that a minimum value of Nu_D will be found at very low Ra_D due to effects caused by the cylinder aspect ratio $L_{cyl.}/D$. The relative size of the cavity in which the cylinder is tested $D_{domain}/D_{cylinder}$ can have similar effects [Ohman 1970]. Previously determined predictions for the values of

Nu_D based on each of these effects individually are [Ohman 1970]:

$$Nu_D = \frac{2}{ln(2L_{cyl.}/D)} \tag{2.23}$$

$$Nu_D = \frac{2}{ln(D_{domain}/D)} \tag{2.24}$$

Where: D_{domain} = diameter of cylindrical domain

L_{cyl} = length of cylinder

In order to solve for these two effects simultaneously, the finite cylinder and domain were modelled by Ohman as two concentric ellipsoids. The combined result of these two effects was analytically estimated to be [Ohman 1970]:

$$Nu_D = \frac{2}{ln\left[\frac{2 \cdot D_{domain}/D}{1+\sqrt{(D_{domain}/L_{cyl.})^2+1}}\right]} \tag{2.25}$$

Morgan found experimental results have yielded higher values for Nu_D than those predicted by Ohman [Ohman 1970]. These results are given in Table 2.1.

Table 2.1: Experimental Nu_D Results for Low Ra_D [Morgan 1975]

Ra_D	10^{-7}	10^{-8}	$3.8 * 10^{-9}$
Nu_D	0.27	0.23	0.18

Vertical Cylinder

In the case of a vertical cylinder, the diameter to length ratio can be used to determine whether or not the cylinder can be treated as a flat plate [Jaluria 1980]. If the thickness of the boundary layer is small in relation to the cylinder diameter, the curvature present in the boundary layer will be small and thus the wall surface can be treated as planar [Jaluria 1980].

As the boundary layer becomes thicker, the planar wall assumption cannot be made and the problem needs to be solved as a case distinct from that of a vertical plane. Jaluria recommends the following criterion as an upper limit of an acceptable $L_{cyl.}/D$ ratio for use of the flat-plate model [Jaluria 1980].

$$\frac{L_{cyl.}}{D} < \frac{Ra_L^{1/4}}{38} \quad for \quad Pr = 0.7 \tag{2.26}$$

Which gives:

$$L_{cyl.} = \frac{D^4 g\beta\Delta T Pr}{38^4\nu^2} \tag{2.27}$$

For a cylinder diameter of $D = 0.1mm$ and air with a temperature difference of 10^oC from the screen, Equation 2.27 predicts a maximum height of cylinder of about $4 * 10^{-14}m$. Clearly for fine cylindrical elements in a window screen, the $L_{cyl.}/D$ ratio will be too great for the planar model to be applied.

2.3 Forced Convection

The convective heat transfer from an indoor insect screen is driven by natural convection since air currents in an indoor space are considered negligible. Even though an externally generated flow is not present and thus heat-transfer is entirely due to natural convection, the study of forced convection can be helpful in understanding the convective heat transfer process occurring. Clearly a heated or cooled insect screen will generate a natural convection flow. If a small sub-section of the screen is studied, the convection in the local vicinity may be looked at as forced convection. In this case, the driving force behind the local forced convection would be the larger scale flow generated by natural convection over the whole screen. The scale of the fluid velocities expected in such a scenario can be obtained from the results of Norris [Norris 2009]. These results indicate that fluid velocities parallel to the screen are on the order of $10^{-1} m/s$.

Forced convection is clearly a widely studied topic. There are several geometries which have been studied that are helpful in understanding convection from an insect screen. These different geometries are separately discussed in the next sub-sections.

2.3.1 Flat Plate

The case of forced convection with the flow parallel to a heated flat plate is a well-studied case. For a flat-plate, laminar flow is expected up to $Re_L \approx 5 * 10^5$ [Fox 2004]. For $300K$ air at a velocity of $0.1 m/s$, $Re_L = 5 * 10^5$ corresponds to a plate length of about $80m$. Since

this is substantially larger than the insect screens contemplated in this work, only models of laminar flow are looked at.

The problem of fluid flow over a flat-plate was solved by Blasius [Blasius 1908] using a similarity method to create an ordinary differential equation which was then numerically solved. By using the flow pattern determined by the Blasius solution in addition to use of the energy equation, the heat transfer co-efficient for an isothermal flat plate can be determined. Equations for the local and average Nu_L for laminar flow are given below for $10 > Pr > 0.6$ [Schlichting 2000].

$$Nu_L = 0.332 Re_L^{1/2} Pr^{1/3}, \qquad Re_L < 5 * 10^5 \tag{2.28}$$

$$\overline{Nu}_L = 0.664 Re_L^{1/2} Pr^{1/3}, \qquad Re_L < 5 * 10^5 \tag{2.29}$$

Where: $Re_L = V \cdot L/\nu$

$V =$ forced fluid velocity

2.3.2 Single Cylinder in Cross-flow

A theoretical treatment of a infinitely long and infinitely fine (i.e., $lim_{D \to 0}$) heat source in a fluid flow was completed by Pikulev [Pikulev 2003]. In order to be able to solve the problem analytically, many assumptions had to be made. A steady-state, isobaric model with constant material properties was considered. The presence of the infinitesimally fine cylinder was assumed to have no impact on the fluid flow streamlines [Pikulev 2003]. The above assumptions neglect natural convection due to the assumption of constant material

properties as opposed to the use of the Boussinesq approximation. The solutions to the continuity and energy equations that represent this simplified model were solved using a Fourier transform and yielded the following [Pikulev 2003]:

$$h_c = \left(\frac{k}{r}\right)\left[\int_0^\infty \frac{cos(\omega)}{\sqrt{0.0625Pe_D^2 + \omega^2}} d\omega\right]^{-1} \tag{2.30}$$

Where: $Re_D = V \cdot D/\nu$

$$Pe_D = \frac{V \cdot D}{\alpha} = Re_D \cdot Pr$$

A key inaccuracy of Pikulev's model is that in the real case of the finite cylindrical heat source, convection inside the cylinder is absent. As such, in order to estimate the accuracy of the model, the amount of convective heat transfer that took place within a radius of r of the fine heat source is compared with the heat source's total thermal flux [Pikulev 2003]. Using this rationale, the scale of error is estimated as:

$$\epsilon = \frac{Q_{conv_r}}{Q_{total}} \tag{2.31}$$

Where: Q_{conv_r} = heat transfer by convection within a radius of r of fine linear source

Q_{total} = total heat flux of linear source

In the real case of a finite solid cylinder, heat transfer inside the cylinder is purely by conduction and there will be no internal convection [Pikulev 2003]. As such, the results

obtained from the theoretical fine heat source will over-predict the heat transfer on the order of ϵ as given above. As would be expected, the magnitude of this error increases with increasing Pe. An error of about 15 % was predicted for $Pe_D = 2$ [Pikulev 2003].

Practical correlations for a finite heated cylinder are readily available and vary based on the applicable Re_D. Based on the results of Norris [Norris 2009], forced air velocities in the range of $0.05 - 0.25 m/s$ and cylinder diameters of $0.1 - 1 mm$ should be considered. These parameters result in $0.3 < Re_D < 15$.

Zukauskas recommends the following correlation to be used for $Pr < 10$ with differing constants for different ranges of of Re_D [Zukauskas 1972]:

$$Nu_D = C \cdot Re_D^n Pr_{T_\infty}^{0.37} \left(\frac{Pr_{T_\infty}}{Pr_{T_s}} \right)^{0.25} \tag{2.32}$$

Where: $Pr_{T_\infty} =$ Pr taken at the ambient temperature

$Pr_{T_s} =$ Pr taken at the surface temperature

Thus for $Pr_{T_s} \approx Pr_{T_\infty}$:

$$Nu_D = C \cdot Re_D^n Pr_{T_\infty}^{0.37} \tag{2.33}$$

The lowest range of Re_D values for which Zukauskus provides values for the constants in Equations 2.32 and 2.33 is $1 < Re_D < 40$ [Zukauskas 1972]. For this range of Re_D, Equation 2.33 becomes:

$$\overline{Nu}_D = 0.75 \cdot Re_D^{0.4} Pr^{0.37}, \qquad 1 < Re_D < 40 \tag{2.34}$$

For scenarios which have low Re_D, natural convection is more likely to be present. In cases where natural convection can be neglected and Re_D is low, Zukauskas recommends the correlation given in Equation 2.35 below. A quantitative $Re_{D_{max}}$ limit for this correlation was not given [Zukauskas 1972].

$$Nu_D = 0.35 + 0.5 \cdot Re_D^{1/2} \tag{2.35}$$

Another correlation is given by Churchill and Bernstein [Churchill & Bernstein 1977] that is valid over a wide range of Re_D:

$$\overline{Nu}_D = 0.3 + \frac{0.62 Re_D^{1/2} Pr^{1/3}}{[1 + (0.4/Pr)^{2/3}]^{1/4}} \left[1 + \left(\frac{Re_D}{282 \cdot 10^3}\right)^{5/8}\right]^{4/5}, \quad Re_D \cdot Pr > 0.2 \tag{2.36}$$

The above correlations for an infinite horizontal cylinder in cross-flow are graphically illustrated in Figure 2.1.

Another factor that may need to be taken into consideration is the surroundings of the cylinder. In looking at cylinders that are in confined spaces, the effects of the surrounding confined space may need to be considered [Churchill & Bernstein 1977]. For the case of a cylinder located inside another cylinder, Morgan has suggested using a modified Re_D value in order to account for blockage effects [Morgan 1975] using the relation given below

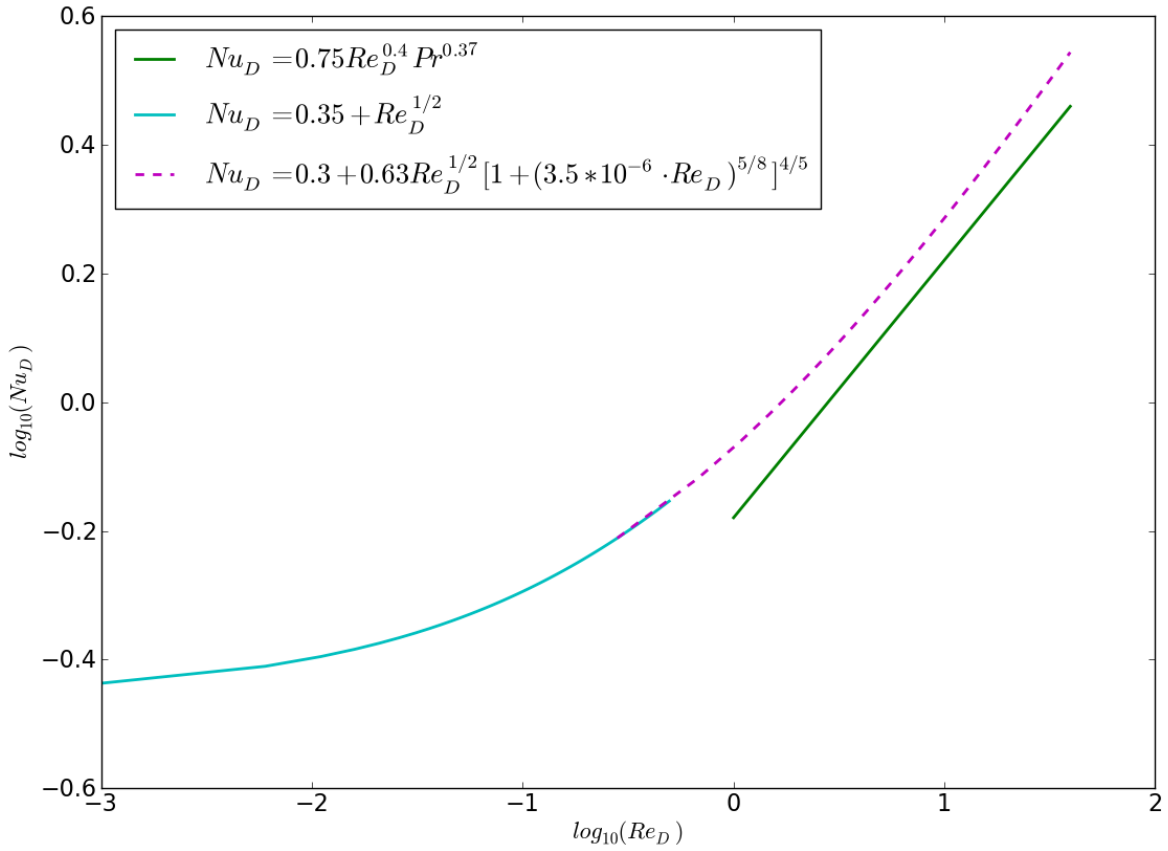

Figure 2.1: Correlations for Forced Convection for a Single Cylinder [Churchill & Bernstein 1977], [Zukauskas 1972]

in Equation 2.37. However Equation 2.37 was developed for higher Reynolds numbers ($10^2 < Re_D < 10^5$) [Morgan 1975] and no equivalent relation for lower values of Re_D was found.

$$Re_{modified} = Re_D \cdot \left[1 + 0.385 \cdot \left(\frac{D}{D_{domain}}\right) + \left(1.356 \cdot \frac{D}{D_{domain}}\right)^2\right] \qquad (2.37)$$

$$\text{for } 10^2 < Re_D < 10^5$$

2.3.3 Multiple Cylinders

Forced convection heat transfer from arrays of multiple cylinders is a common engineering scenario found in many heat exchangers. Correlations are available for two-dimensional arrays of tubes in different geometrical configurations. The case most applicable to an insect screen is the case of a cross-flow past a single row of cylinders spaced along the axis of flow. The single array could also be considered as a special case of the two-dimensional array where the transverse spacing between rows is very large.

Differences in heat transfer between cylinders in different positions in an array is due to a number of factors. The first factor is that as heat is transferred to the fluid, cylinders further downstream see a higher temperature fluid and thus a reduced rate of heat transfer. In addition, the flow past downstream cylinders is altered by the presence of the upstream cylinders. In the case of an insect screen where the cylinders are all arranged in-line with each other, upstream cylinders act as a block and reduce the downstream centreline fluid velocity and the corresponding heat transfer rates [Incropera 2002]. In opposition to this effect is the production of turbulence by the upstream cylinders which increases fluid mixing and heat transfer [Incropera 2002]. As a result, it is found that for laminar flows, the heat transfer from the first cylinder is typically higher due to the dominance of the blockage

effect. In turbulent flow, the heat transfer from the first cylinder is typically lower than for the other cylinders since the turbulence production effect is most significant [Kreith 1997].

It was noted by Zukauskas that there was much less experimental data available for tube banks at low Re than for those at high Re [Zukauskas 1972]. This is likely due to the prevalence of high Re flows in common heat exchanger designs. Zukauskas suggests that for $Re_D < 200$, Nu_D varies as $Re_D^{0.4}$ [Zukauskas 1972]. Research on low Re tube bundles was later completed by Fowler [Fowler 1994]. Fowler found that Nu_D decreased for downstream cylinders before stabilizing after 10-20 cylinders. This work was completed with a square grid of staggered cylinders spaced to produce cross-sectional area densities of $0.6 - 0.95$ [Fowler 1994].

2.4 Mixed Convection

It is useful to be able to quantify the relative significance of natural versus forced convection. In the event that one form of convection can be shown to be negligible, only the other needs to be considered. The Richardson number estimates the ratio of the effects of natural and forced convection, and is given in equation 2.38 [Cengel 2007].

$$Ri = \frac{Gr}{Re^2} \tag{2.38}$$

For $0.1 < Ri < 10$ both natural and forced convection must be taken into consideration [Cengel 2007]. A simple method to estimate the combined effects of natural and forced convection is:

$$Nu_{mixed} = \left(Nu^n_{forced} \pm Nu^n_{natural}\right)^{1/n} \qquad \text{[Kakac 1987]} \tag{2.39}$$

In Equation 2.39 the forced and natural component terms are added if both components are in the same direction or transverse to one another; if the components are in opposition to each other the terms are subtracted. For a vertical plate, the recommended exponent is $n = 3$ [Kakac 1987].

Chapter 3

Model Setup

Since a building is a large and complex system to model in its entirety, building energy modelling is completed by treating finer details as simpler elements. In the case of windows, it is desirable to implement what is known as the centre-glass approximation. In this approximation, the heat transfer through the window is assumed to be constant over the area of the window. This approximation is only used to model the heat transfer through the window glazing; heat transfer through the window frame is treated separately [Lomanowski 2008]. The approximation of constant heat transfer for all locations over the glazing allows it to be viewed as a one-dimensional system of thermal resistances as is shown in Figure 3.1.

In order to find the thermal resistances for the centre-glass approximation, a two-dimensional model of a window, taken along a central vertical cross-section is used. This was the approach used by Norris when creating a two-dimensional CFD model of a window

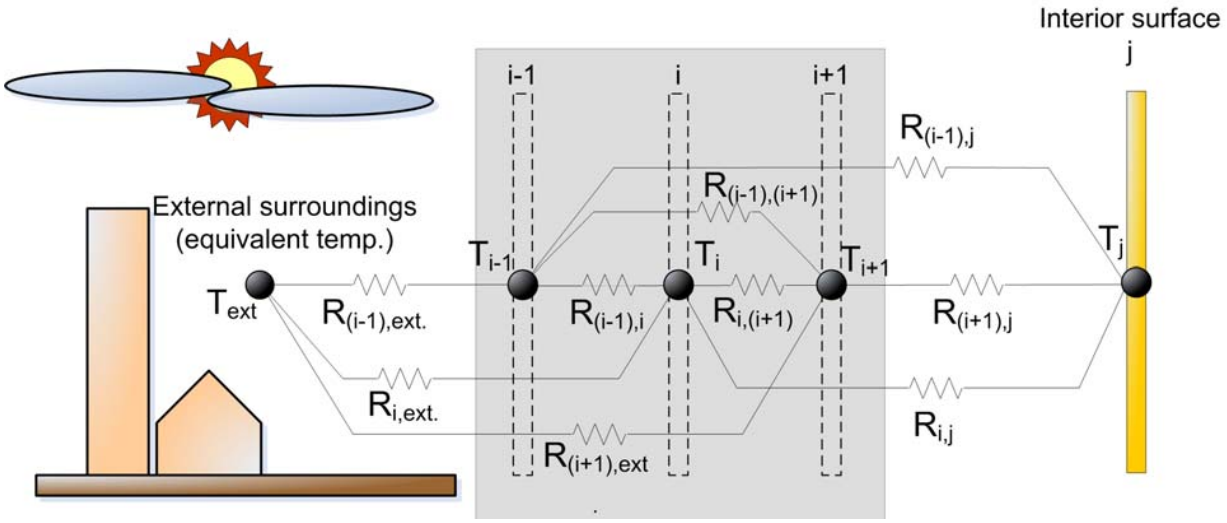

Figure 3.1: Schematic Description of the Centre Glass Approximation [Lomanowski 2008]

with an insect screen [Norris 2009]. Figure 3.2 shows this model. Edge effects from the sides of the windows were neglected [Norris 2009]. Note also that the model used by Norris places the insect screen on the indoor side of the window glazing. The present investigation uses the same position for the insect screen. Insect screens placed on the outdoor side of the window glazing are not considered here.

The convective heat transfer coefficient on both sides of the insect screen must be known for these thermal resistances to be calculated. The heat transfer coefficient for a given

screen could reasonably be expected to vary as a function of the following variables:

$$h_c = F(D, \gamma, \Delta T, V, \theta, y, \text{position effects}) \tag{3.1}$$

Where: D = Diameter of screen filaments

γ = Screen density

ΔT = Temperature difference between ambient air and screen

V = Velocity of air being forced past the screen

θ = Direction of forced convection

y = Height of the screen

Position Effects = Spatially variable heat transfer over the area of the screen

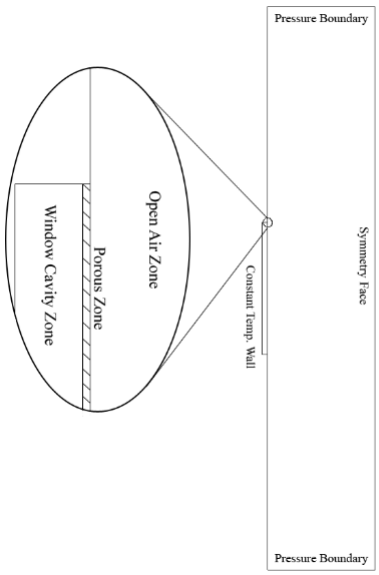

Figure 3.2: Window With Screen 2-D Cross Section Model [Norris 2009]

Thus finding the heat transfer coefficient would appear to be at least a seven-dimensional problem. As such, varying each parameter to determine a correlation of the heat-transfer co-efficient to all of the seven possibly coupled parameters would take a prohibitive number of models. The number of models required would be Ω^7 where Ω is the number of values for which a given parameter is modelled. Clearly, explicitly modelling all cases is not feasible.

The approach taken is to initially look at simpler geometries. The results for these simpler geometries can be more easily and conclusively determined. The complexity associated with a real screen is then modelled and compared to the simpler models. The relation between the simpler and more complex models can then be used and the results for other specific geometries determined using a perturbational methodology.

Furthermore, all of the geometries require simulations separately for the cases of both forced and natural convection. The simulation of forced convection on the insect screen also allows the use of analyses which consider the overall natural convection flow developed around the screen/window assembly to be modelled a source of localized forced convection when portions of the screen are considered on a smaller scale.

The models were completed as follows:

- Single Cylinders: Correlations for single cylinders, either horizontal or vertical, are readily available. CFD models of single cylinders were created and compared to available correlations to validate the CFD models used.

- Multiple Cylinders: CFD models were created of vertical arrays of horizontal cylinders. The heat transfer coefficients determined from these can be compared to those of the

single cylinders. By modelling infinite cylinders, a 2D CFD model can be used which substantially decreases the model complexity and computational time. Thus a larger number of these models can be created than for those of a full screen.

- Rectangular Grid of Cylinders: A grid of horizontal and vertical cylinders was simulated using CFD. These models are by necessity three-dimensional and thus have greater complexity and required computational time. The results of these models can be compared to those from the corresponding two-dimensional models and a correlation between the two determined. Once this correlation is determined, the results for a larger set of screen geometries can be predicted using the correlation between the three-dimensional models' results and the more voluminous data obtained from the two-dimensional models.

All of the above model scenarios were modelled using the CFD package FLUENT.

3.0.1 Size Limits

Certain size restrictions apply to the use of a CFD model. The FLUENT software discretizes the Navier-Stokes equations of fluid mechanics. In order to use this approach, the continuum nature of the fluid must be assumed. The appropriateness of this assumption can be analyzed using the Knudson number which is defined below [White 2006].

$$Kn = \frac{\lambda}{\iota} \tag{3.2}$$

Where: $\lambda =$ Molecular mean free path

$\iota =$ Characteristic length

The mean free path of fluid particles can be calculated as follows [Kittel 1997]:

$$\lambda = \frac{1}{n\pi d^2} \tag{3.3}$$

Where: $n =$ particle concentration

$d =$ molecular diameter

To calculate the mean free path, the fluid surrounding the screen was simplified to be diatomic nitrogen at $300K$. Material data was taken from [Incropera 2002] and [Zumdahl 1992] and the diameter of N_2 was assumed to be $d_{N_2} = \sqrt{2} \cdot d_N$.

$$\rho = 1.1\ kg/m^3 \quad \text{[Incropera 2002]}$$

$$N_A = 6.0 * 10^{23}\ mol^{-1} \quad \text{[Zumdahl 1992]}$$

$$m_{N_2} = 28.0\ g/mol \quad \text{[Zumdahl 1992]}$$

$$d_{N_1} = 0.18\ nm \quad \text{[Zumdahl 1992]}$$

Where: $N_A =$ Avogadro's Number

$m =$ molecular mass

Using the values given above, the characteristic length can be calculated as follows:

$$n = \frac{\rho N_A}{m_{N_2}} = 2.4 * 10^{25}\ m^{-3}$$
$$\lambda = \frac{1}{\pi(2.4 * 10^{25} m^{-3})(0.18nm)^2} = 0.4\ \mu m \tag{3.4}$$

For the continuum model of a gas to be appropriate, the Knudson number should be much less than 1 [White 2006]. If the Knudsen number becomes as large as $Kn \approx 0.1$, slip condition models at wall boundaries are recommended [White 2006]. The finest insect screen investigated had a filament diameter of $0.1mm$ and $Kn = 0.002$. Therefore it was deemed appropriate to model heat transfer and fluid flow phenomena using continuum approaches.

3.1 Natural Convection

In simulating natural convection, only laminar flow was considered. For natural convection, the flow is expected to be laminar for $Ra_i < 10^9$ [Gebhart 1988]. For air at $300K$, $Ra_i = 10^9$ corresponds to a length dimension of $i \approx 1m$ for $\Delta T = 10K$ or $i \approx 0.6m$ for $\Delta T = 50K$. The models described in this section all involve screen segments that are substantially smaller than this and hence it was not necessary to consider turbulence for them.

3.1.1 Single Cylinder Models

The simplest case of a single horizontal cylinder is investigated first. Numerical models were created for horizontal cylinders with diameters ranging between $0.1mm$ and $1.0mm$. These models were run with surface temperatures of the cylinder ranging from 1^oC to 50^oC above the temperature of the ambient fluid.

0.1mm Diameter Cylinder

A cylinder diameter of $0.1mm$ was used as a base case on which to judge the accuracy of the model meshes used. Two-dimensional models with different domain sizes and mesh densities were compared to find the minimum mesh density and domain size required for the $0.1mm$ diameter wire case. Table 3.1 summarizes the different mesh densities and domain sizes used.

Figures 3.3 and 3.4 show mesh D2-M2 which uses a structured boundary layer mesh around the wire and a triangular unstructured mesh for the rest of the domain. The thickness of the first boundary layer cell is 25% of its length. The size of the mesh in each layer of cells in the boundary layer increases by a factor of 1.2. There are a total of 10 cell layers in the grid boundary layer. Symmetry conditions were imposed on the vertical boundaries of the domain. The lower horizontal domain boundary was modelled as a pressure inlet while the upper domain boundary was modelled as a pressure outlet. The cylinder edge was modelled as a wall with a no-slip momentum condition and a constant temperature thermal condition.

Table 3.1: Meshes Used for Single Cylinder, Natural Convection

Model #	X-Size	Y-Size	Cylinder Grid Count	Outside Grid Size	Cell Count
D1-M2	40D	60D	36	2.5D	5800
D2-M2	80D	120D	36	2.5D	9406
D3-M2	160D	240D	36	5D	22 810
D4-M1*	160D	480D	9	20D	3039
D4-M2*	320D	480D	18	10D	12 346
D4-M3*	160D	480D	36	5D	51 811
D5-M2*	640D	960D	18	20D	17 982

D = cylinder diameter

X-Size = horizontal width of model domain

Y-Size = vertical height of model domain

Cylinder Grid Count = number of grid cells adjacent to cylinder boundary wall

Outside Grid Size = edge length of grid cells along outer model domain boundaries

*these meshes use vertical mirror half-symmetry to reduce cell counts

Models using the different domain and mesh densities were run using a cylinder surface temperature 10^0C above ambient. Results from these models are presented graphically in Figures 3.5 through 3.8 and numerically in Table 3.2. The optimum domain size and mesh density for further use is determined by looking for independence of model results from domain size and mesh density. All models were run using the following residual criteria: continuity = 10^{-3}, energy = 10^{-6} and x,y,z momentum = 10^{-3}.

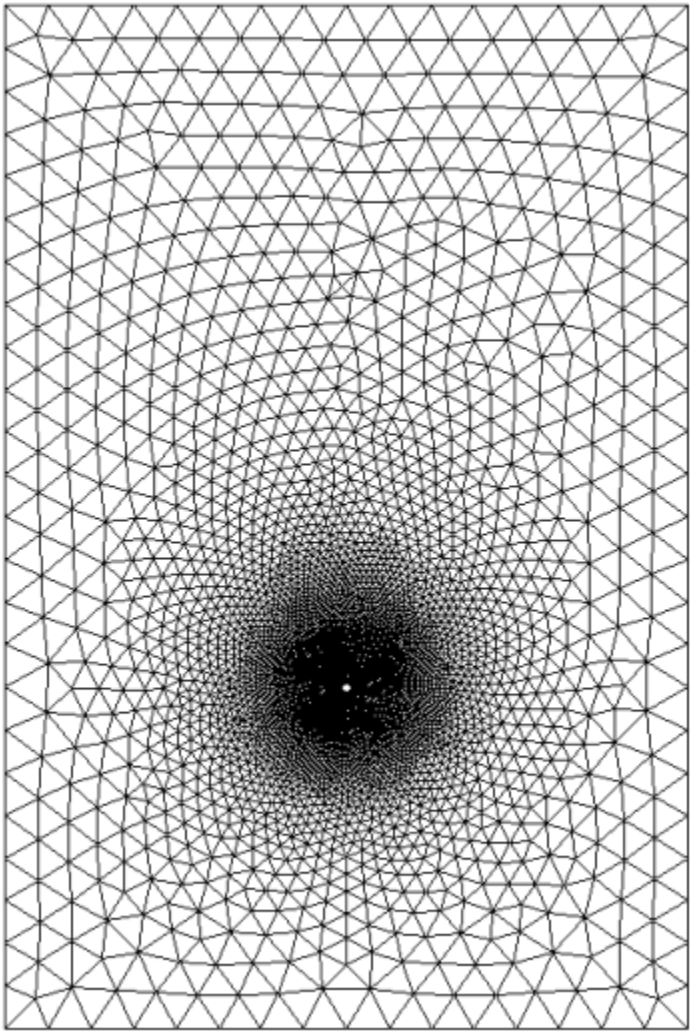

Figure 3.3: Grid for Mesh # D2-M2, Natural Convection for a Single Cylinder

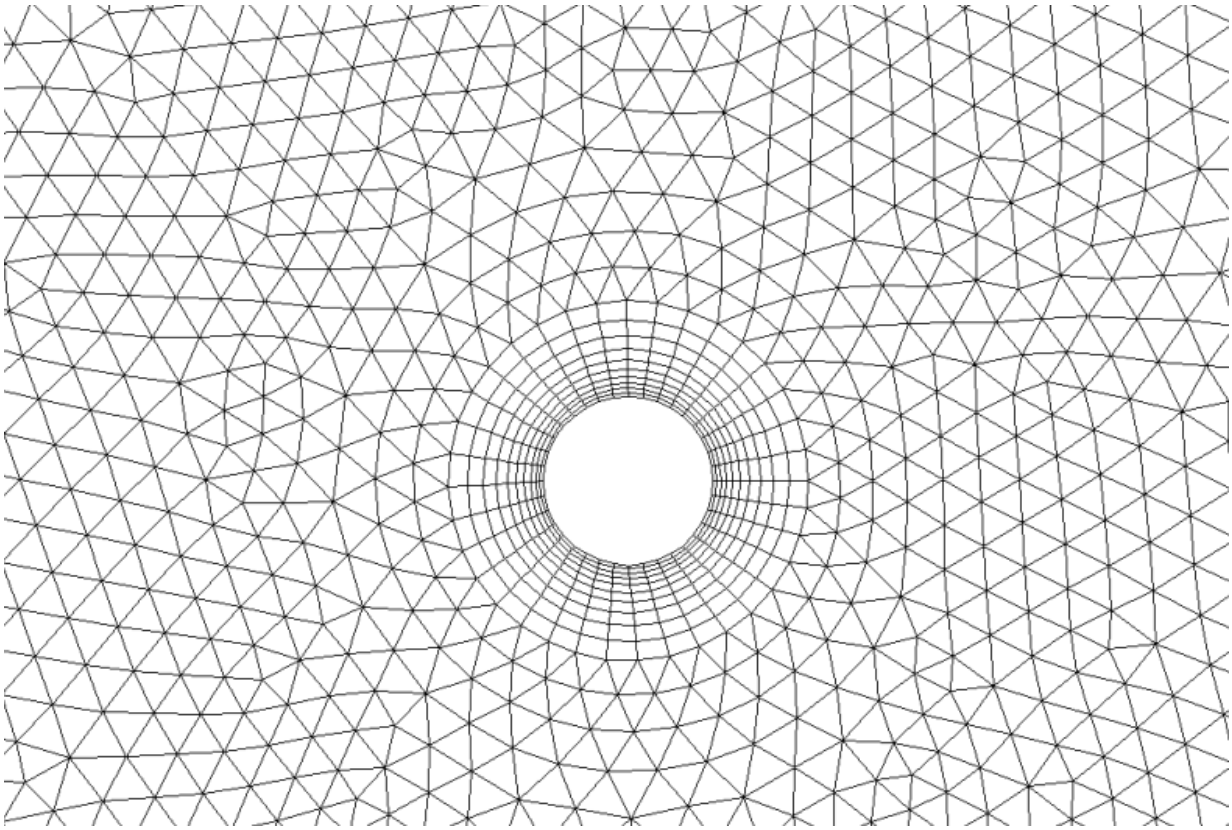

Figure 3.4: Centre Close-up of Grid for Model # D2-M2, Natural Convection for a Single Cylinder

Table 3.2: h_c Values for Natural Convection from a Single $0.1mm$ Cylinder

Mesh	$Q \ \ W/m$	$h_c \ \ W/(m^2 \cdot K)$
D1-M2	0.418	133
D2-M2	0.367	117
D3-M2	0.366	116
D4-M1	0.376	120
D4-M2	0.374	119
D4-M3	0.364	116
D5-M2	0.376	120

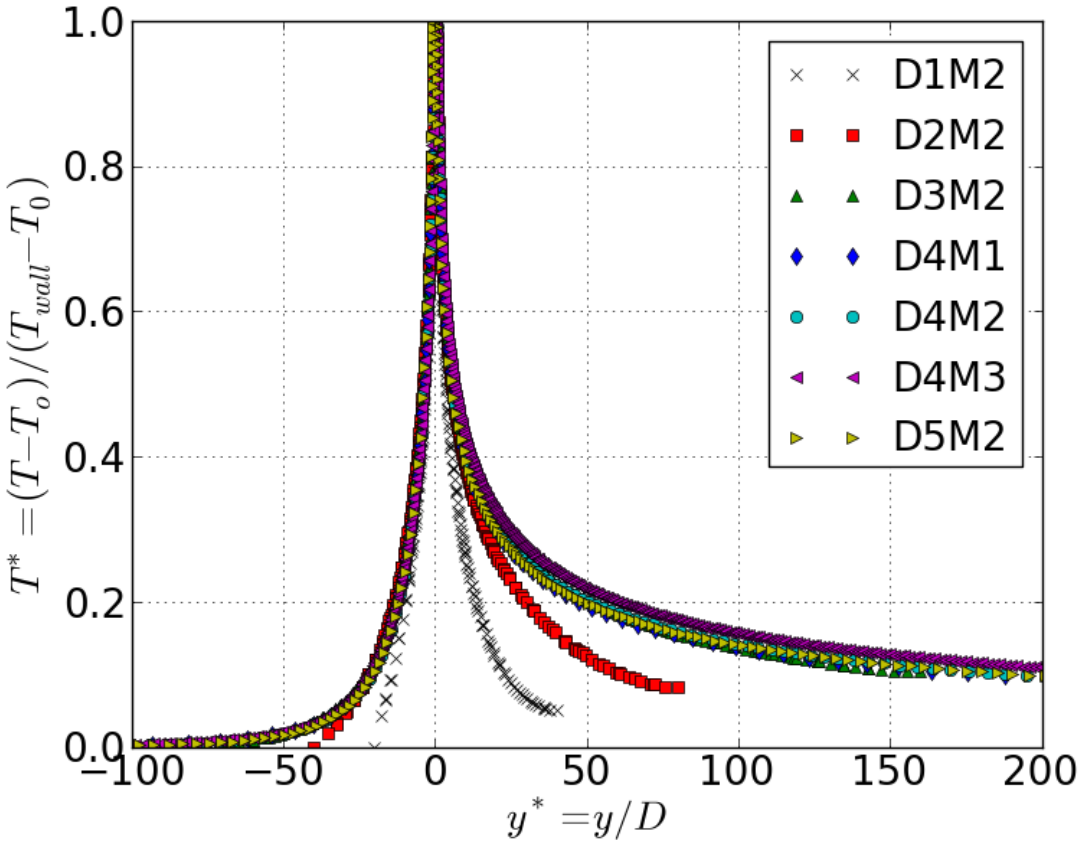

Figure 3.5: Temperature along Vertical Cross Section for $0.1mm$ Cylinder, Natural Convection Models at $\Delta T = 10^oC$

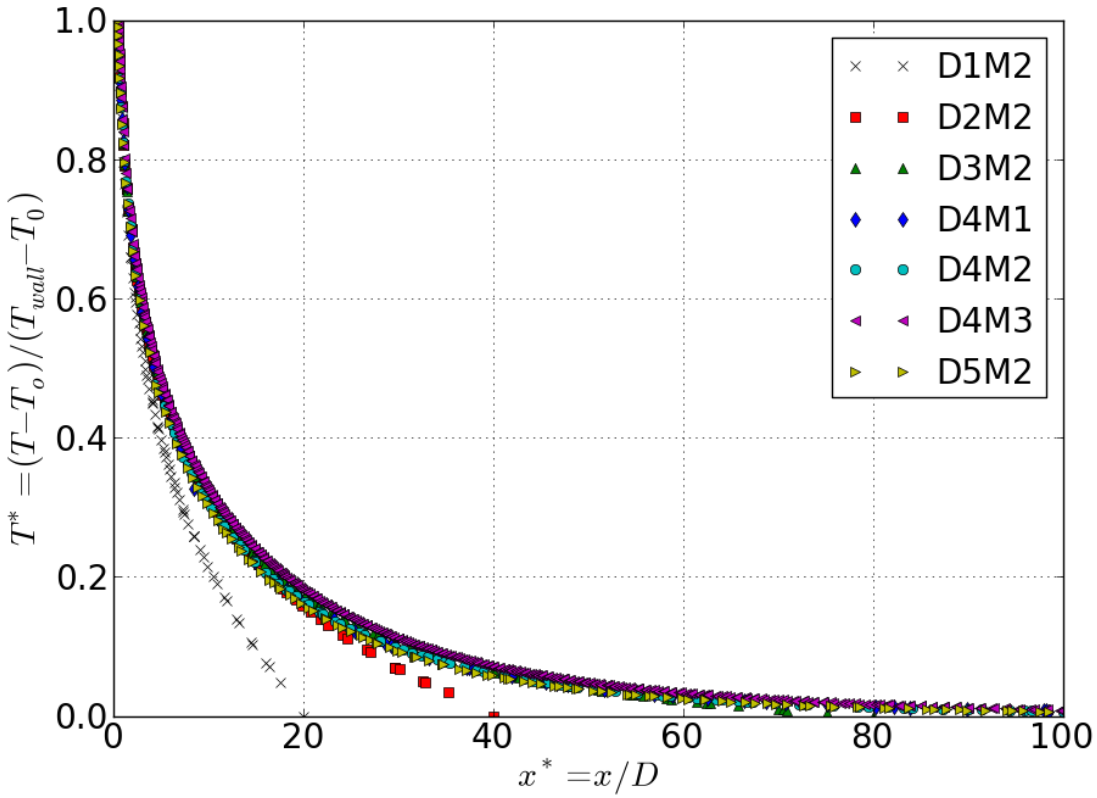

Figure 3.6: Temperature along Horizontal Cross Section for $0.1mm$ Cylinder, Natural Convection Models at $\Delta T = 10^oC$

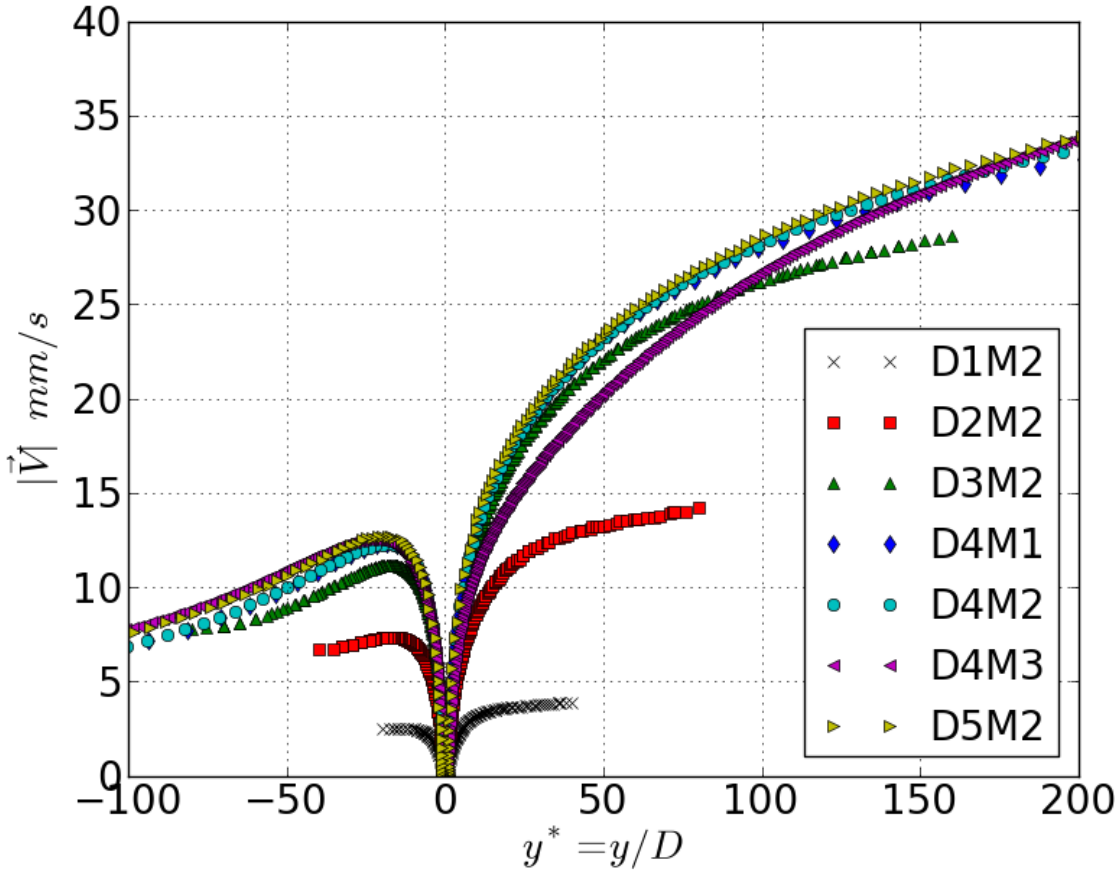

Figure 3.7: Air $|\vec{V}|$ along Vertical Cross Section for $0.1mm$ Cylinder, Natural Convection Models at $\Delta T = 10^oC$

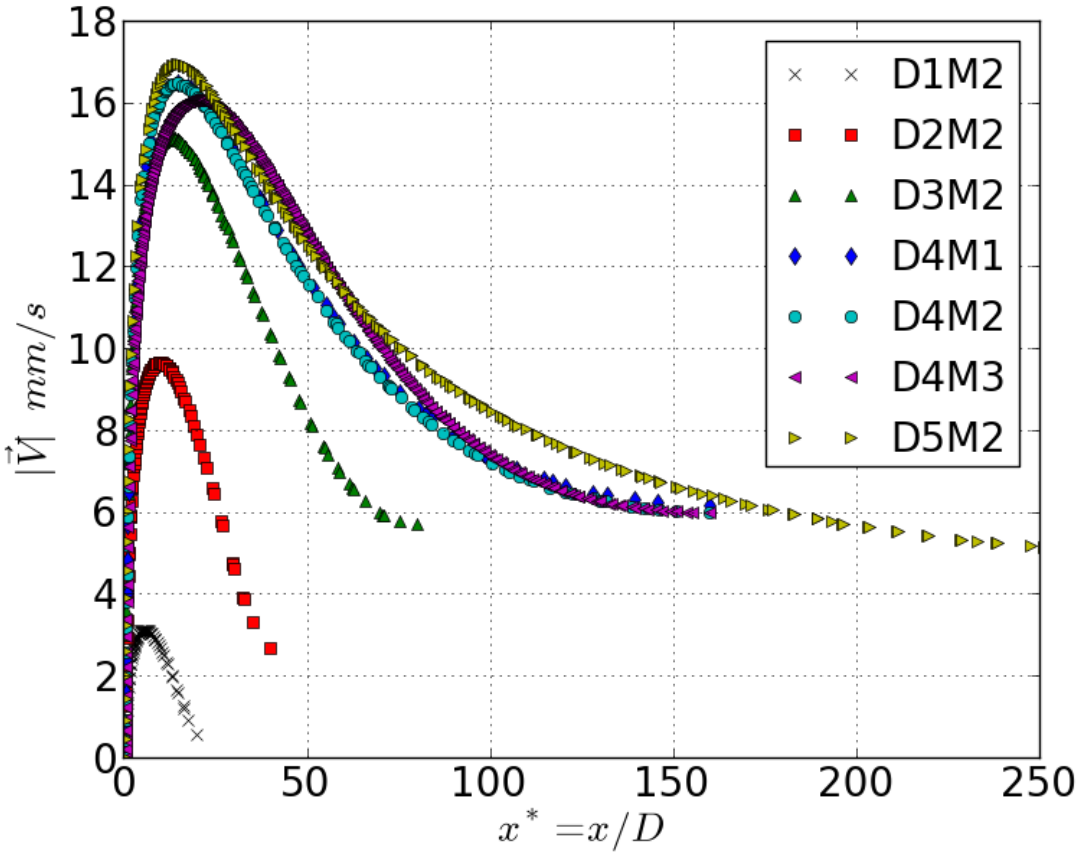

Figure 3.8: Air $|\vec{V}|$ along Horizontal Cross Section for $0.1mm$ Cylinder, Natural Convection Models at $\Delta T = 10^oC$

The values of h_c given in Table 3.2 show a reasonable degree of independence from the domain size and mesh density used for all meshes except D1-M2. The values of h_c were in the narrow range of $116 - 120\ W/m^2K$ except for the result from the mesh D1-M2 which differed somewhat at $133\ W/m^2K$. These compare to those predicted by the correlations of Morgan and Churchill which predict h_c values of $100\ W/m^2$ and $114\ W/m^2$ respectively [Morgan 1975] & [Churchill & Chu 1975(1)].

However, it can be seen in Figures 3.5 and 3.6 that the temperature distribution across the domain is more sensitive to the domain size than the value of h_c at the cylinder surface . Based on the temperature distributions, a domain size of 160D x 240D (domain D3) appears to be the minimum domain size. Likewise, it appears from the velocity distributions shown in Figures 3.7 and 3.8 that a domain size of 320D x 480D (domain D4) is the minimum domain size.

In order to provide the greatest confidence in the accuracy of the models, domain D4 (320D x 480D) was chosen since it was the minimum domain size for which the both the velocity and temperature distributions were similar to larger domains tested. Once D4 was chosen as the domain size, it was meshed at different densities with the results being compared to show independence from the mesh density. Similar results were obtained for the three mesh densities tested. Since convergence was rapidly obtained using the middle-density meshes M1 and M2, mesh M2 was chosen as the optimum one and D4-M2 was chosen for further use.

1.0mm Diameter Cylinder

The largest diameter cylinder modelled was $1.0mm$. For the case of a $1.0mm$ cylinder, all of the models used for the $0.1mm$ cylinder were simply scaled by a factor of 10. The results from these models were used to determine the appropriate domain and mesh sizes required. The data from the different domain and mesh sizes are presented in Figures 3.9 through 3.12 and in Table 3.3.

Table 3.3: h_c Values for Natural Convection from a Single $1.0mm$ Cylinder

Mesh	$Q \ \ W/m$	$h_c \ \ W/(m^2 \cdot K)$
D1-M2	0.765	24.4
D2-M2	0.740	23.6
D3-M2	0.786	25.0
D4-M2	0.786	25.0
D4-M3	0.788	25.1
D5-M2	0.786	25.0

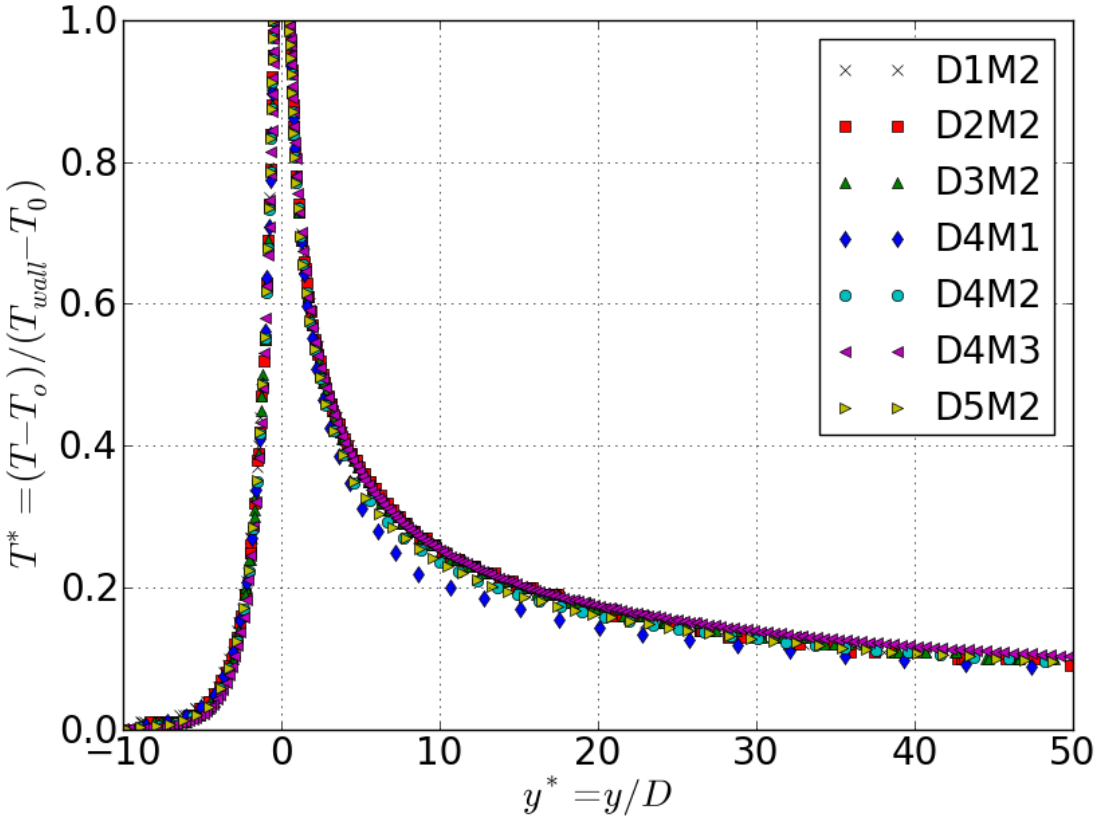

Figure 3.9: Temperature along Vertical Cross Section for $1.0mm$ Cylinder, Natural Convection Models at $\Delta T = 10^oC$

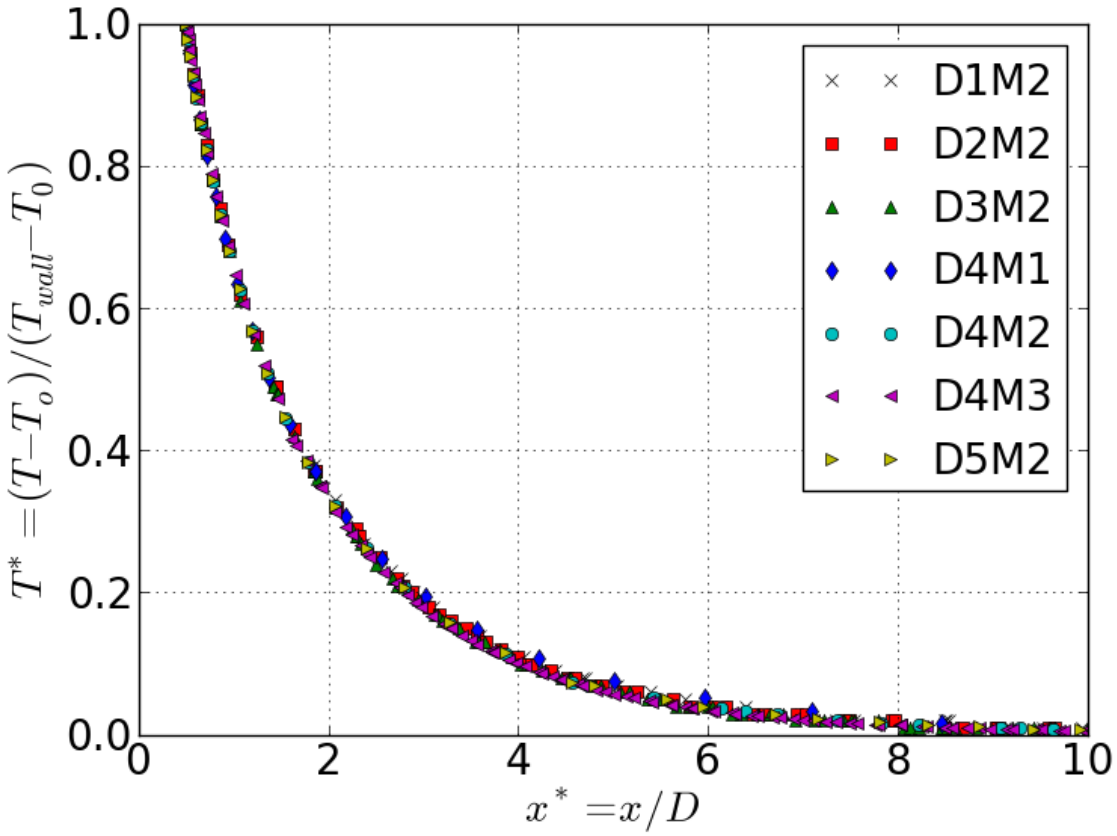

Figure 3.10: Temperature along Horizontal Cross Section for $1.0mm$ Cylinder, Natural Convection Models at $\Delta T = 10^oC$

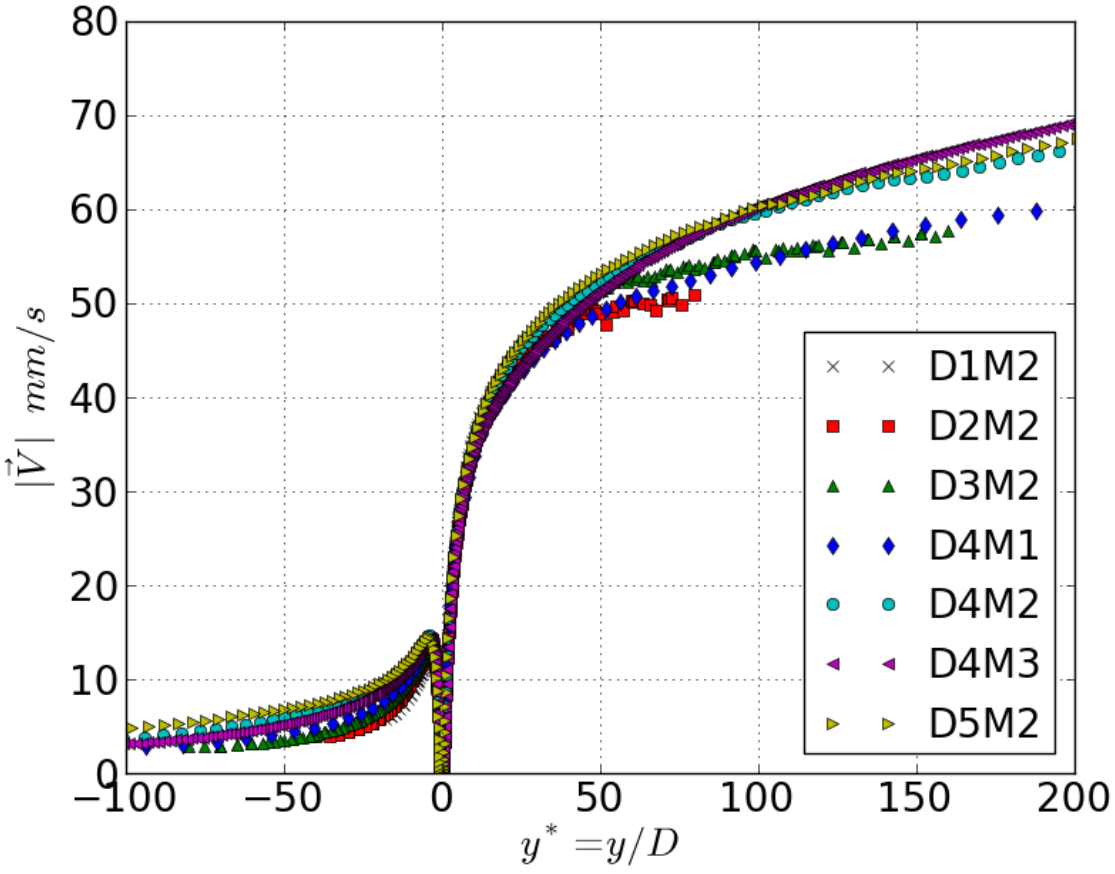

Figure 3.11: Air $|\vec{V}|$ along Vertical Cross Section for $1.0mm$ Cylinder, Natural Convection Models at $\Delta T = 10^oC$

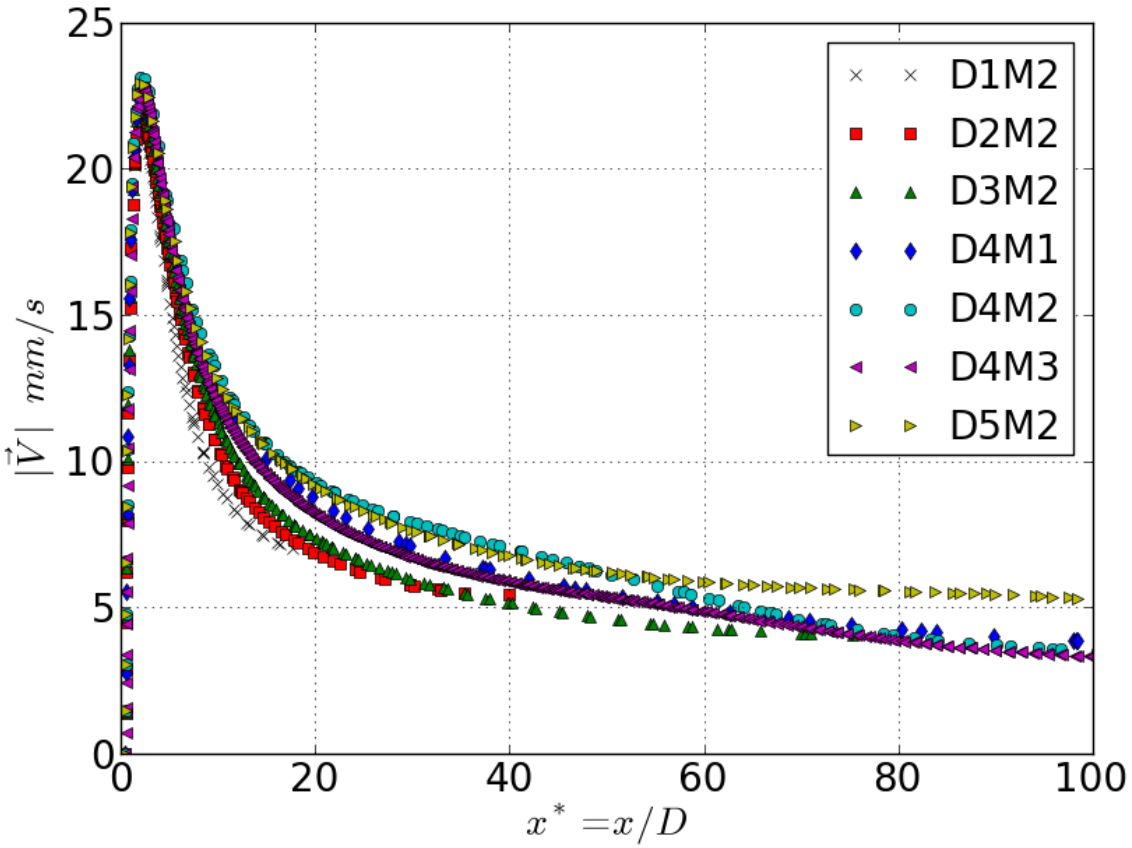

Figure 3.12: Air $|\vec{V}|$ along Horizontal Cross Section for $1.0mm$ Cylinder, Natural Convection Models at $\Delta T = 10^oC$

As can be seen in Table 3.3, the values of h_c predicted by models using the different meshes fall in a narrow range from $23.6-25.1\ W/m^2K$. This compares to values predicted by the correlations of Morgan and Churchill of $h_c = 15\ W/m^2$ and $h_c = 17\ W/m^2$ respectively [Morgan 1975] & [Churchill & Chu 1975(1)].

In addition, Figures 3.9 and 3.10 show very similar temperature distribution predictions for the different domain sizes and mesh densities used. The velocity distributions in Figure 3.11 do show lower predicted velocities for the smaller domains at distances greater than 60*D downstream (above for a heated cylinder) from the cylinder. Despite this, the distributions all show less dependence on the domain size compared to the smaller 0.1mm diameter cylinder models. Based on this finding, it can be deduced that the minimum domain size required (where domain size L^*_{domain} is measured as the size of the domain relative to the cylinder diameter) to give independent results appears to decrease with increasing wire diameter. Thus, the minimum domain size to give domain-independent results for the smallest cylinder used ($0.1mm$) was used for all cylinder sizes as a conservative size selection.

3.1.2 Vertical Array of Cylinders

After modelling a horizontal cylinder, the next step in the modelling progression was to model vertical arrays of infinite horizontal cylinders. An array of five cylinders was modelled for diameters of 0.1mm, 0.25mm, 0.5mm and 1.0mm as well as for temperature differences of 5^oC, 10^oC, 20^oC and 50^oC. A centre-centre spacing of ten diameters was used between the cylinders. The mesh used for these models was based on the D4-M1 mesh used for the single cylinder case. Details of the D4-M1 mesh are given above in Table 3.1. The coarser M1 mesh density was used in the multi-cylinder models to reduce computational time which is already necessarily increased from the higher complexity of a multi-cylinder model. Due to the space taken up by the array of cylinders, the domain height was increased over that used by a single cylinder by 40 cylinder diameters. By doing this, the distances from the first and last cylinders to the lower/upper domain boundaries were kept the same as those used for the single cylinder case. Figure 3.13 gives a sketch of the model domain used. Boundary conditions were the same as for the single-cylinder case.

In addition to the models of a five-cylinder array, a single case for a 10-cylinder array was modelled for comparison. The case modelled was a 0.1mm cylinder with $\Delta T = 10^oC$. The model setup was the same as that for the five cylinder array with the only changes being the addition of five cylinders and a domain height increase of 50*D.

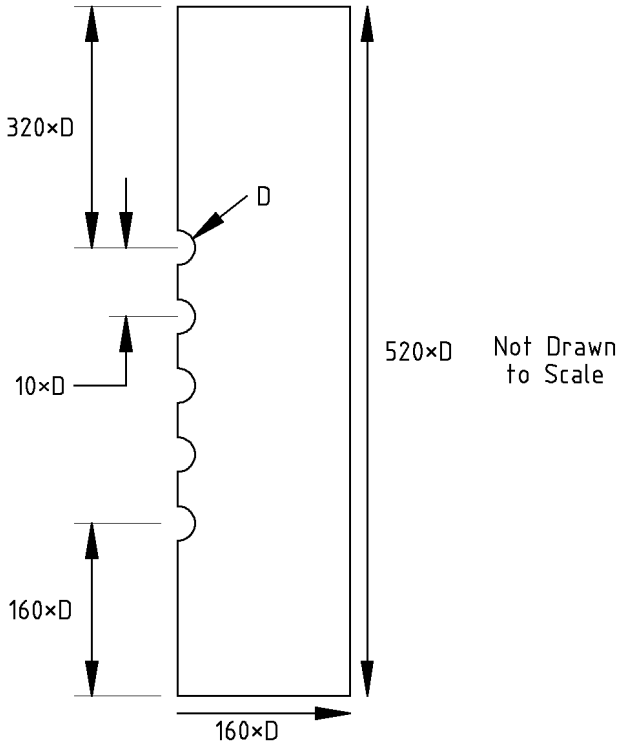

Figure 3.13: Sketch of 2D Model Domain for Five Cylinder Array, Natural Convection

3.1.3 3D Models

The final model created was a three-dimensional section of the screen. The screen was treated as rectangular pattern of intersecting cylinders. The same domain size of 160*D wide and 520*D tall that was used for the two-dimensional multiple-cylinder case was used for the 3D case as well. This domain is shown in Figures 3.14 and 3.15. Geometrical symmetry allowed for the use of a 1/8th model using three mirror planes. The modes of symmetry utilized are described given below:

- xy plane = mirror through centre of mesh
- yz plane = mirror through centre of vertical cylinder
- parallel to yz plane = mirror through midpoint of horizontal cylinders represents horizontal repetition of mesh pattern

Where the co-ordinate axes used are:

x-axis $\rightarrow$ parallel to horizontal cylinders

y-axis $\rightarrow$ parallel to vertical cylinders

z-axis $\rightarrow$ normal to rectangular cylinder array

Note that there is a fifth boundary parallel to the xy plane which has a symmetry boundary condition. This symmetry plane represents a far-field condition of ambient

conditions at infinity. The walls of the cylinders were assigned a constant temperature thermal condition and a no-slip momentum condition.

In order to avoid effects from the abrupt interruption of the flow by the blunt end of a cylinder, frustums were added to both ends of the horizontal cylinder. These frustums had a height of 30*D and an end diameter of D/10. Frustums were used to avoid meshing issues which arose when cones were used. Adiabatic and no-slip boundary conditions were assigned to the end-cap frustums.

Due to the added complexity and computational time required for a three-dimensional model, only a single case was considered. The case modelled was an array with horizontal and vertical centre-centre spacing of the cylinders of 10*D. Note that this produces a mesh screen with a screen density of $\gamma = 0.19$. The modelled screen filaments were 0.1mm diameter cylinders with surface temperatures 10^oC above ambient.

Two different meshes were created. The first one used is labelled D4-M2. This mesh is an unstructured tetrahedral mesh created using FLUENT's size function system to manage the density of grid cells based on proximity to specified surfaces. The domain volume was divided into two volumes, each of which had a size function defined for it. The inner volume was a 40*D wide, 170*D tall and 5*D thick rectangular prism with its lower surface 20*D below the lowest horizontal cylinder. The first size function applied created a grid inside this volume that had cells with side lengths of 0.25*D at the cylinder wall surfaces. A growth factor of 1.2x and a maximum edge length of 5*D was applied to progressively decrease the density of the mesh away from the modelled screen surfaces. The outer volume which contained the rest of the domain had cell side lengths of 5*D at its inner boundary.

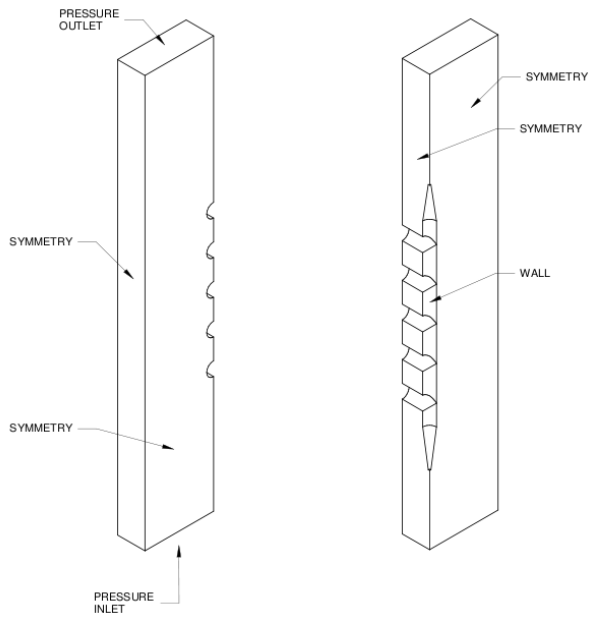

Figure 3.14: Domain Geometry for 3D Natural Convection Models

Thus the grid densities on both sides of the boundary between the two domains were matched. A growth factor of 1.2x was also applied in the outer region with the maximum cell length allowed set at 20*D.

The second mesh was created with the same procedure used for the first mesh but with smaller grid cell sizes. The grid lengths on the cylinder wall surfaces for the finer mesh were specified to be 0.1*D while those at the inner/outer volume junctures were set at 2.5*D and the maximum size allowed was 10*D. This mesh is labelled D4-M3. Table 3.4 gives the details of these meshes.

To identify the variability of the heat transfer based on location on the mesh surface, Nu_L vs Ra_L values were calculated for different sections of the modelled screen. The

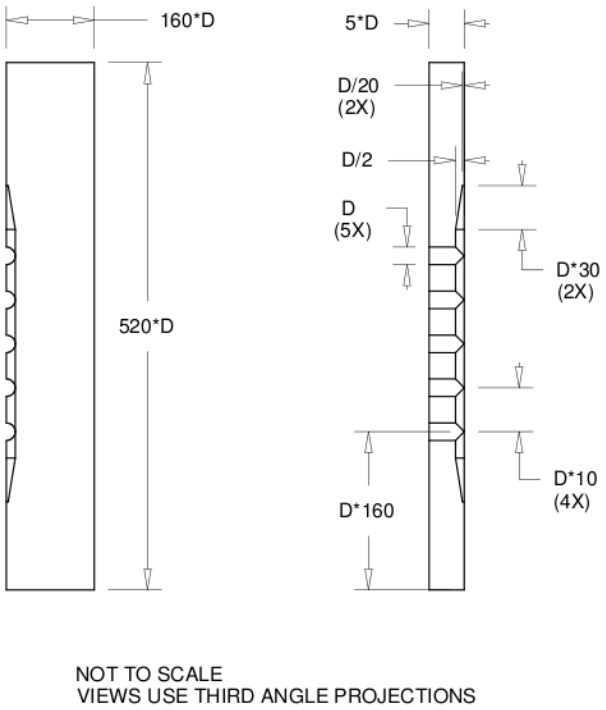

Figure 3.15: Domain Dimensions for 3D Natural Convection Models

Table 3.4: Meshes Used for 3D Natural Convection Models

Mesh	L_{wall}/D	L_{mid}/D	L_{max}/D	Cell Count
D4-M2	0.25	5	20	145 748
D4-M3	0.1	2.5	10	820 964

L_{wall} = grid cell edge length along cylinder wall boundary
L_{mid} = maximum grid cell edge length in inner volume
L_{max} = maximum grid cell edge length in outer volume

dimension L is the vertical distance above the centre of the bottom horizontal cylinder. Each horizontal cylinder was considered as an individual surface. The vertical cylinder was broken into 6 individual segments divided by the horizontal cylinders. The value of L was taken at the centre of the cylinder for the horizontal cylinders. Using this definition of L,

the first cylinder has ill-defined values for Ra_L and Nu_L of 0 and ∞ respectively. For the vertical cylinders, L was taken at halfway between the top and bottom of the section. Note that for the lowest and highest sections of the vertical cylinder, this is not equivalent to the geometrical centre. The values for Ra_L and Nu_L are defined as follows:

$$L = \text{vertical distance above centre of first wire} \tag{3.5}$$

$$A = \text{wall area of a given section of mesh} \tag{3.6}$$

$$h_c = \frac{q}{(T_{wall} - T_\infty) * A} \tag{3.7}$$

$$Ra_L = \frac{Pr * g\beta(T_{wall} - T_\infty)L^3}{\nu^2} \tag{3.8}$$

$$Nu_L = \frac{h_c}{kL} \tag{3.9}$$

The results obtained are given in Figure 3.16. The C1,C2 or C3 suffixes on the end of the mesh labels in Figure 3.16 refer to different convergence criteria used. The applied parameters of these convergence criteria are summarized in Table 3.5.

Table 3.5: Convergence Limits for Natural Convection 3D Models

Mesh	Continuity Residual	Energy Residual	X,Y,Z Velocity Residuals
D4-M2-C1	10^{-3}	10^{-6}	10^{-3}
D4-M2-C2	10^{-4}	$3 * 10^{-7}$	10^{-4}
D4-M3-C1	10^{-3}	10^{-6}	10^{-3}
D4-M3-C2	10^{-4}	10^{-7}	10^{-4}
D4-M3-C3	10^{-5}	$3 * 10^{-8}$	10^{-5}

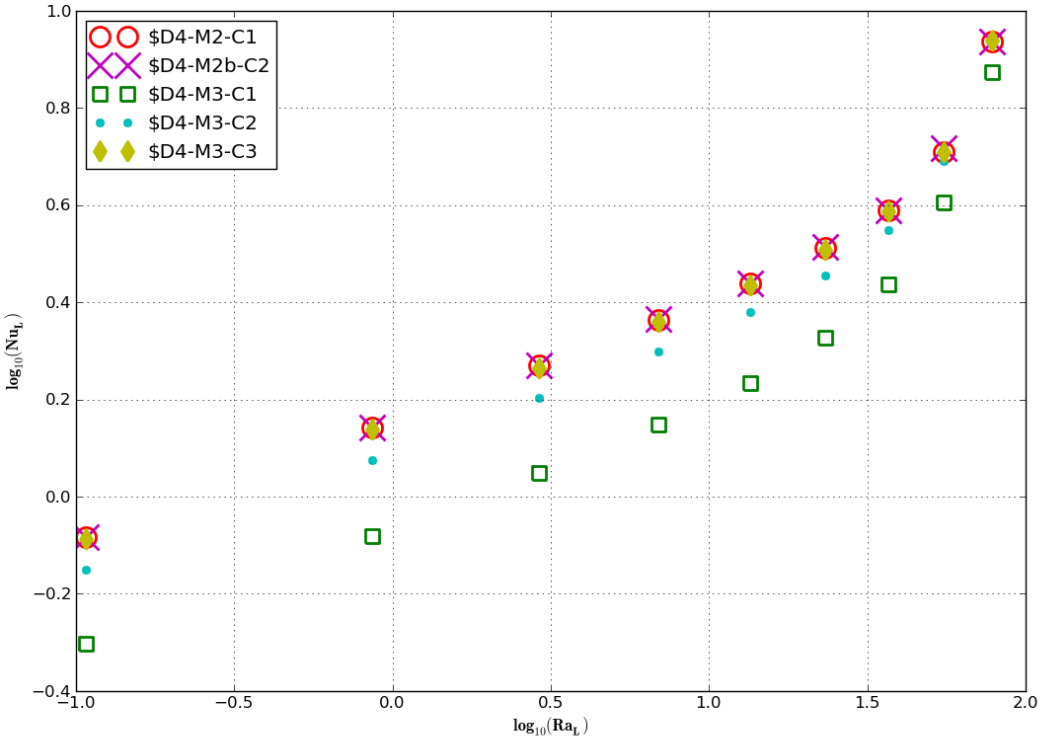

Figure 3.16: Nu_L vs Ra_L for 3D Natural Convection Models, $D = 0.1mm$ & $\Delta T = 10^oC$

The results shown in Figure 3.16 for the D4-M2 mesh are similar for both sets of convergence criteria. Thus it appears that the residual limits used are adequate to yield a convergence-independent solution. The results for the D4-M3 mesh indicate that stricter residual limits are required for the finer mesh. For the largest residual size used, the Nu_L values were lower for all surfaces. As the residual limits were dropped, the Nu_L values increased and approached those found with the coarser D4-M2 mesh. The D4-M3-C3 model's limiting residual was the energy residual. The energy residual for this model was the lowest obtainable at $3 * 10^{-8}$.

Based on the similarity of the results between the two mesh densities, the increased computational time required for D4-M3 and the increased difficulty of obtaining residual-independent results for D4-M3, mesh D4-M2 was chosen as the preferred mesh for further use.

3.2 Forced Convection

As previously noted, investigating forced convection is helpful to understanding the convective heat transfer from an insect screen, even if natural convection is the main driving force of convective heat transfer from the screen. As such, forced convection over the screen was investigated.

As was done with natural convection, simpler two-dimensional models were created for a wide range of scenarios. By using the two-dimensional models, a larger number

of parameters could be varied and the corresponding models completed. The significant parameters that were varied between different forced-convection models were:

- Cylinder diameter
- Cylinder spacing
- Temperature difference between the cylinder surface and ambient fluid
- Velocity of fluid flowing past cylinders
- Orientation of fluid velocity relative to cylinders

Depending on these parameters, the relative significance of natural and forced convection will vary. The relative importance of each type of convection is quantified using the Richardson number which is given here as $Ri = Gr/Re^2$. A plot of Ri versus the forced velocity is given in Figure 3.17 for different screen filament diameters. Furthermore, parameters of the two-dimensional models created along with the corresponding non-dimensional numbers are given in Table 3.6.

Table 3.6: Range of Parameters Used for 2D Models of Forced Convection

Parameter	Range of Values
$D_{cylinder}$	$0.1mm$ - $0.5mm$
ΔT	10^oC
V_{forced}	$0.05m/s$ - $0.25m/s$
Re_D	0.3 - 8
Gr_D	$1.2 * 10^{-3}$ - 0.15
$Ri = Gr_D/Re_D^2$	$2.1 * 10^{-5}$ -1.6

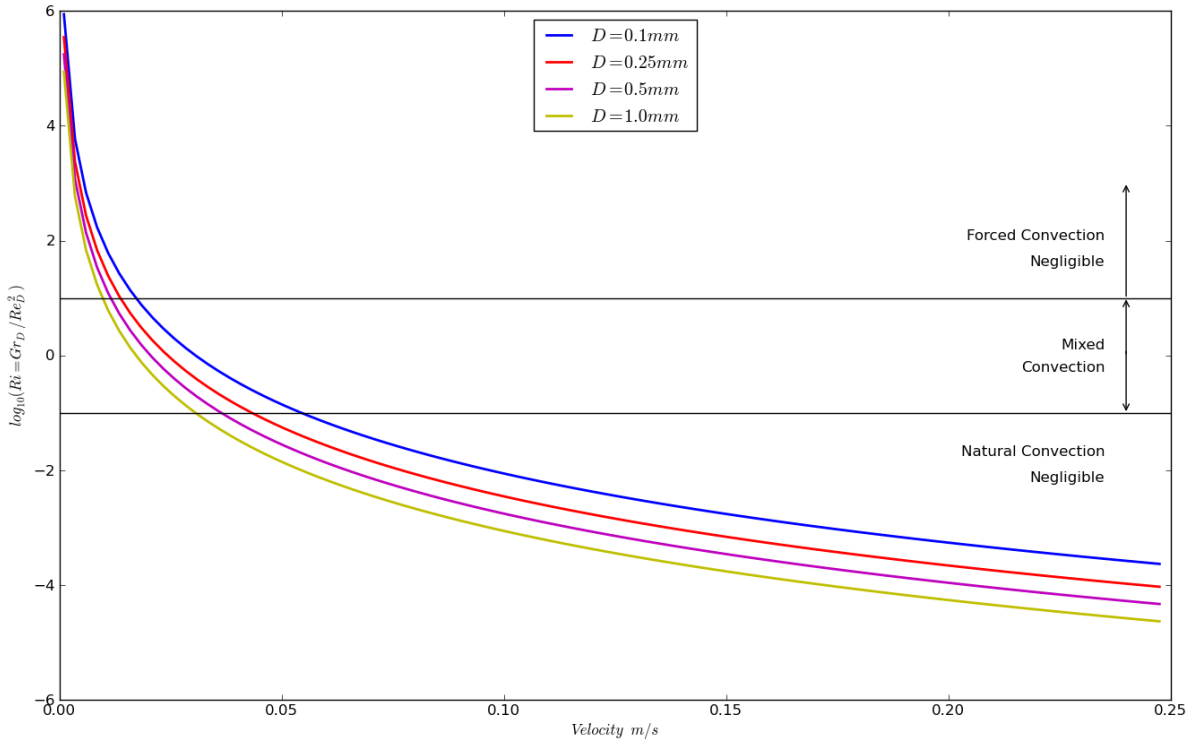

Figure 3.17: Richardson Number vs. Forced Velocity

It is also necessary to examine whether or not turbulence needs to be considered. For flow over a flat plate the transition to turbulence is estimated to occur at $Re_i \approx 5 * 10^5$ [Fox 2004]. For $V = 0.25m/s$, the largest velocity simulated, $Re_i = 5 * 10^5$ corresponds to a length dimension of $i \approx 33m$. As such, it was not necessary to consider turbulent effects.

3.2.1 Forced Convection Normal to Vertical Array of Cylinders

The first case looked at for forced convection was that of horizontal forced flow orthogonal to a vertical array of infinite horizontal cylinders. This case can be examined in two spatial dimensions. The model included gravity so that the total, or mixed convection could be examined. This case should be very similar to horizontal flow over a single cylinder, if the cylinders are spaced widely enough.

The first mesh created to model the 'forced-perpendicular' case was named 'D4-M1'. Figure 3.18 gives a schematic diagram of the domain geometry of mesh 'D4-M1'. The array of cylinders consisted of five infinite horizontal cylinders with a centre-centre spacing of $10 * D$. A structured mesh was created around the heated cylinders. The surface of each cylinder was subdivided into 18 sections. The first row of grid cells was given a height equal to 20% of its width. The height of each successive ring of structured grid cells was increased by a factor of 1.2. A total of 15 layers of grid cells was used for the structured mesh. The purpose of this structured mesh was to capture the details of the boundary layer flow adjacent to the cylinder's surface. The structured meshes from all of the cylinders were combined with an unstructured triangular mesh that filled the rest of the domain. The outside boundaries of the domain were divided into sections $20 * D$ long. The unstructured mesh was then automatically generated with its element sizes gradated to meet the sizes specified at the domain boundaries and outside edges of the structured meshes. Figure 3.19 illustrates this mesh.

A second mesh named 'D5-M1' was created with a larger domain size than mesh 'D4-M1'. Aside from the different domain sizes, mesh 'D4-M1' and 'D5-M1 are identical. Table 3.7

summarizes the properties of these two meshes. Note that the use of a half-geometry to reduce the number of grid cells is not possible in this case. The horizontal forced convection clearly negates the possibility of using a vertical mirror plane. A horizontal mirror plane would only be possible if gravity was neglected (i.e., pure forced convection).

Table 3.7: Meshes Used For Forced Convection Normal to Vertical Array of Cylinders

Model #	X-Size	Y-Size	Cylinder Grid Count	Outside Grid Size	Cell Count
D4-M1	480D	480D	18	20D	21730
D5-M1	960D	480D	18	20D	25086

D = cylinder diameter
X-Size = horizontal width of model domain
Y-Size = vertical height of model domain
Cylinder Grid Count = number of grid cells adjacent to cylinder boundary wall
Outside Grid Size = edge length of grid cells along outer model domain boundaries

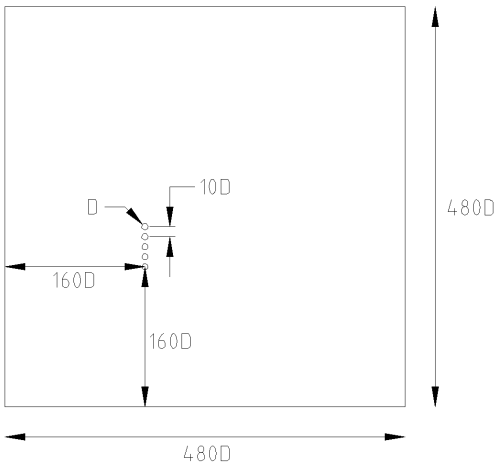

Figure 3.18: Schematic of Domain of D4-M1 for Forced Convection Normal to Array

Results from meshes D4-M1 and D5-M1 were compared to test domain size independence. A single reference case was used for this purpose. The reference case used $0.1mm$ cylinders

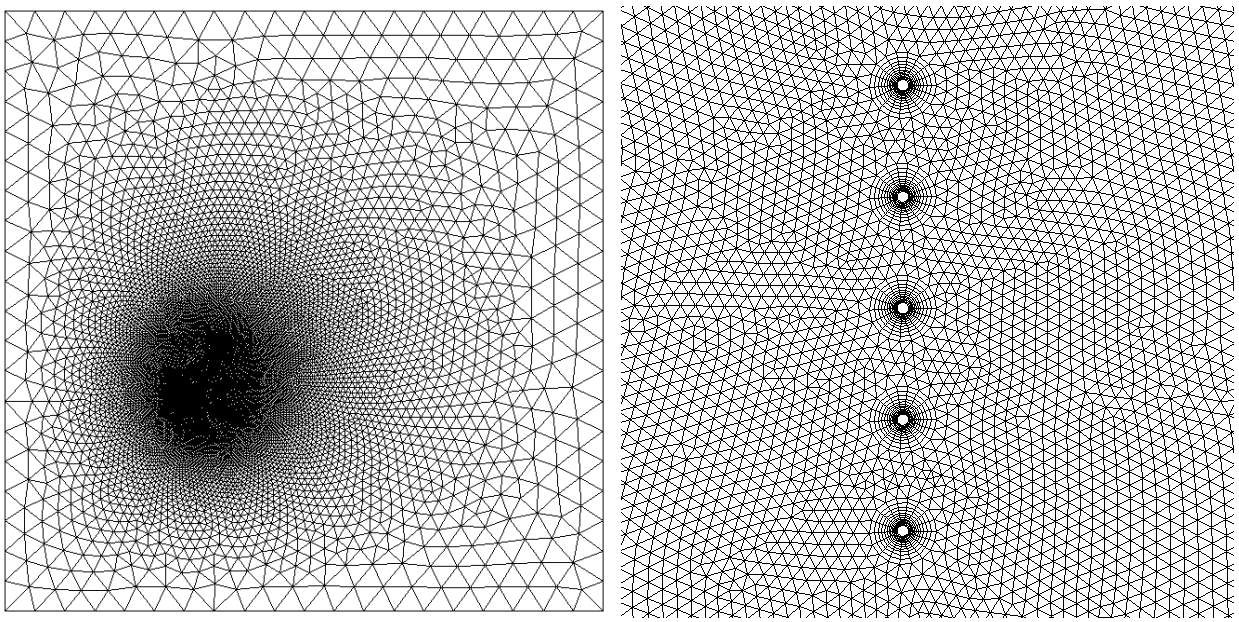

(a) Whole Mesh (b) Close-up of Mesh Near Cylinders

Figure 3.19: Forced Convection Normal to Array, Mesh D4-M1

with surface temperatures 10^oC above ambient. The heat-transfer co-efficients found are given in Table 3.8. As can be seen in Table 3.8, the heat-transfer co-efficients obtained from the two models' results are very similar. To further investigate the similarities of the results, temperature and velocity profiles were also obtained. These profiles are shown graphically in Figures 3.20 through 3.25. The horizontal cross-sections illustrated cut through the centre of the lowest cylinder while the vertical cross-sections cut through the centres of all five of the cylinders. It can be seen in Figures 3.20 to 3.22, that the temperature profiles obtained using the two meshes were very similar. The velocity profiles in Figures 3.23 through 3.25 also show similarity for the most part. The velocity profiles downstream of the cylinders do differ somewhat, with the velocities in model 'D4-M1' being somewhat

higher than those in 'D5-M1'. The discrepencies in the velocity profiles however were not considered to be sufficient to be of concern and mesh 'D4-M1' was used for further models using different temperature differences, fluid velocities and cylinder diameters.

While the results from two different domain sizes were compared, results obtained using different mesh densities were not compared. Rather than retest different grid densities, the grid density that was found to be optimum in the natural convection case was reused for the forced convection case. Further confidence in the accuracy of the models' results can be gained by comparison to previously published correlations. These comparisons are given in the Results section.

Table 3.8: h_c (W/m^2K) Values for Forced Convection Normal to Array

Models	D4-M1	D5-M1
Cylinder 1	234	232
Cylinder 2	231	229
Cylinder 3	231	229
Cylinder 4	231	230
Cylinder 5	235	233

Values are for 0.1mm cylinders
with 0.25 m/s horizontal forced airflow

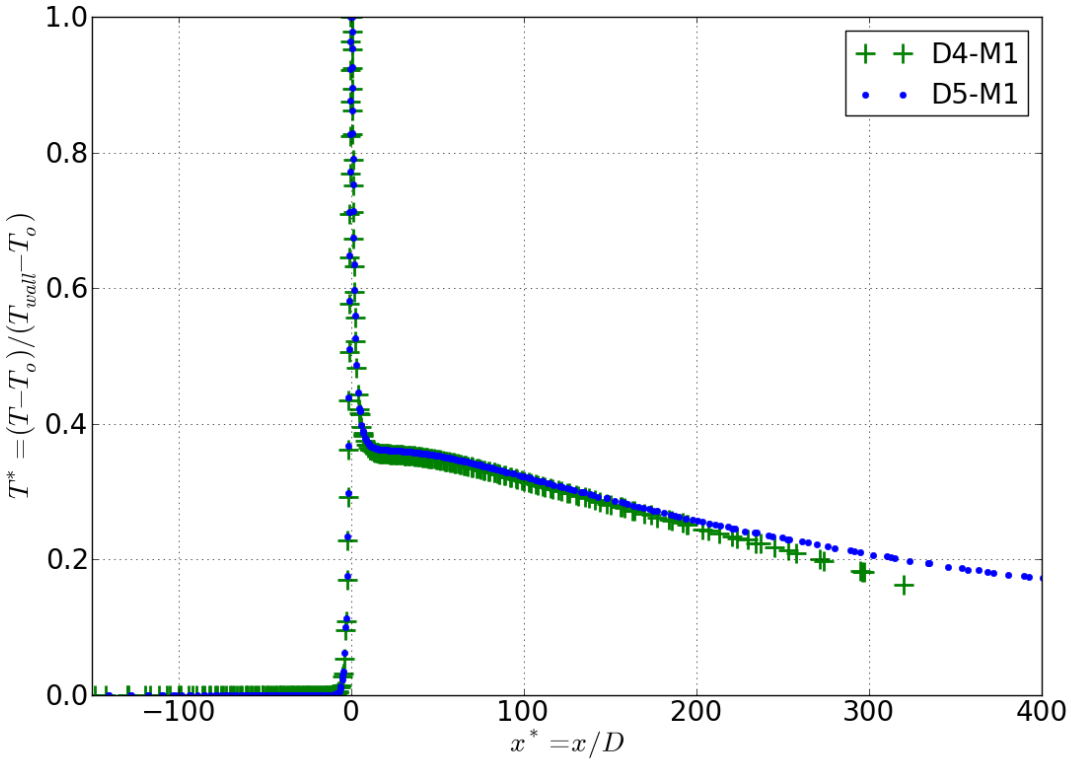

Figure 3.20: Temperature Along Horizontal Cross Section for Forced Convection Normal to Vertical Array of Cylinders, $D = 0.1mm$ & $\Delta T = 10^oC$

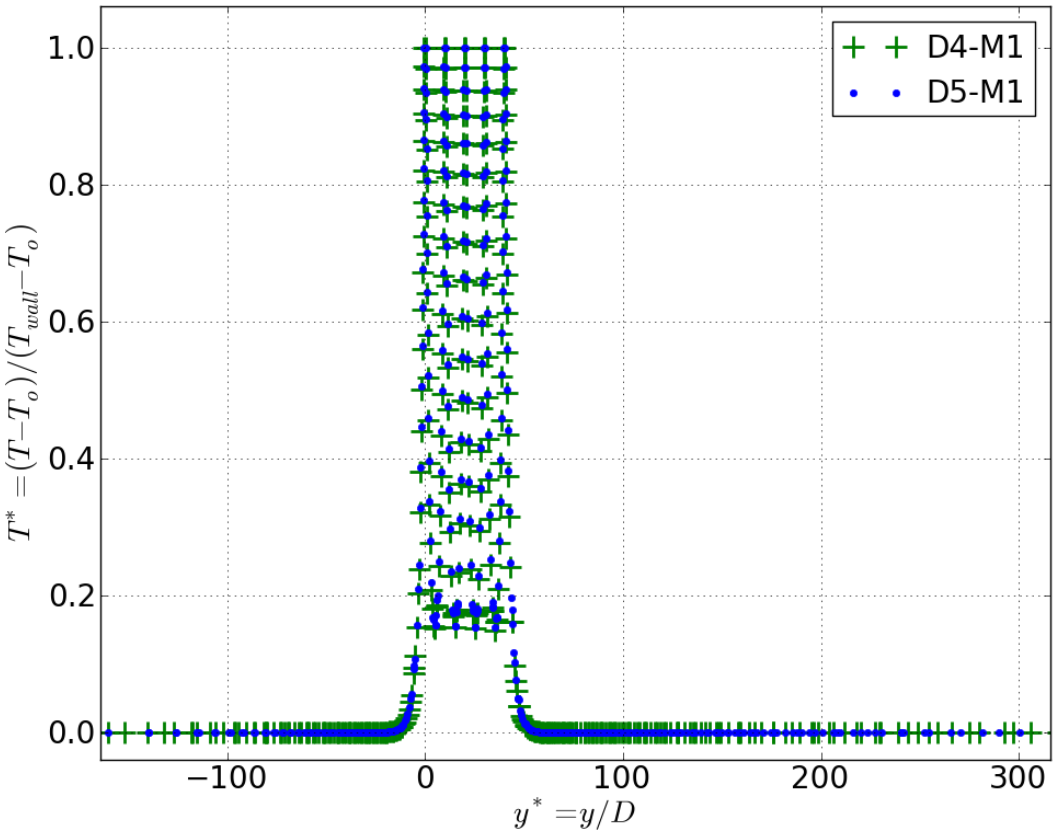

Figure 3.21: Temperature Along Vertical Cross Section for Forced Convection Normal to Vertical Array of Cylinders, $D = 0.1mm$ & $\Delta T = 10^oC$

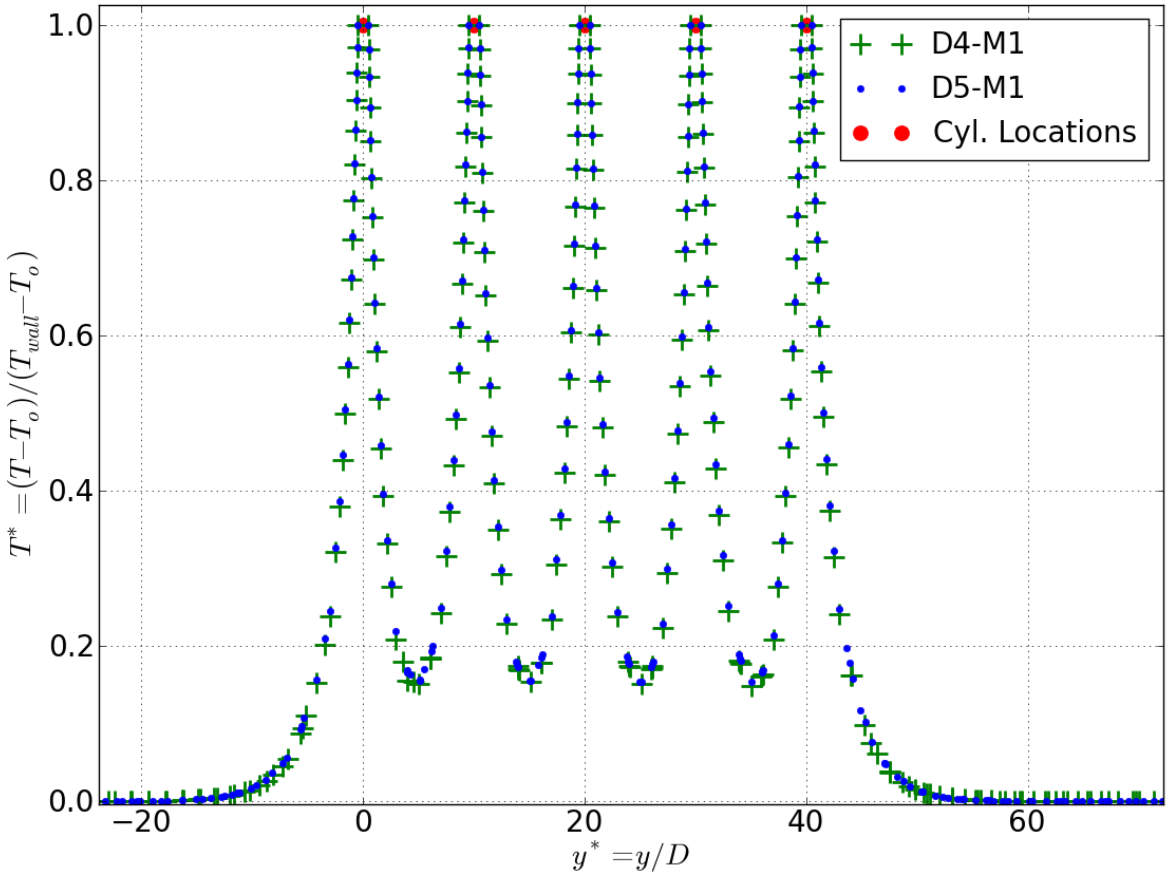

Figure 3.22: Zoomed Plot of Temperature Along Vertical Cross Section for Forced Convection Normal to Vertical Array of Cylinders, $D = 0.1mm$ & $\Delta T = 10^oC$

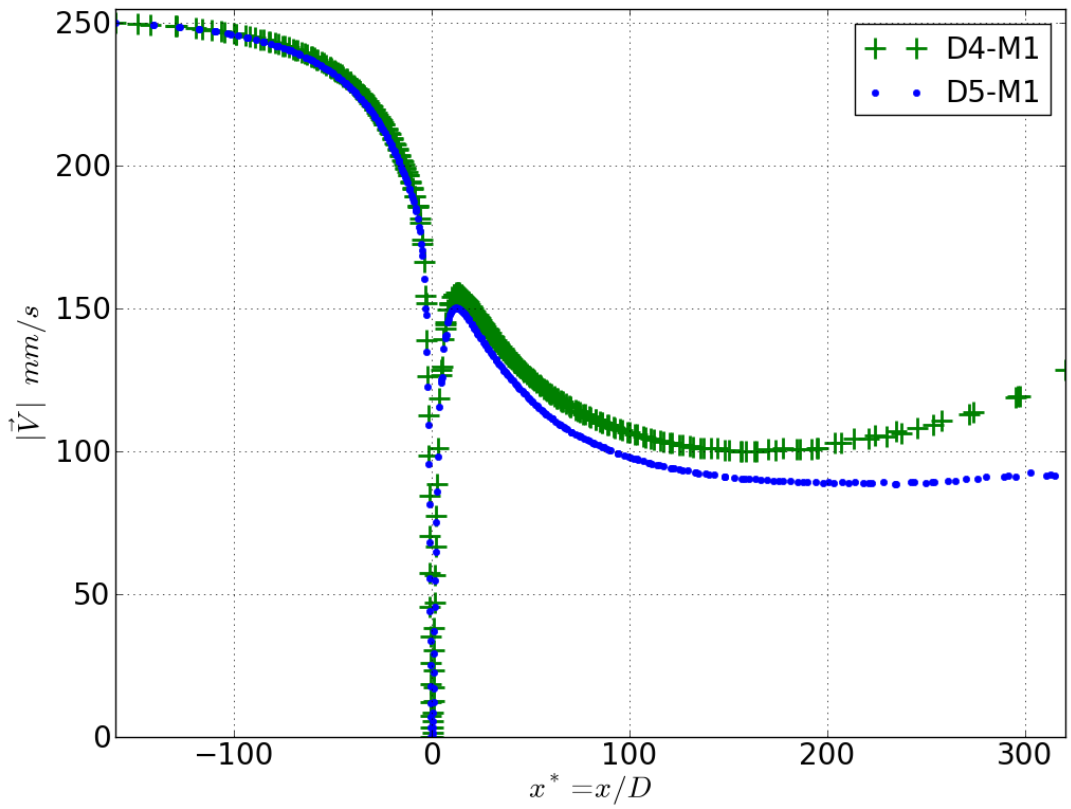

Figure 3.23: Air $|\vec{V}|$ Along Horizontal Cross Section for Forced Convection Normal to Vertical Array of Cylinders, $D = 0.1mm$ & $\Delta T = 10^oC$

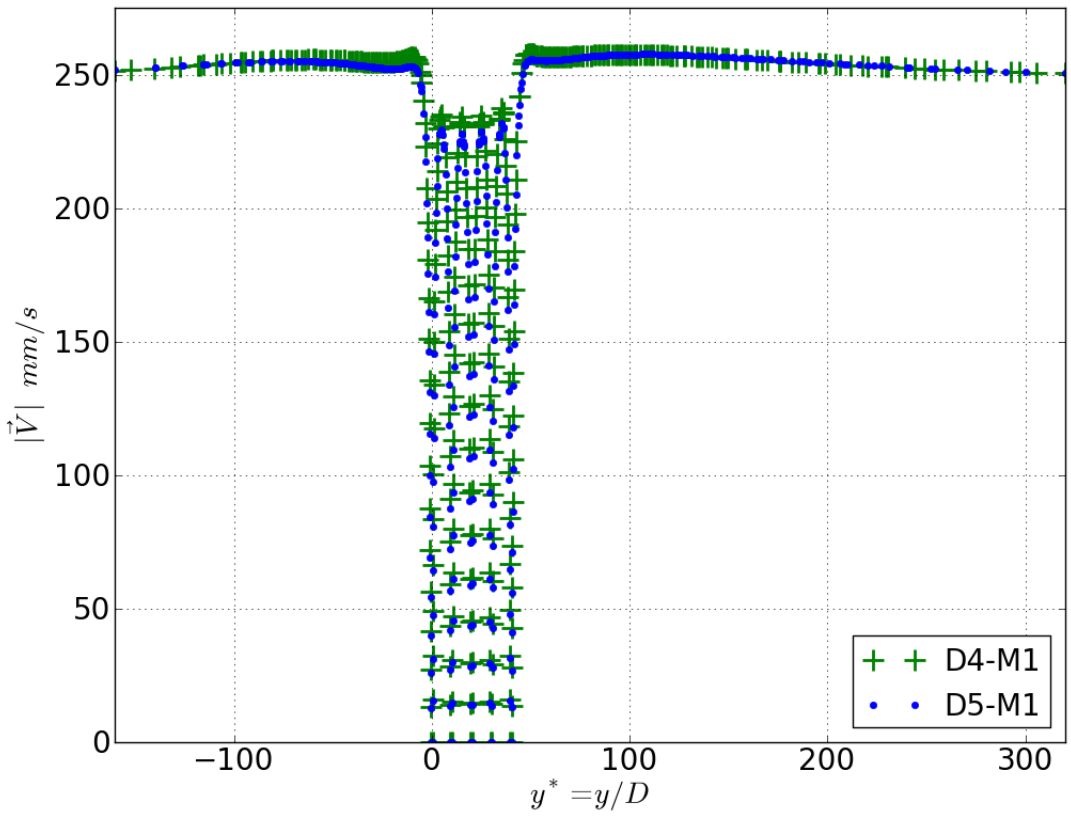

Figure 3.24: Air $|\vec{V}|$ Along Vertical Cross Section for Forced Convection Normal to Vertical Array of Cylinders, $D = 0.1mm$ & $\Delta T = 10^oC$

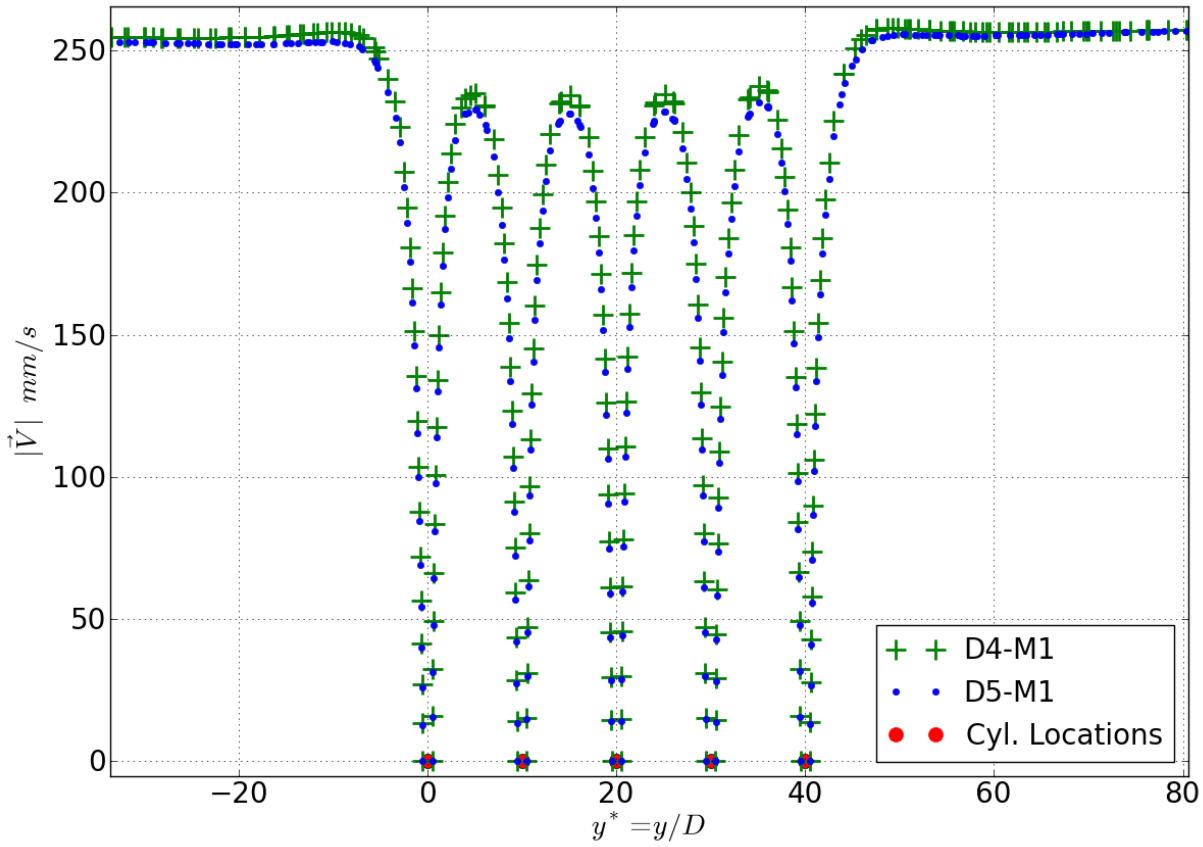

Figure 3.25: Zoomed Plot of Air $|\vec{V}|$ Along Vertical Cross Section for Forced Convection Normal to Vertical Array of Cylinders, $D = 0.1mm$ & $\Delta T = 10^oC$

3.2.2 Forced Convection Normal to Vertical 3-D Screen

The first three-dimensional case for forced convection that was considered was that of forced fluid flow normal to a vertical screen. Symmetry can be used to reduce the size of models for this case as is shown in Figure 3.26. If the screen shown in Figure 3.26a is considered to consist of an infinite array of identical rectangular sections, a single section with symmetrical boundary conditions on four sides can be used as is shown in Figure 3.26b. The geometrical section shown in Figure 3.26b can be further split along a vertical centre mirrorline. If gravity is neglected, a horizontal centre mirrorline can also be used, the result being illustrated in Figure 3.26c. One more symmetrical mirror can be used if, as is the case being considered, the mesh section is square rather than merely rectangular. In this case, the section can be divided along a diagonal from its centre to one corner. The resulting section of the mesh that needs to be modelled is shown in Figure 3.26d.

In selecting the model domain for this case, only the length in the flow direction needed to be chosen as the cross-sectional shape and size was fixed by the screen dimensions. The length of the domain in the flow direction was chosen to be $480 * D$, the same as that used in the two-dimensional case. A schematic of the model domain is given in Figure 3.27.

The screen density γ is defined as the fraction of the cross-sectional area of the screen taken up by the screen filaments. In two-dimensional cases this fraction is simply the ratio of the diameter of the cylindrical screen filaments to the centre-centre spacing of those same filaments. In the three-dimensional models created, this is not the case as the screen is modelled as a rectangular array of intersecting cylinders. For a rectangular array of cylinders, the screen density γ is given by Equation 3.11.

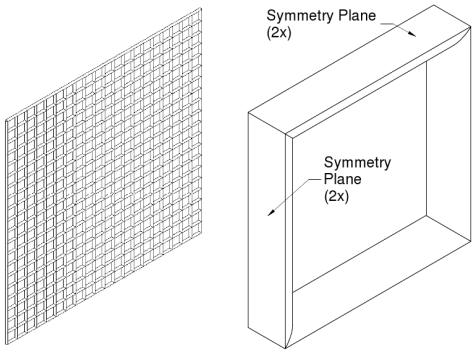

(a) Full Screen (b) Single Section

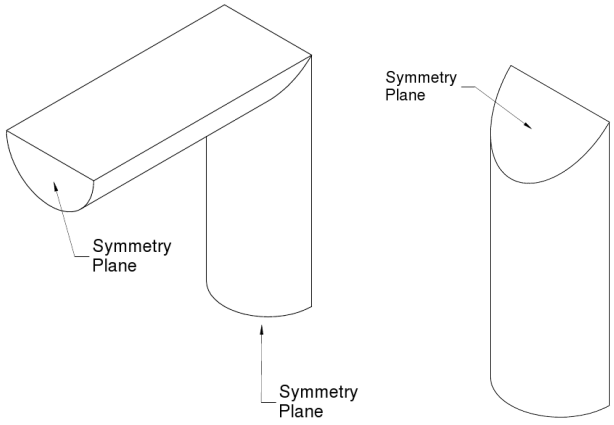

(c) 1/4 Section (d) 1/8 Section

Figure 3.26: Forced Convection Normal to Screen, 3D Model Symmetry

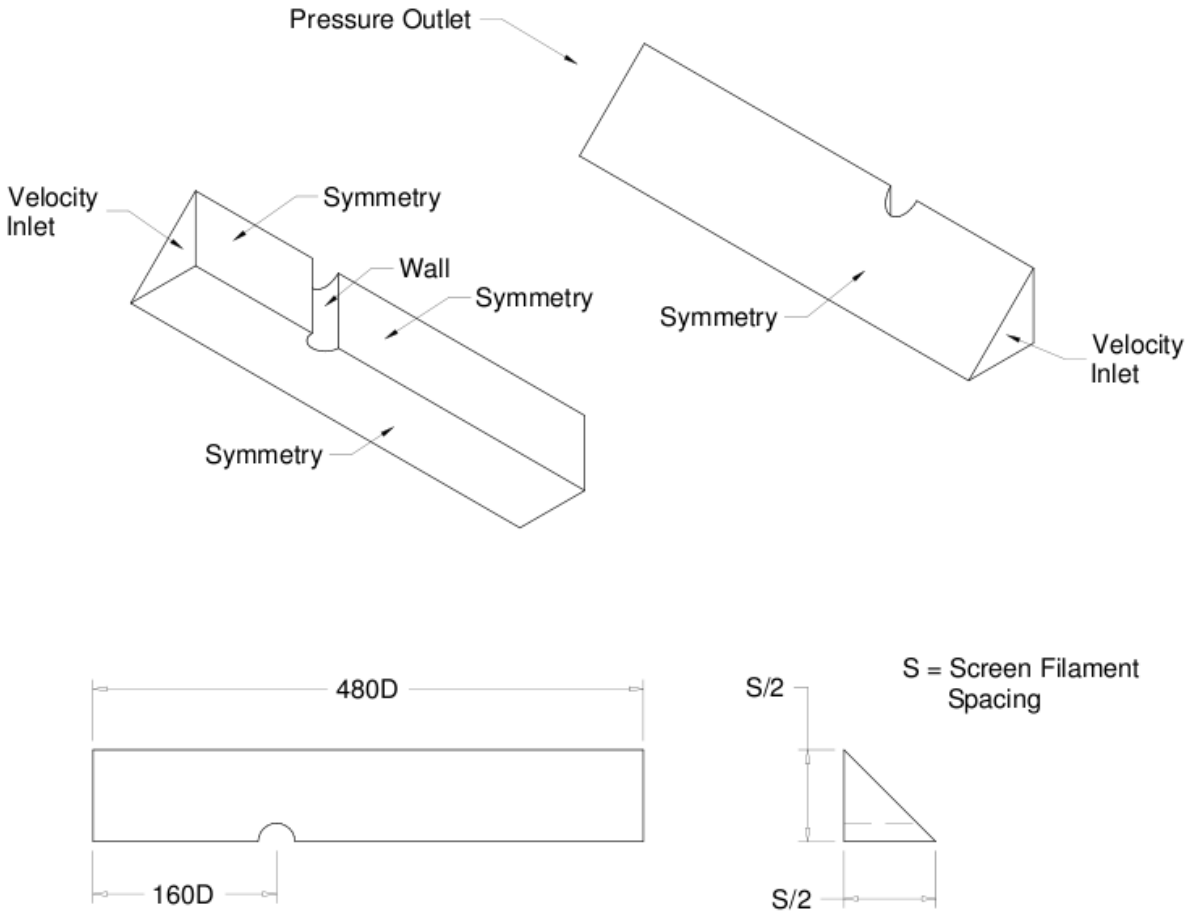

Figure 3.27: 3D Model Domain for Forced Convection Normal to Screen

$$\phi = (1 - 1/s)^2 \tag{3.10}$$

$$\gamma = 1 - (1 - 1/s)^2 \tag{3.11}$$

Where:

$\phi =$ Screen porosity

$\gamma =$ Screen density

$s =$ Filament spacing to diameter ratio

20% Screen Density

The first screen modelled had a mesh filament spacing of $10 * D$. It therefore had a screen porosity of $\gamma = 0.2$ as determined by Equation 3.11.

Two separate meshes were created of the domain illustrated in Figure 3.27. A coarser mesh was created first. For this mesh, dimensions of cells on the screen walls were set at $0.2 * D$. The cell sizing was increased by a factor of 1.2 per cell layer for each layer of cells successively further away from the screen walls. The maximum cell dimension was set to a limit of $2.5 * D$. In order to mesh the domain volume, an unstructured mesh was created using the T-Grid meshing scheme [Gambit 2005]. This meshing scheme created a mesh of mostly tetrahedral cells plus possibly some hexahedral, pyramidal or wedge cells. The total mesh size was 13 098 cells. This mesh was labelled 'D4-M1'

The second, finer mesh created was labelled 'D4-M2'. This mesh was created using the same methodology as mesh 'D4-M1' but with finer parameters. The changed parameters

were as follows: cell dimensions on the screen walls were set at $0.1 * D$, cell dimensions increased by a factor of $1.1/layer$ with distance from the screen walls and the maximum cell dimension was set at $1 * D$. The resulting mesh size was 107 131 cells.

To evaluate the suitability of the meshes, a test case was run using both meshes as well as different convergence criteria. The test case selected used a screen filament with $0.1mm$ diameter and screen surface temperature 10^oC above the ambient fluid along with a $0.25m/s$ forced convection velocity. Gravity was neglected. The results obtained for this case are given in Table 3.9. As can be seen in Table 3.9, the results obtained are in fair agreement. The ratio of the highest/lowest results' values was 1.08. Based on these results mesh 'D4-M1' was chosen for further use. The 'b' set of convergence criteria given in Table 3.9 was used.

Table 3.9: Forced Convection Normal to Screen, 3D Model Grid Comparison, $\gamma = 0.2$

Mesh	Convergence	Q W/m	$h_{c_D} W/(m_2 \cdot K)$
D4-M1	a	$1.59 * 10^{-4}$	217
D4-M1	b	$1.63 * 10^{-4}$	223
D4-M1	c	$1.65 * 10^{-4}$	226
D4-M2	a	$1.53 * 10^{-4}$	209
D4-M2	b	$1.57 * 10^{-4}$	214

Convergence Criteria Residuals
a: Continuity 10^{-3}, X,Y,Z Momentum 10^{-3}, Energy 10^{-6}
b: Continuity 10^{-4}, X,Y,Z Momentum 10^{-4}, Energy 10^{-7}
c: Continuity 10^{-5}, X,Y,Z Momentum 10^{-5}, Energy 10^{-7}

75% Screen Density

The $\gamma = 0.2$ model domain discussed above was modified to simulate screens with different densities. Only the filament spacing, dimension 's' as shown in Figure 3.27, needed to be changed to change the screen porosity being simulated. For a screen of with a density of $\gamma = 0.75$, $s = 2$ as determined by Equation 3.11

As the domain size used for this model was much smaller than that used for the 20% density model, a grid independence study was completed. Two meshes were created for the model. These two meshes were created using the same procedure used for the $\gamma = 0.2$ case. However, due to the much smaller domain size, different parameters were used. The finer mesh, labelled 'D4-M2', was created using the following parameters: cell dimensions on the screen walls were set at $0.1 * D$, cell dimensions increased by a factor of $1.1/layer$ with distance from the screen walls and the maximum cell dimension set at $1 * D$. The resulting mesh had 35 871 cells. The second, coarser mesh labelled 'D4-M3' was created using the following parameters: cell dimensions on the screen walls were set at $0.05 * D$, cell dimensions increased by a factor of $1.1/layer$ with distance from the screen walls and the maximum cell dimension was set at $0.5 * D$. The resulting mesh has 8 133 cells. A test case was used to compare these two meshes. The test case used a filament diameter of $0.1mm$, a forced convection velocity of $0.25m/s$ and a screen wall temperature of 10^oC above ambient. Results obtained using both meshes for this test case are given in Table 3.10. The results given in Table 3.10 show close agreement between the two meshes. As a result, the coarser mesh, mesh 'D4-M2' was used for further modelling. Furthermore, as

differing convergence criteria did not appear to affect the results, the milder convergence criteria listed as criteria set 'a' in Table 3.10 were considered adequate.

Table 3.10: Forced Convection Normal to Screen, 3D Model Grid Comparison for $\gamma = 0.75$ Screen

Mesh	Convergence	Q W/m	$h_{c_D} W/(m_2 \cdot K)$
D4-M2	a	$1.41 * 10^{-5}$	132
D4-M2	b	$1.42 * 10^{-5}$	132
D4-M3	a	$1.43 * 10^{-5}$	133

Convergence Criteria Residuals
a: Continuity 10^{-3}, X,Y,Z Momentum 10^{-3}, Energy 10^{-6}
b: Continuity 10^{-4}, X,Y,Z Momentum 10^{-4}, Energy 10^{-7}

3.2.3 Forced Convection Inline with Vertical Array of Cylinders

The next case to be modelled was that of forced convection with the flow direction parallel to the array of horizontal cylinders. In this case, the forced convection can either supplement or counteract the effects of natural convection depending on the direction of the flow relative to gravity. Only the complementary case was investigated. Since heated cylinders were modelled, an upwards forced convection flow direction was used to generate complementary natural/forced convection.

Two different screen densities were tested for this case. The first screen density used was $\gamma = 10\%$ (i.e. cylinder centre-centre spacing of $10 * D$), the same density as was used for the horizontal flow models. The second screen density investigated was $\gamma = 50\%$, corresponding to a cylinder centre to centre spacing of $2 * D$.

10% Screen Density Case

The model domain used to simulate a screen with $\gamma = 0.1$ is illustrated in Figure 3.28. The mesh created for this model is similar to that used for the horizontal forced convection model D4-M1. The main difference is in the domain dimensions and location of the screen cylinders. The domain dimensions used for the vertical flow were rotated 90^o compared to those used for the horizontal convection case. Thus, the larger dimension of the domain was in the direction of the flow so that a larger section of the flowstream passing by the cylinders was captured by the model. Two different domain sizes were tested. Table 3.11 gives the dimensions and grid parameters used, while Figure 3.28 illustrates the geometry of the domain for mesh 'D4-M1'. Due to the similarities of this model and the horizontal forced convection case, a grid density study was not completed. The values for the heat-transfer coefficients found using each mesh to model a single test case are given in Table 3.12. As can be seen in Table 3.12, the results obtained using the two meshes are similar. As such, the mesh with the smaller domain, mesh 'D4-M1', was selected for further use.

Table 3.11: Meshes Used For Vertical Forced Convection Past a Vertical Array of Cylinders, $\gamma = 0.1$

Model #	X-Size	Y-Size	Cylinder Grid Count	Outside Grid Size	Cell Count
D4-M1	320D	520D	18	20D	24464
D5-M1	320D	840D	18	20D	28000

D = cylinder diameter
X-Size = horizontal width of model domain
Y-Size = vertical height of model domain
Cylinder Grid Count = number of grid cells adjacent to cylinder boundary wall
Outside Grid Size = edge length of grid cells along outer model domain boundaries

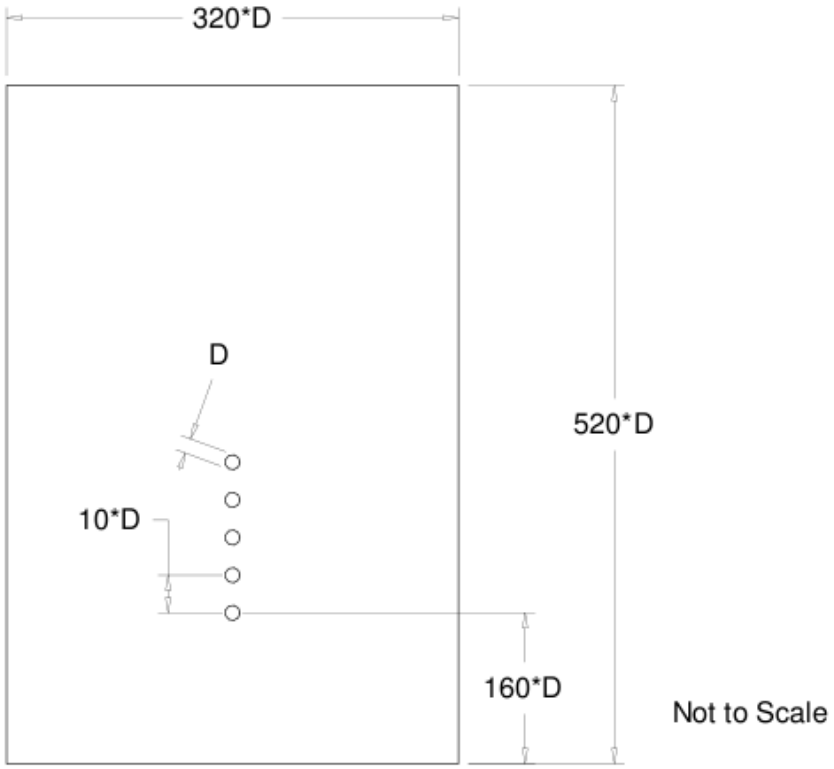

Figure 3.28: Schematic of Domain of D4-M1 for Vertical Forced Convection, $\gamma = 0.1$

Table 3.12: h_c (W/m^2) Values for Vertical Forced Convection Past a Vertical Array of Cylinders, $\gamma = 0.1$

Models	D4-M1	D5-M1
Cylinder 1	225	226
Cylinder 2	147	147
Cylinder 3	117	117
Cylinder 4	99	100
Cylinder 5	91	92

Values are for 0.1mm cylinders with 0.25 m/s horizontal forced airflow. Cylinders are numbered starting at the bottom of the array.

50% Screen Density Case

The model domain used to model the screen with $\gamma = 0.5$ is shown in Figure 3.29. Due to the closer spacing of the cylinders, an array of 5 cylinders would only represent a screen with a height of '$9 * filament\ diameter$' compared to '$41 * filament\ diameter$' for the $\gamma = 0.1$ screen. To partially compensate for this, the number of cylinders used in the model was increased to 20. A completely different mesh structure was required for this model since the structured mesh surrounding the cylinders illustrated in Figure 3.19 would interfere with the adjacent cylinders' meshes due to the closer cylinder spacing. As a result, a wholly unstructured mesh was used.

Two unstructured meshes were tested with different mesh densities. Both of the meshes created used the same domain; this domain is illustrated in Figure 3.29. The coarser mesh created was labelled 'D4-M1'. In order to resolve detail close to the cylinders without using an excessive number of grid cells, a gradated mesh was used. For mesh 'D4-M1', grid cell lengths on the cylinders' surfaces were set at $0.2 * D$ where D is the cylinder diameter. The cell size was then increased with distance away from the cylinders by a factor of 1.2 for each successively adjacent grid cell. The maximum grid cell length was set at $10 * D$. The total grid cell count for mesh 'D4-M1' was 10 404; the mesh itself is shown in Figure 3.30. The finer mesh created was labelled 'D4-M2'. This mesh was created using the same process as mesh 'D4-M1' but with modified parameters. The cell lengths on the cylinders' surfaces were set at $0.1 * D$. The rate of growth of cell size with distance away from the cylinders was set at a factor of 1.1 per cell layer while the maximum cell size was maintained at

$10 * D$. The resulting total cell count was 27 058. Mesh 'D4-M2' is shown in Figure 3.31. Table 3.13 lists the parameters of these two meshes.

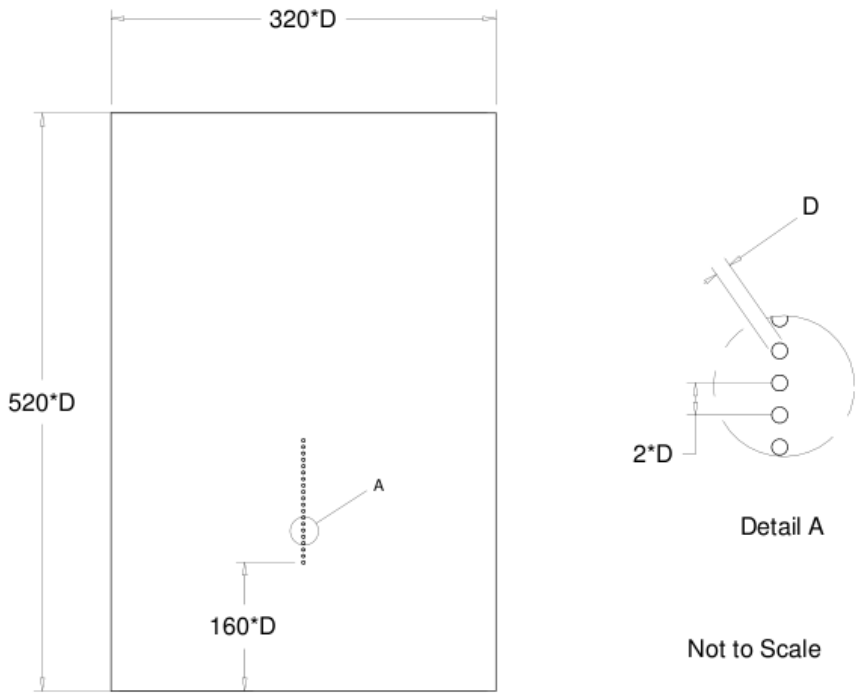

Figure 3.29: Schematic of Domain of D4-M2 for Vertical Forced Convection, $\gamma = 0.5$

Initially, both meshes were used for the case of $0.1mm$ cylinders with a forced convection velocity of $0.25m/s$. The resulting heat transfer co-efficients for selected cylinders in the array are given in Table 3.14. Temperature and velocity profiles obtained using the two meshes are also given in Figures 3.32 through 3.36.

It can be seen in Figures 3.32 and 3.35 that the horizontal temperature profiles plotted are similar for the two meshes used. These profiles were taken as a horizontal slice through

Table 3.13: Meshes Used For Vertical Forced Convection Past Vertical Cylinder Array, $\gamma = 0.5$

Model #	X-Size	Y-Size	Cylinder Grid Size	Outside Grid Size	Cell Count
D4-M1	320D	520D	0.2D	10D	10 404
D4-M2	320D	520D	0.1D	10D	27 058

D = cylinder diameter
X-Size = horizontal width of model domain
Y-Size = vertical height of model domain
Cylinder Grid Count = number of grid cells adjacent to cylinder boundary wall
Outside Grid Size = edge length of grid cells along outer model domain boundaries

Table 3.14: h_c Values (W/m^2) for Vertical Forced Convection Past a Vertical Array of Cylinders, $\gamma = 0.5$

Models	D4-M1	D4-M2
Cylinder 1	166	149
Cylinder 5	36	29
Cylinder 10	26	21
Cylinder 15	22	17
Cylinder 20	41	40

Values are for 0.1mm cylinders with 0.25 m/s horizontal forced airflow. Cylinders are numbered starting at the bottom of the array.

the centre of the lowest cylinder in the array. However the vertical cross-sections (Figures 3.33, 3.34, 3.36 and 3.37) taken through the centre of all the cylinders in the array, show differences. It does not appear that mesh 'D4-M1' has enough grid cells to resolve the detail between the closely spaced cylinders. In addition, the downstream velocities from mesh 'D4-M1' are larger than those from 'D4-M2'. The heat-transfer co-efficients given in Table 3.14 show moderate agreement with the differences between corresponding values ranging from 2% to 20%. A higher degree of grid independence would be preferred. However due to

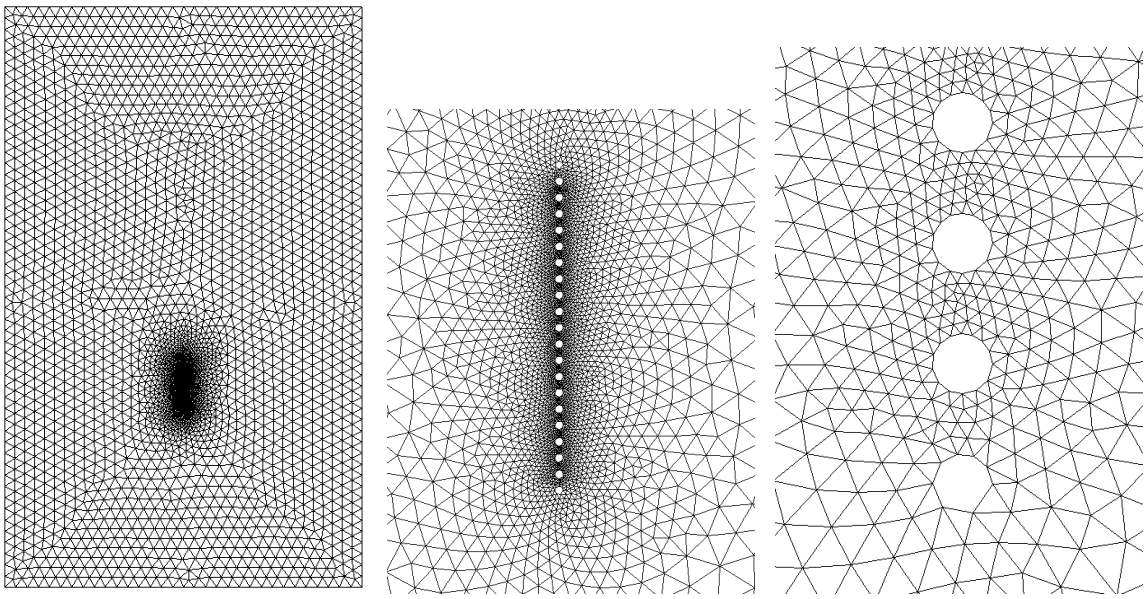

(a) Full Domain (b) Centre of Domain (c) Cylinder Close-up

Figure 3.30: Vertical Forced Convection, $\gamma = 0.5$, Mesh 'D4-M1'

difficulties in getting convergence from meshes using a greater mesh density, mesh 'D4-M2' was chosen for further use. The accuracy of these results needs to be considered with a view to the lower degree of grid-independence found.

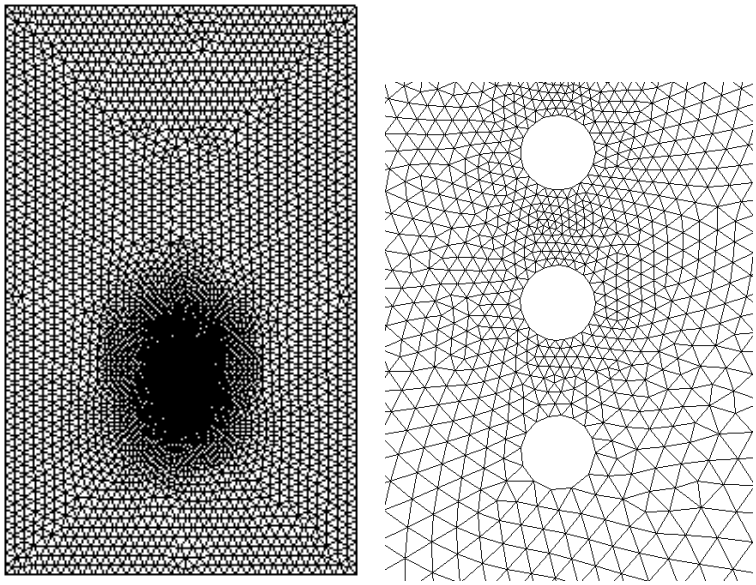

(a) Full Domain (b) Cylinder Close-up

Figure 3.31: Vertical Forced Convection, $\gamma = 0.5$, Mesh 'D4-M2'

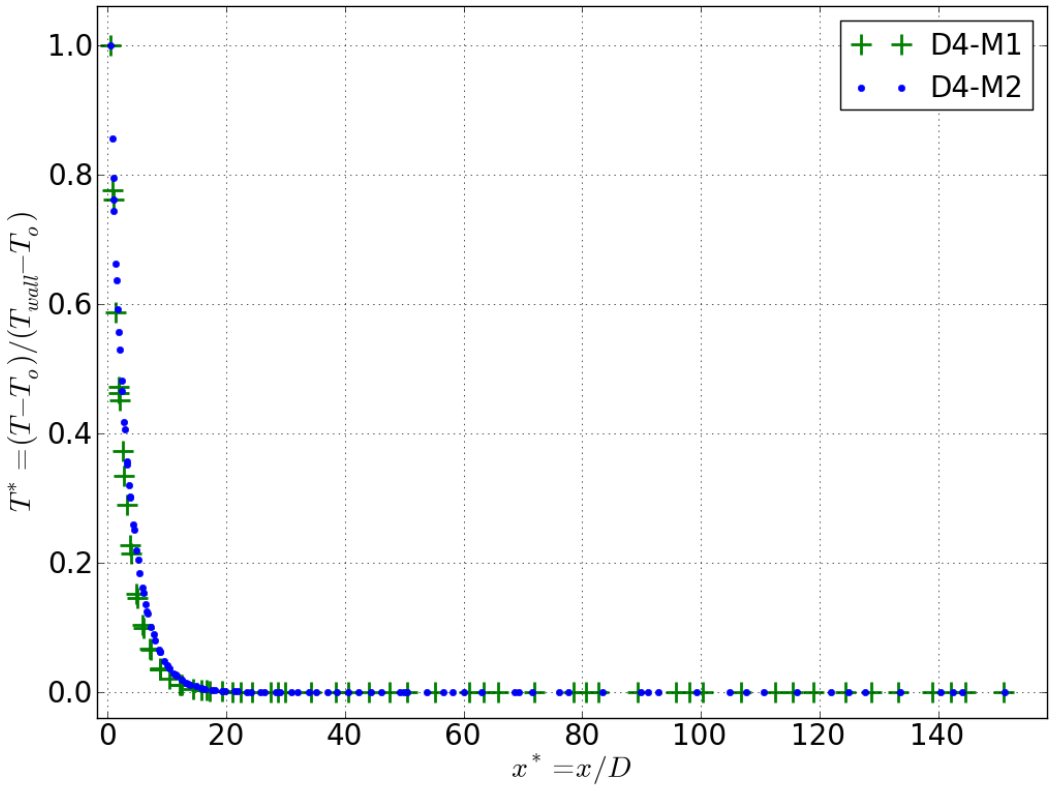

Figure 3.32: Temperature Along Horizontal Cross Section for Vertical Forced Convection $\gamma = 0.5$ Model

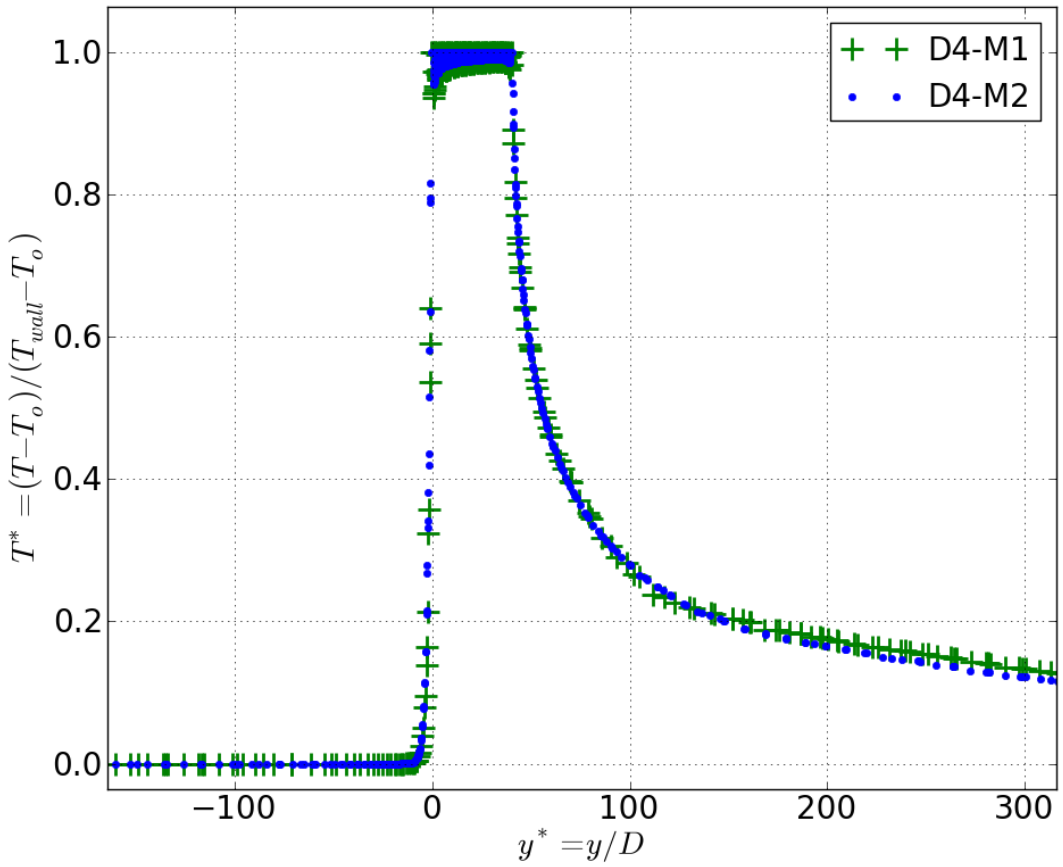

Figure 3.33: Temperature Along Vertical Cross Section for Vertical Forced Convection $\gamma = 0.5$ Model

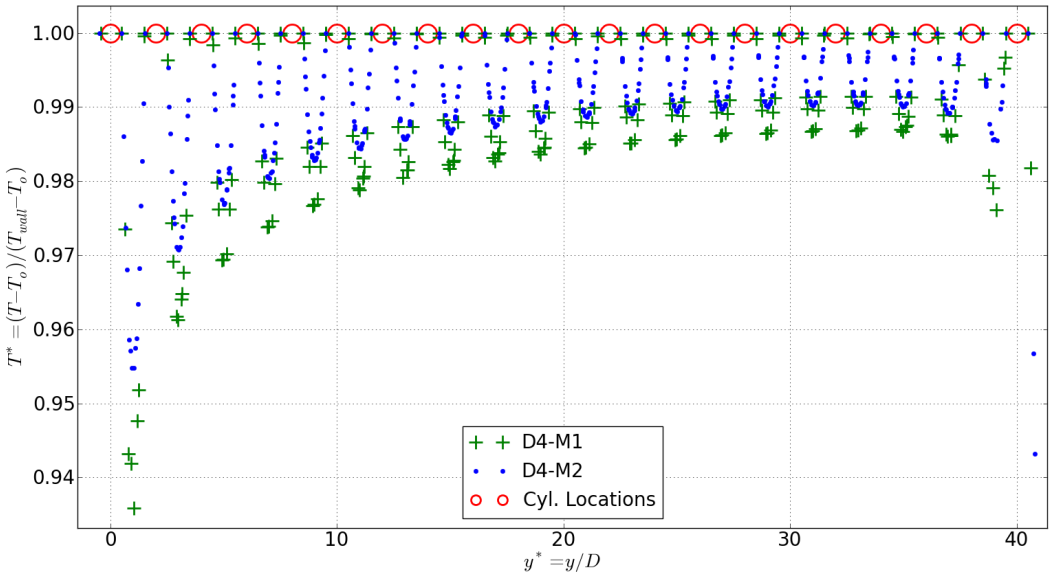

(a)

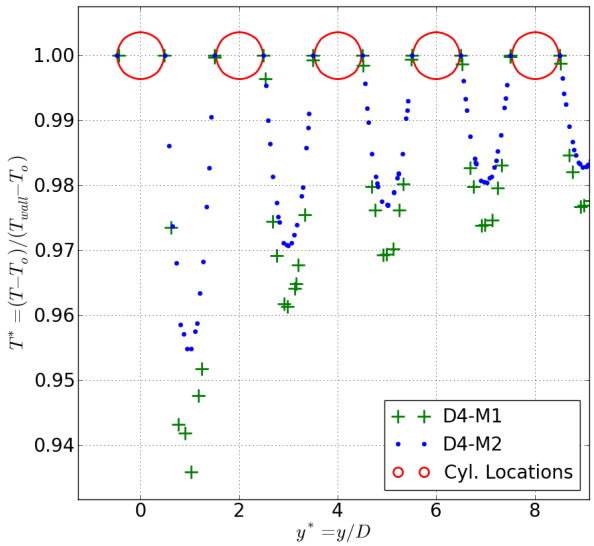

(b)

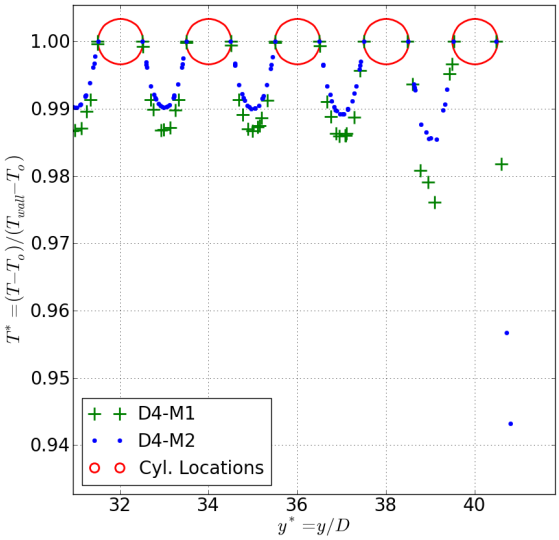

(c)

Figure 3.34: Close-up Views of Temperature Along Vertical Cross Section for Vertical Forced Convection, $\gamma = 0.5$ Model

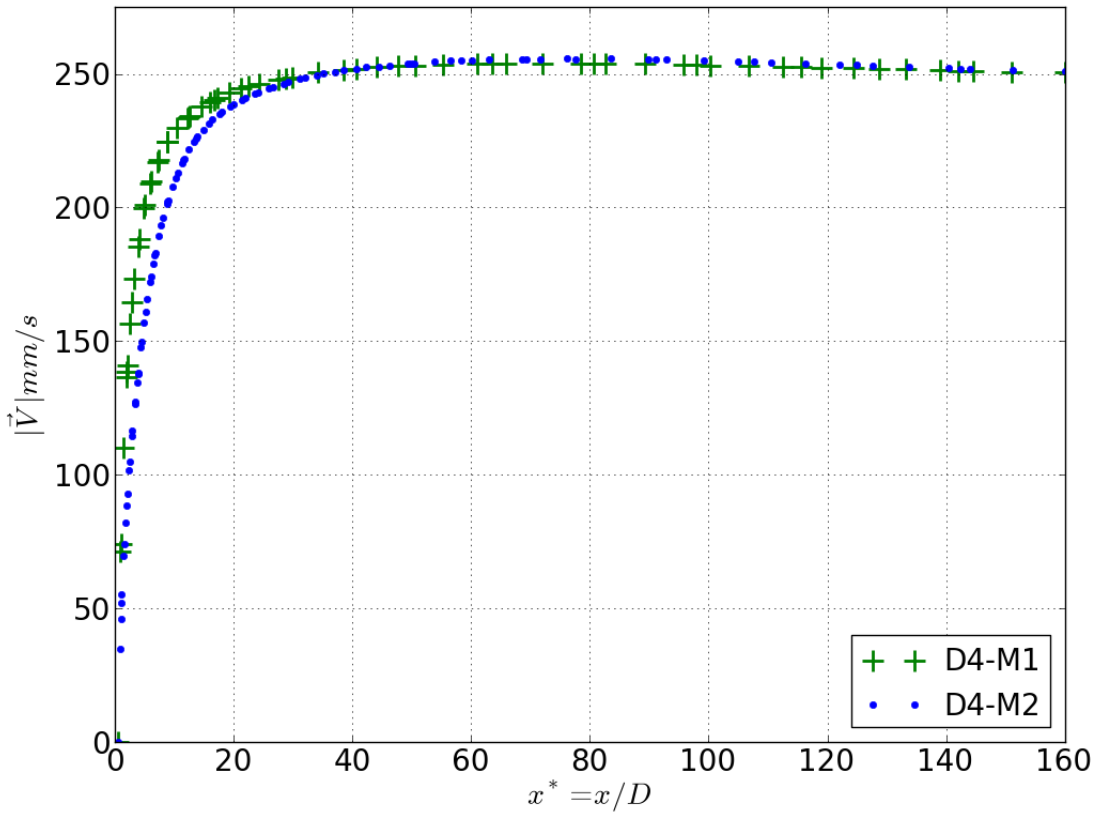

Figure 3.35: Fluid $|\vec{V}|$ Along Horizontal Cross Section for Vertical Forced Convection, $\gamma = 0.5$ Model

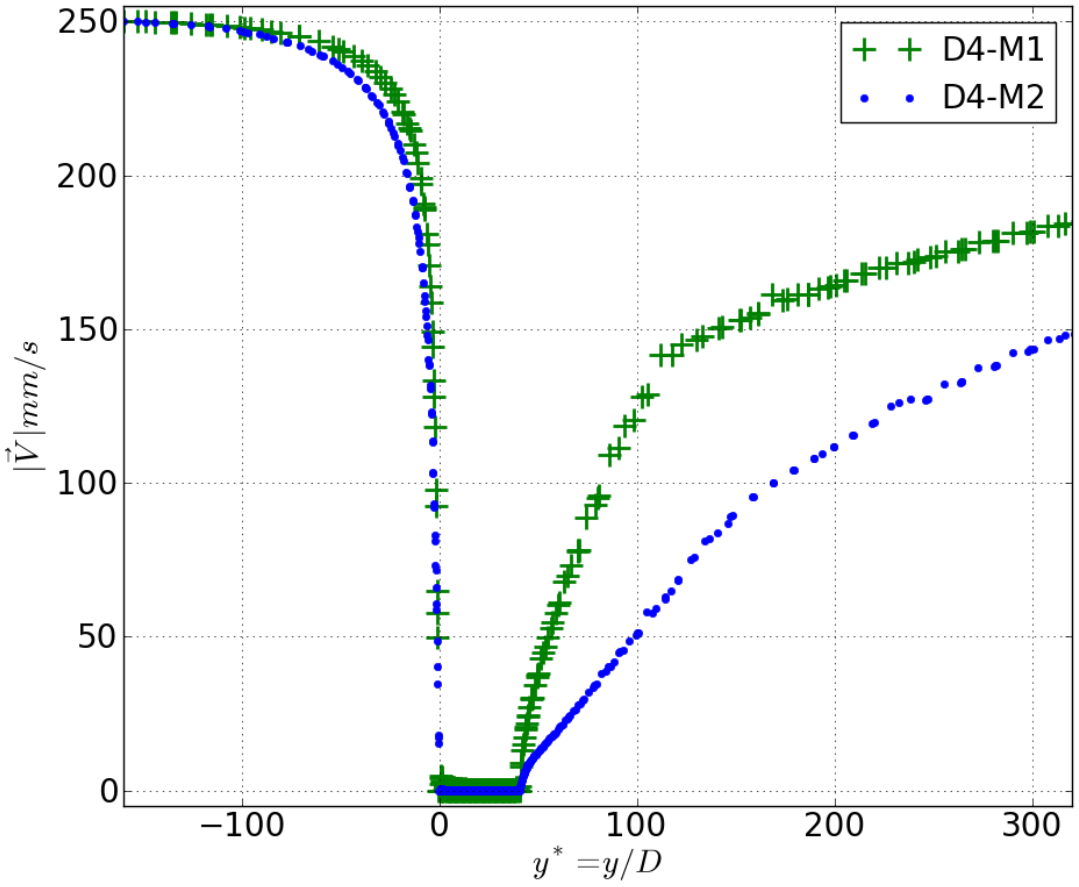

Figure 3.36: Fluid $|\vec{V}|$ Along Vertical Cross Section for Vertical Forced Convection, $\gamma = 0.5$ Model

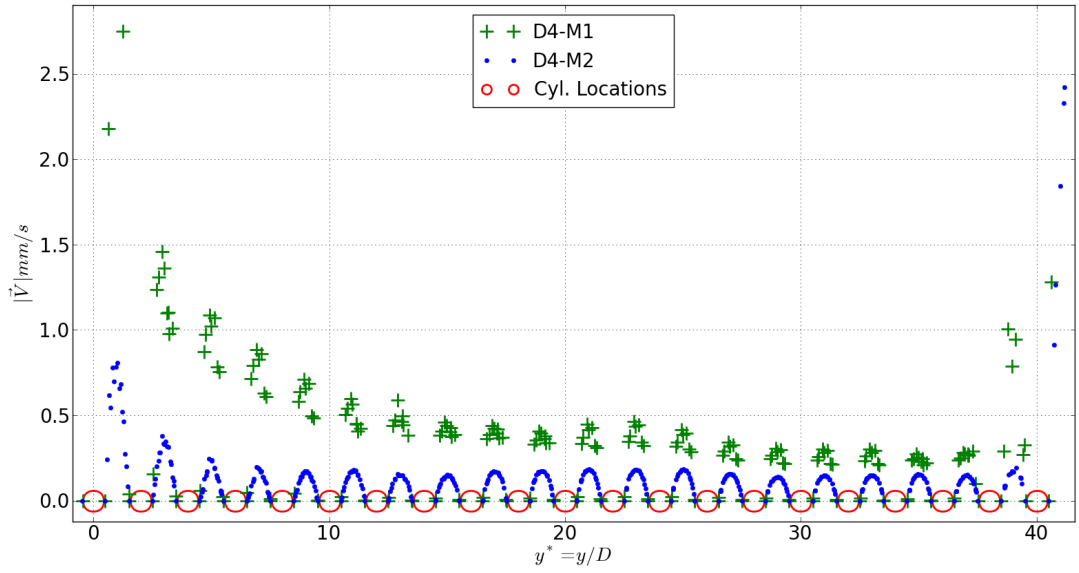

(a)

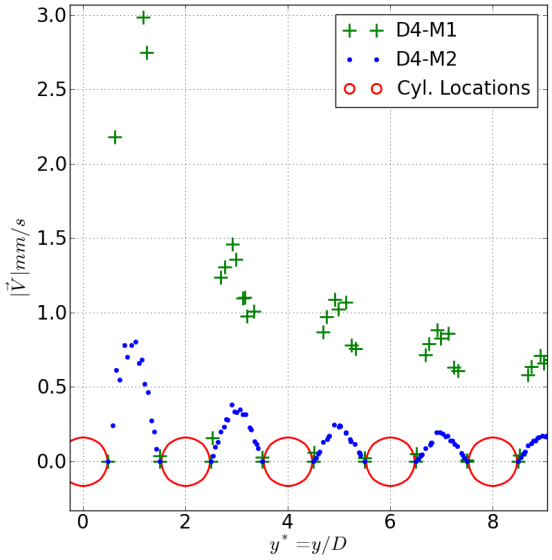

(b)

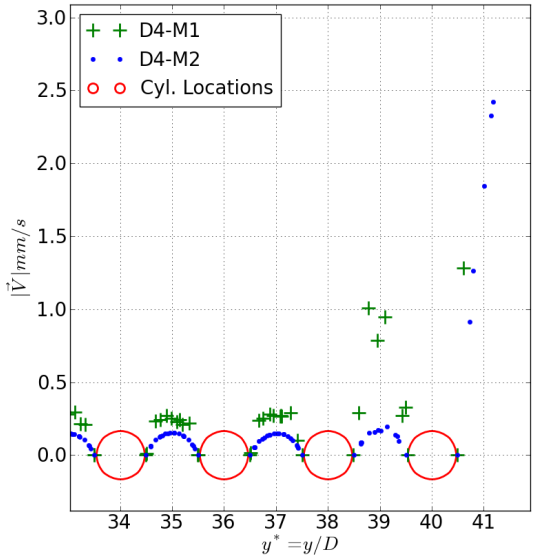

(c)

Figure 3.37: Close-up Views of Fluid $|\vec{V}|$ Along Vertical Cross Section for Vertical Forced Convection, $\gamma = 0.5$ Model

3.2.4 Forced Convection Inline With Vertical 3-D Screen

The next three-dimensional case that was considered was forced convection parallel to an insect screen. Less symmetry is available to reduce the domain size for this case than for that of horizontal forced convection. The screen filament spacing is considered to be small compared to the size of the screen. Thus, due to symmetry, a single vertical section with a width equal to the filament spacing can be used to model the screen. Symmetry also indicates that a vertical mirror plane through the centre of this section can be used to further reduce the domain in half. The symmetry used and the resulting portion of the screen are illustrated in Figure 3.38. Note that the direction of the forced convection prevents the use of horizontal planes of symmetry. However the fine screen filament spacing would require an excessively large model domain to model the flow over the entire height of the screen. As such, a section of the screen with five horizontal filaments was used to gain some information on the nature of heat transfer from the screen. Figure 3.39 gives a schematic diagram of the domain used to model this case. The frustums at the top and bottom of the screen segment were added to reduce artificial end effects that could occur if a blunt end was added to the screen section modelled. The overall height and width of the domain were chosen to be $520 * D$ and $320 * D$ respectively. These were chosen to be the same as what was found to be sufficient for the two-dimensional case. The thickness of the domain is determined by the screen filament spacing. A screen filament spacing of $10 * D$ was chosen and thus the thickness of the domain was set at $5 * D$, half the screen filament spacing. Changing the screen filament spacing requires the use of different domain sizes and only the single case of $\gamma = 0.19, s = 10 * D$ was modelled.

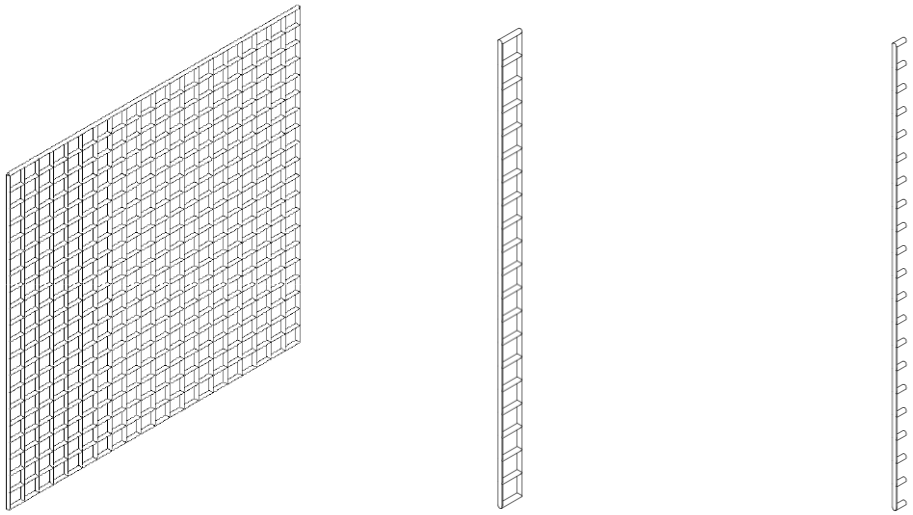

(a) Full Screen (b) Single Section Vertical Slice (c) Half-Section Vertical Slice

Figure 3.38: 3D Screen Model Symmetry For Vertical Forced Convection

While the domain size was chosen based on studies done in two dimensions, different mesh densities were tested to test for grid density independence. For the coarser mesh, which was labelled 'D4-M1', the dimensions of grid cells along the screen filament walls were set at a size of $0.2 * D$. The cell sizes were increased by a factor of 1.2 per cell layer for each layer of cells successively further away from the screen walls. The maximum cell dimension was limited to $2.5 * D$. The domain volume was meshed using the T-Grid meshing scheme [Gambit 2005]. This meshing scheme created an unstructured mesh of mostly tetrahedral cells plus possibly some hexahedral, pyramidal or wedge cells. The resulting mesh size was 306 290 cells.

A second, finer mesh was created and labelled 'D4-M2'. This mesh was created in the same way but with finer parameters. These parameters are as follows: cell dimensions on

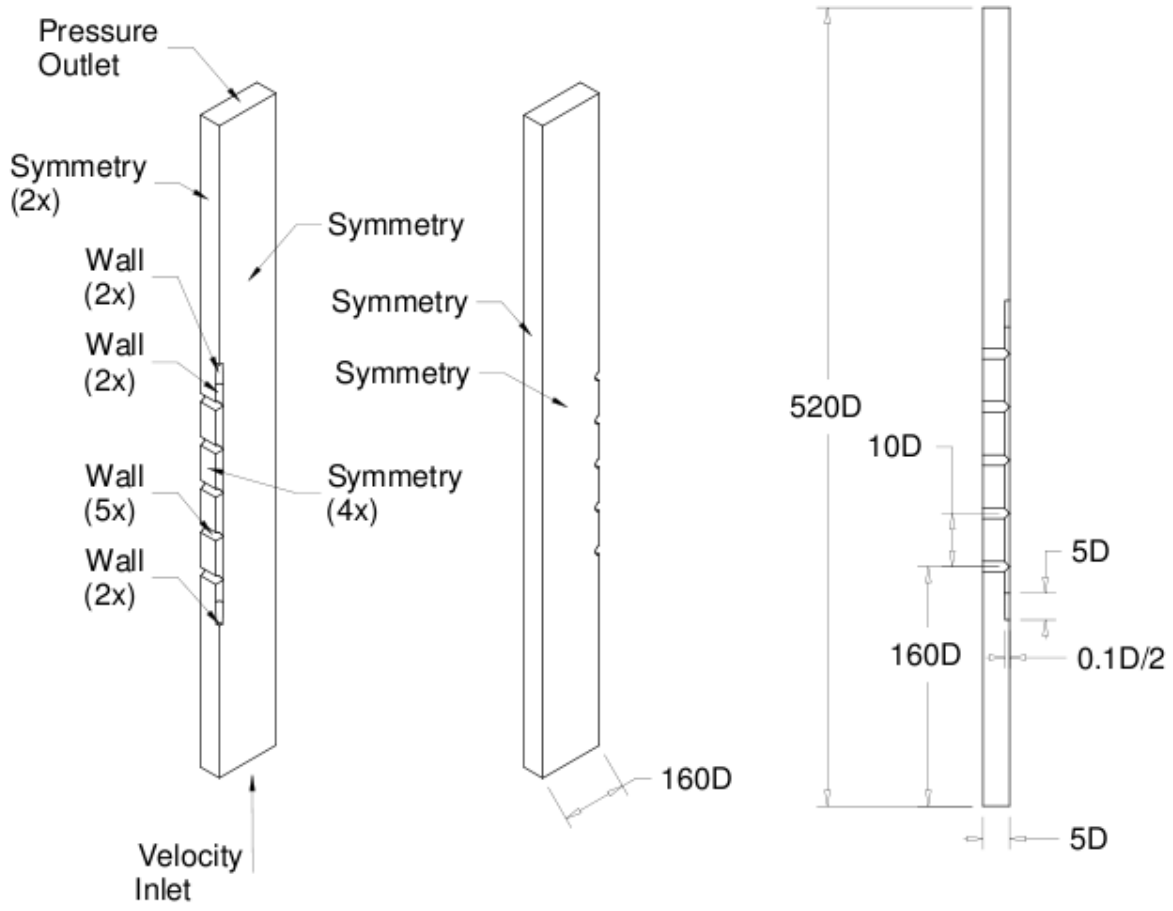

Figure 3.39: 3D Model Domain for Forced Convection Inline With Screen

the screen walls were set at $0.1 * D$, cell dimensions increased by a factor of $1.2/layer$ with distance from the screen walls and the maximum cell dimension was set at $1 * D$. The resulting mesh size was 502 874 cells.

The above two meshes were compared by using them both to separately model a single test case. The chosen test case was for a screen with $0.1mm$ diameter filaments, a 10^oC temperature difference between the screen filament walls and the ambient fluid

and a forced convection velocity of $0.25m/s$. The results obtained are given in both Table 3.15 and Figure 3.40. In Figure 3.40, Nu_L and Ra_L are defined as $Nu_L = h_c * L/k$ and $Ra_L = Pr * g\beta\Delta TL^3/(\nu^2)$ where L is defined as follows:

For Vertical Cylinders;

L = Distance from bottom of lowest vertical cylinder to vertical midpoint on cylinder

For Horizontal Cylinders;

L = Distance from bottom of lowest vertical cylinder to cylinder centreline

Table 3.15: 3-D Vertical Convection Grid Comparison for $\gamma = 0.19$ Screen

Mesh	Convergence	$Q\ W/m$			$h_cW/(m_2 \cdot K)$		
		Horizontal	Vertical	Overall	Horizontal	Vertical	Overall
D4-M1	a	$1.83 * 10^{-4}$	$1.53 * 10^{-4}$	$3.36 * 10^{-4}$	50.1	46.5	48.4
D4-M1	b	$3.17 * 10^{-4}$	$2.48 * 10^{-4}$	$5.65 * 10^{-4}$	86.7	75.3	81.3
D4-M1	c	$3.36 * 10^{-4}$	$2.63 * 10^{-4}$	$5.98 * 10^{-4}$	91.8	79.8	86.2
D4-M2	a	$1.79 * 10^{-4}$	$1.51 * 10^{-4}$	$3.30 * 10^{-4}$	48.9	45.6	47.3
D4-M2	b	$3.05 * 10^{-4}$	$2.39 * 10^{-4}$	$5.44 * 10^{-4}$	83.0	72.4	78.0

Convergence Criteria Residuals

a: Continuity 10^{-3}, X,Y,Z Momentum 10^{-3}, Energy 10^{-6}

b: Continuity 10^{-4}, X,Y,Z Momentum 10^{-4}, Energy 10^{-7}

c: Continuity 10^{-5}, X,Y,Z Momentum 10^{-5}, Energy $5 \cdot 10^{-8}$

It can be seen from the results given in Table 3.15 and Figure 3.40 that mesh 'D4-M1' gives different results for the 'a' convergence criteria than for the 'b' and 'c' criteria. The results obtained using the 'b' and 'c' criteria are similar. Furthermore, the results obtained with mesh 'D4-M1' with convergence criteria 'b' and 'c' are similar to those obtained using

mesh ‘D4-M2’ with convergence criteria ‘b’. Based on these results, mesh ‘D4-M1’ and convergence criteria ‘b’ were chosen for further use.

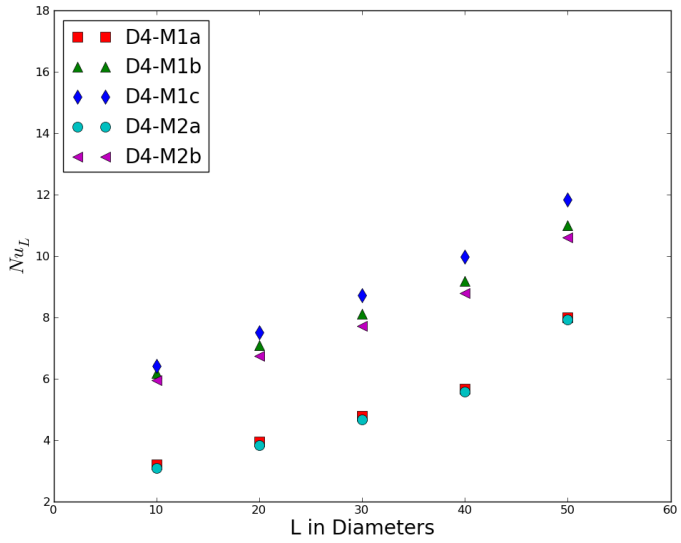

(a) Horizontal Segments

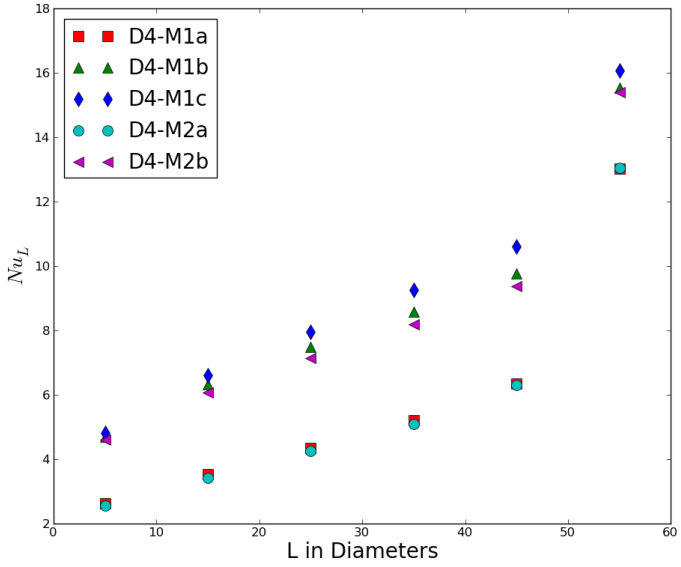

(b) Vertical Segments

Figure 3.40: Comparison of Nu_L vs. L Results for Different Meshes, 3D Convection Inline with Screen

Chapter 4

Results

The numerical models developed in the previous chapter were used to simulate a range of input parameters and geometries. The results from these simulations are given in this chapter. The results are presented in the same order as the models were described.

4.1 Natural Convection

4.1.1 Single Cylinder

Results for the case of a single, infinite horizontal cylinder are given here. Table 4.1 lists the cases for which CFD models were created. The results obtained for these cases are shown in Figure 4.1 along with the following correlations:

$$\overline{Nu}_D = 0.675 Ra_d^{0.058} \; for \; 10^{-10} < Ra_D < 10^{-2} \quad \text{[Morgan 1975]}$$
$$\overline{Nu}_D = 1.02 Ra_d^{0.148} \; for \; 10^{-2} < Ra_D < 10^{2} \quad \text{[Morgan 1975]} \tag{2.15}$$

$$\overline{Nu}_D = \left\{ 0.6 + \frac{0.387 Ra_D^{1/6}}{[1 + (0.559/Pr)^{9/16}]^{8/27}} \right\}^2 \quad \text{[Churchill \& Chu 1975(1)]} \tag{2.17}$$

It can be seen in Figure 4.1 that the results of the CFD models are in close agreement with the correlations of both Morgan [Morgan 1975] as well as Churchill and Chu [Churchill & Chu 1975(1)]. This agreement with multiple published correlations gives confidence in the accuracy of these CFD model results.

Table 4.1: Cases Modelled for Single Horizontal Cylinder in Natural Convection

Diameter mm	$\Delta T \; ^oC$
0.1	1,5,10,20,50
0.25	1,5,10,20,50
0.5	1,5,10,20,50
1.0	1,5,10,20,50

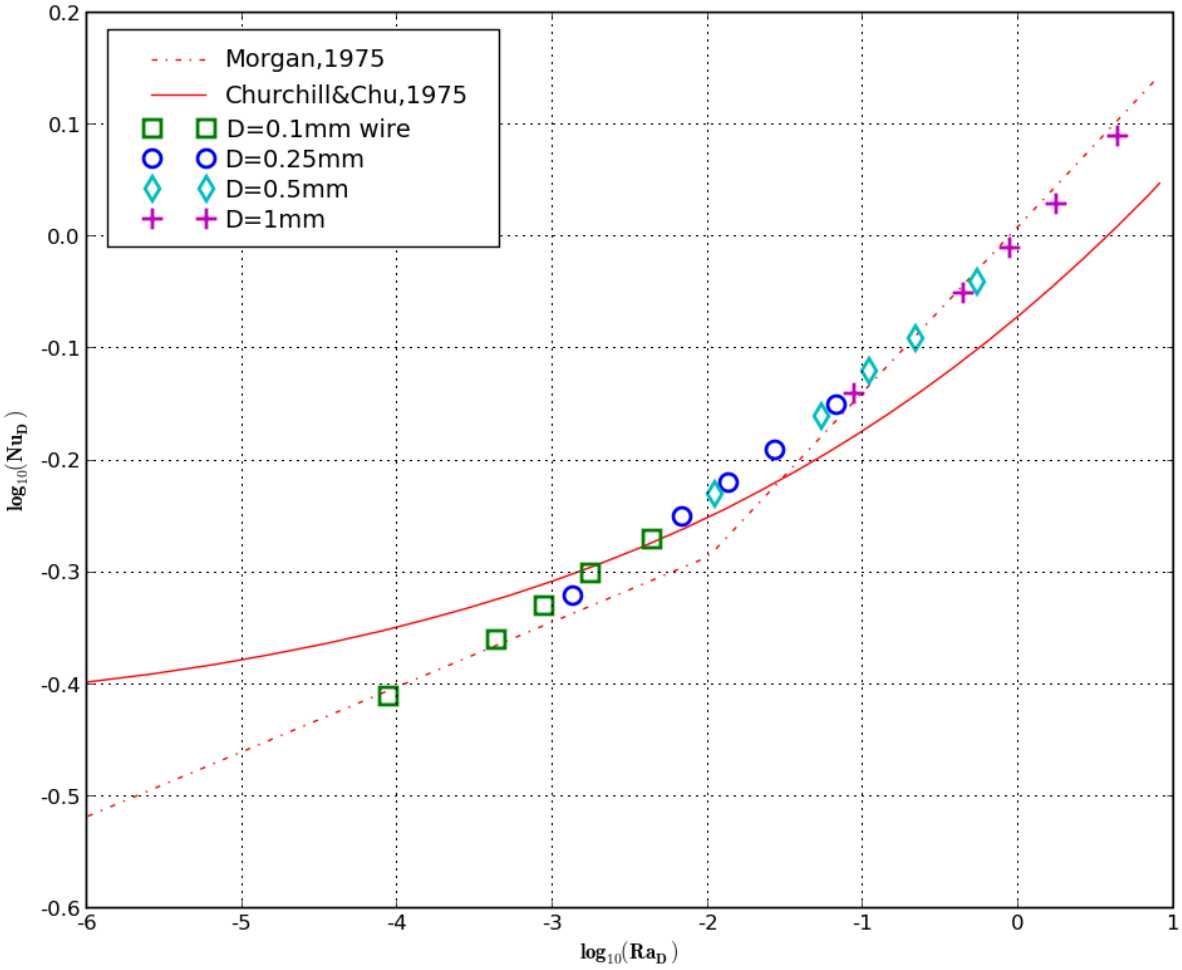

Figure 4.1: Correlations and Results for Single Cylinders, Natural Convection

4.1.2 Multiple Cylinders

Vertical arrays of multiple infinite horizontal cylinders are listed next. Table 4.2 lists the cases simulated for arrays of five cylinders. All models used centre-centre vertical spacing of the cylinders of 10 diameters. Results from these models can be seen in Figure 4.2 along with the single cylinder results and correlations for comparison.

Table 4.2: Cases Modelled for Vertical Arrays of Five Horizontal Cylinders in Natural Convection

Diameter mm	$\Delta T\ ^oC$
0.1	5,10,20,50
0.25	5,10,20,50
0.5	5,10,20,50
1.0	5,10,20,50

Based on the results given in Figure 4.2, the following trends can be seen:

- Nu_D is highest for the bottom wire in the array.
- With the exception of the top wire, Nu_D decreases for each subsequent ascending wire in the vertical array .
- The Nu_D spread within a vertical array decreases with increasing Ra_D.
- For $Ra_d > 0.01$, Nu_D for the lowest cylinder in the multiple cylinder array approaches that of the single cylinder case.
- $\overline{Nu}_D$ over all cylinders for a multiple cylinder array is less than Nu_d for a single cylinder with an identical Ra_D.

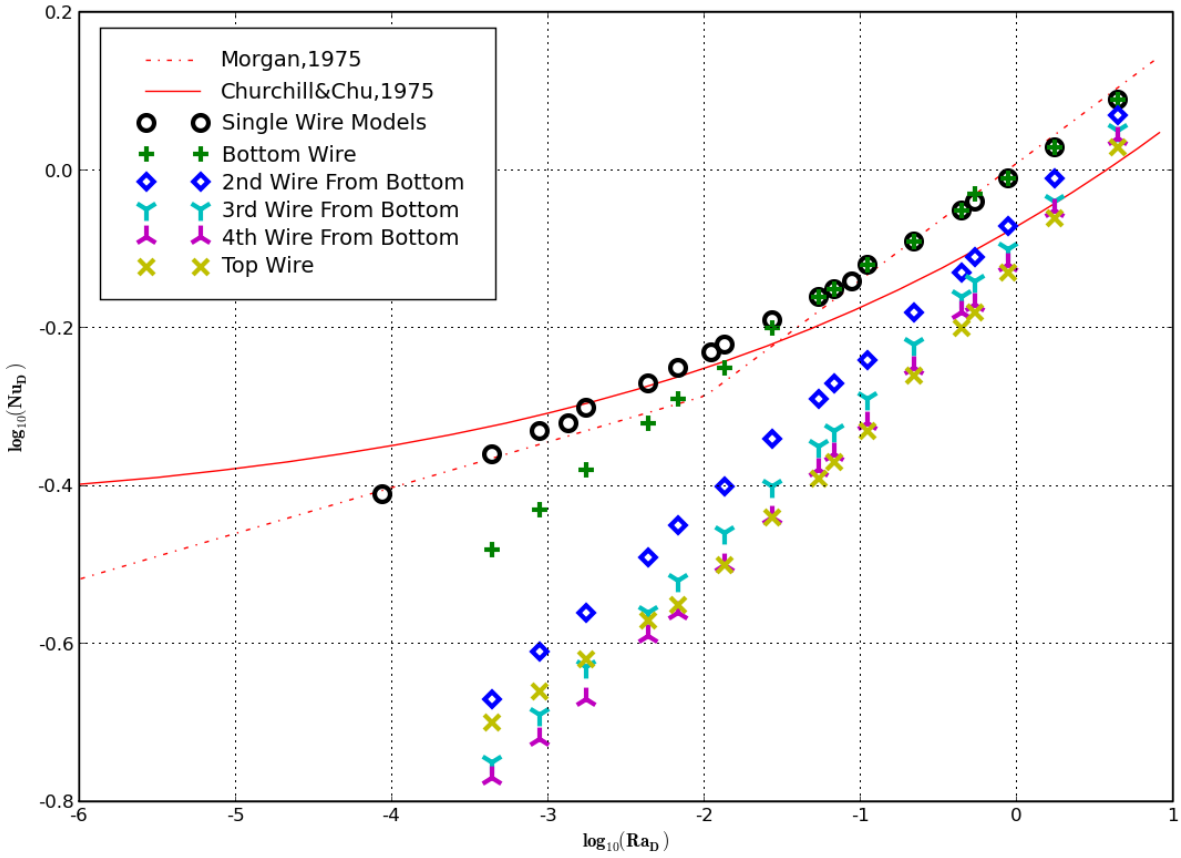

Figure 4.2: Correlations and Results for Vertical Arrays of Five Cylinders, Natural Convection

The results discussed above and shown in Figure 4.2 give Ra_d where Ra_D is the Rayleigh number based on the cylinder diameter. As seen in the results in Figure 4.2, the heat transfer varies with the vertical position of a cylinder in an array. It can be hypothesized that Nu for a cylinder will vary with vertical position in a manner similar to the variation of Nu with respect to height on a vertical flat plate. To compare the variation of heat transfer with vertical position with that of a flat plate, the Nusselt and Rayleigh numbers

can be reformulated to use the vertical position as the relevant length dimension. The height above the centre of the bottom cylinder was used as the length dimension and labelled L. Using this definition of L in calculating Ra_L results in $Ra_L = \infty$ for the bottom cylinder. As such, results from the bottom cylinder were not calculated.

In order to view the variation of heat transfer over a wider range of array heights, a single model was created with an array of ten cylinders. The single ten-element array utilized 0.1mm cylinders with surface temperatures 10^oC above ambient and with the same 10*D centre-centre cylinder spacing as used in the five-element arrays. Figure 4.3 shows the Nu_L versus Ra_L results. A best-fit line of the following form was fit to the data:

$$Nu_L = A \cdot {Ra_L}^B \tag{4.1}$$

Using a least-squares method, the resulting best-fit equation was found to be:

$$Nu_L = 2.8 \cdot {Ra_L}^{0.21} \tag{4.2}$$

Two correlations for a vertical flat plate from Eckert ($Nu_L = 0.41 \cdot Ra_L^{1/4}$) [Eckert 1963] as well as Churchill and Chu ($Nu_L = \left[0.825 + 0.324 \cdot Ra_L^{1/6}\right]^2$) [Churchill & Chu 1975(2)] are also shown for comparison. Note that a correlation of the form $Nu_L = A \cdot {Ra_L}^{1/3}$ corresponds to a heat-transfer co-efficient h_c independent of length L [Kreith 1997].

Figure 4.4 shows the results for 0.1mm cylinders only. Since all of the data in this plot are for the same diameter, for a given temperature, increasing Ra_L corresponds to cylinders higher in the array. It can be seen in Figure 4.4 that Nu_L for the first and last cylinders in

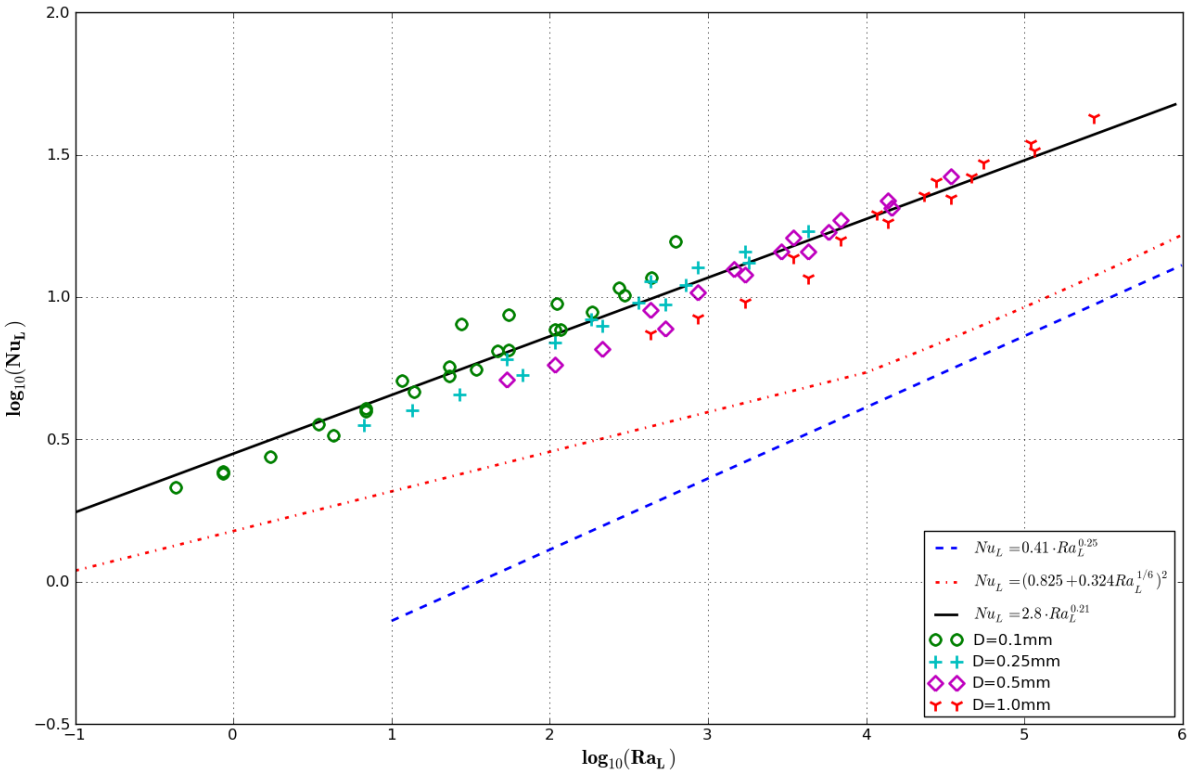

Figure 4.3: Nu_L vs Ra_L for Vertical Array of Cylinders

a given model array are larger than predicted by the correlation. This is likely the case due to the competing momentum and thermal effects as described by [Corcione 2005] and discussed in the Background chapter.

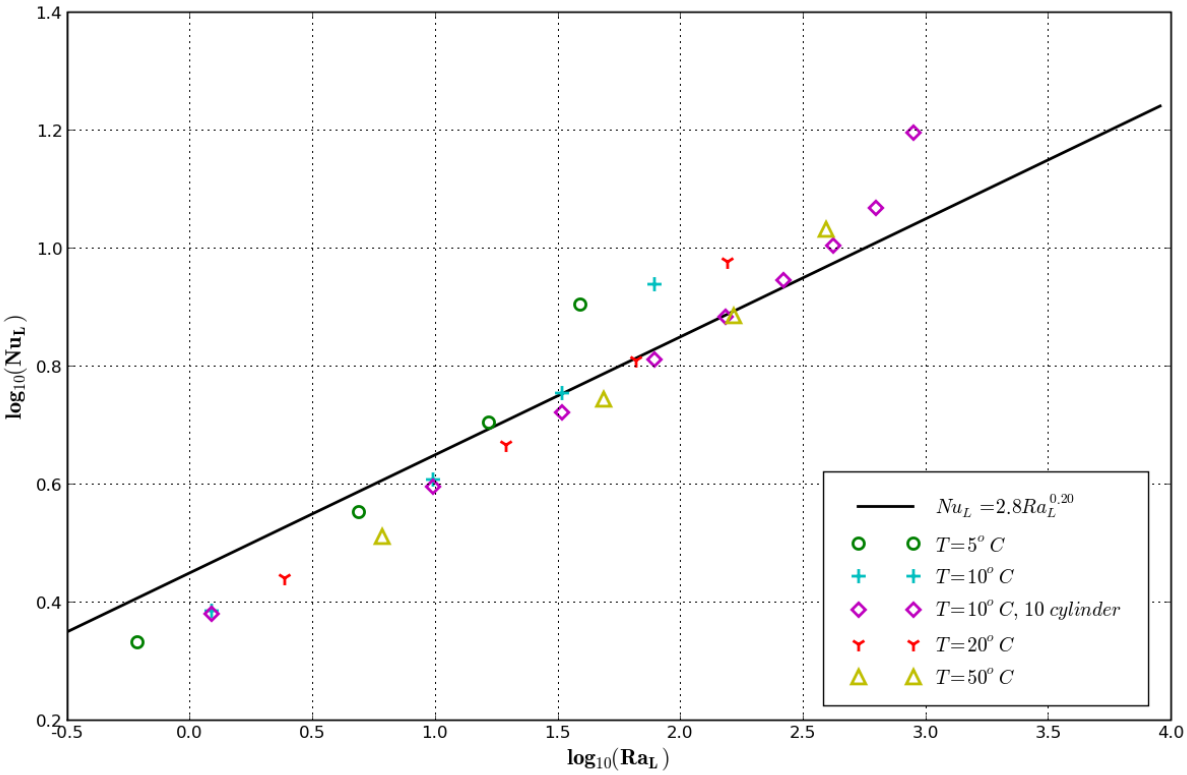

Figure 4.4: Nu_L vs Ra_L for Vertical Array of 0.1mm Cylinders

4.1.3 3D Models

A three-dimensional model of a vertical array of five $0.1mm$ cylinders at a centre-centre spacing of $10 * D$ was created and run at $\Delta T = 10^oC$. Table 4.3 gives the results of Nu_D for this model and how they compare to the results from the 2D models for single and multiple horizontal cylinders. Figure 4.5 graphically presents the Nu_L vs Ra_L results.

Table 4.3: Ra_D by Surface for 3D Natural Convection Models with $D = 0.1mm$ & $\Delta T = 10^oC$

Single Cylinder		2D 5-Cylinder		3D 5-Cylinder	
Surface	Nu_D	Surface	Nu_D	Surface	Nu_D
				3D-Ver1	0.385
Hor1	0.468	2D-Hor1	0.373	3D-Hor1	0.229
				3D-Ver2	0.165
		2D-Hor2	0.243	3D-Hor2	0.139
				3D-Ver3	0.124
		2D-Hor3	0.203	3D-Hor3	0.115
				3D-Ver4	0.110
		2D-Hor4	0.190	3D-Hor4	0.108
				3D-Ver5	0.111
		2D-Hor5	0.217	3D-Hor5	0.128
				3D-Ver6	0.192

Hor: Horizontal Cylinder Surfaces

Ver: Surfaces part of vertical Cylinders

Surface numbering is from bottom to top

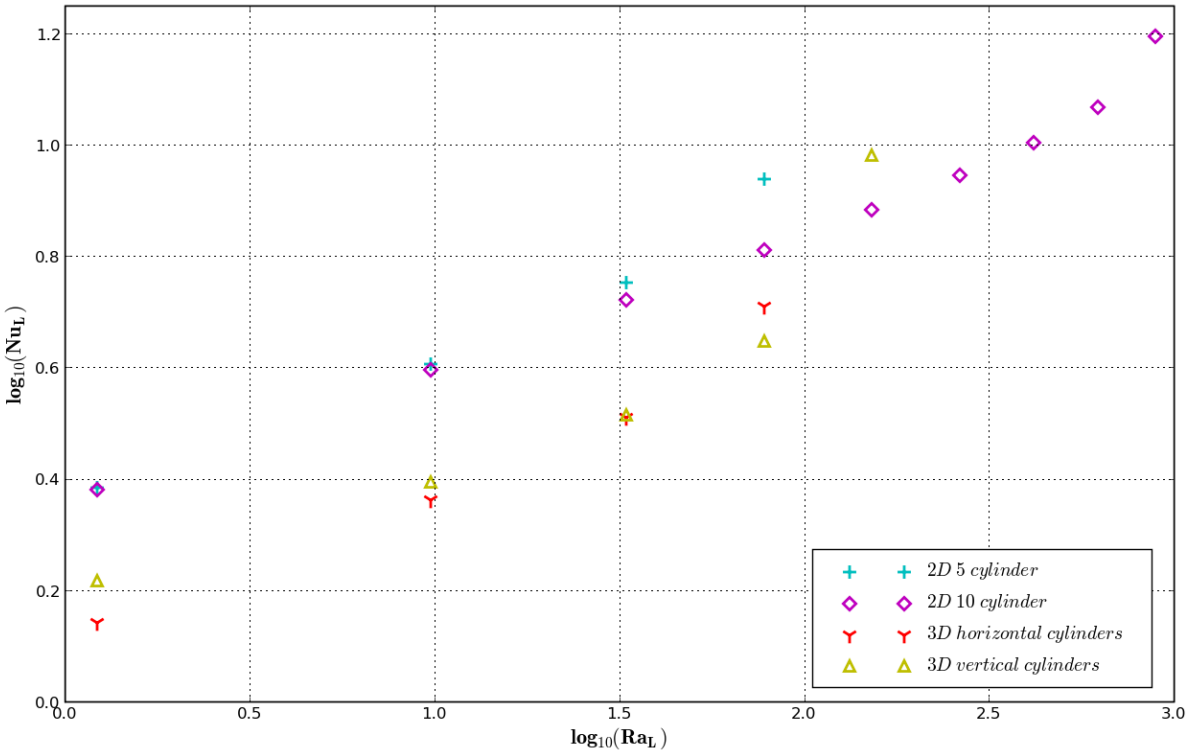

Figure 4.5: Nu_L vs Ra_L for Natural Convection in 2D and 3D Models

4.2 Forced Convection

4.2.1 Forced Convection Normal to an Array of Cylinders

Results for the case of forced convection with the fluid flow direction perpendicular to the array of cylinders are given first. Table 4.4 lists the cases run and the corresponding results along with values predicted by correlations. The results are also shown graphically in Figure 4.6. All of the models were run with a simulated temperature difference of $\Delta T = 10^oC$.

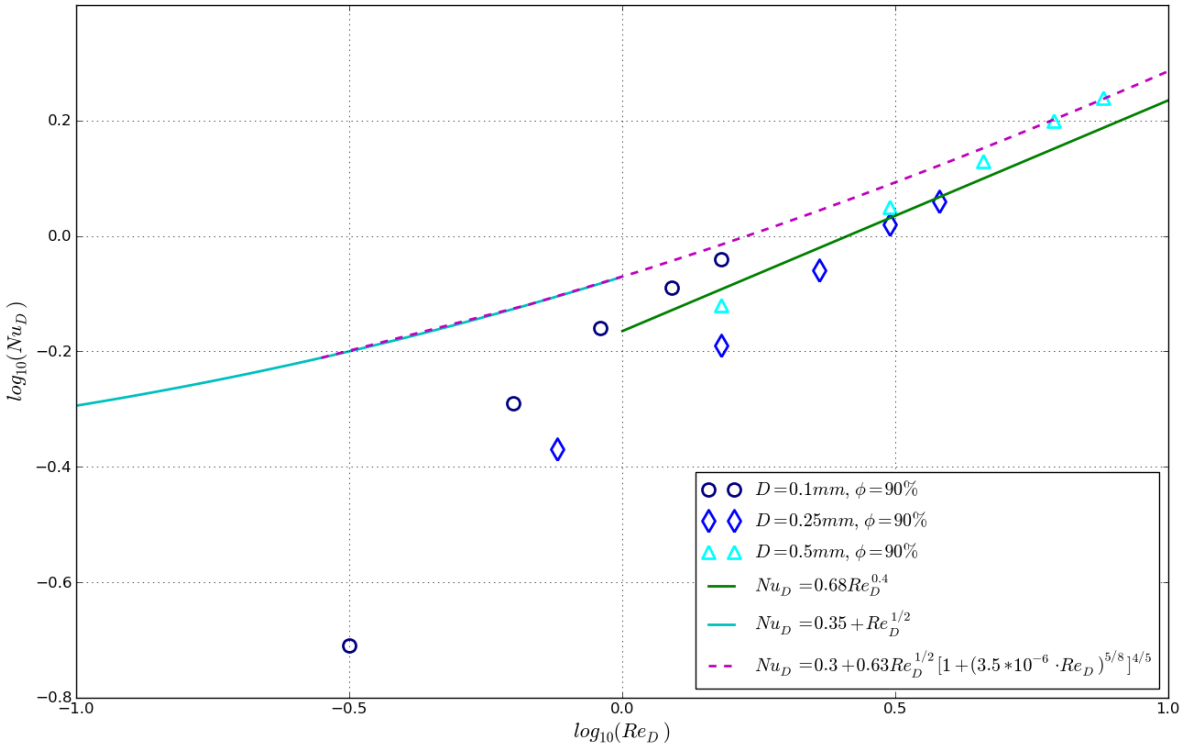

Figure 4.6: Nu_D vs. Re_D for Forced Convection Normal to Cylinder Array [Zukauskas 1972] & [Churchill & Bernstein 1977]

Table 4.4: Results for Forced Convection Normal to Cylinder Array, $\gamma = 10\%$

D mm	V m/s	Re_D	Gr_D/Re_D^2	Nu_D			
				Numerical Results	Correlations		
					#1	#2	#3
0.10	0.05	0.31	$1.3 * 10^{-2}$	0.19	x	0.90	0.65
0.10	0.10	0.61	$3.3 * 10^{-3}$	0.51	x	1.1	0.80
0.10	0.15	0.92	$1.5 * 10^{-3}$	0.69	x	1.3	0.90
0.10	0.20	1.2	$8.2 * 10^{-4}$	0.82	0.74	1.4	1.0
0.10	0.25	1.5	$5.2 * 10^{-4}$	0.91	0.81	1.6	1.1
0.25	0.05	0.76	$3.3 * 10^{-2}$	0.43	x	1.2	0.85
0.25	0.10	1.5	$8.2 * 10^{-3}$	0.64	0.81	1.6	1.1
0.25	0.15	2.3	$3.6 * 10^{-3}$	0.86	0.95	1.9	1.3
0.25	0.20	3.0	$2.0 * 10^{-3}$	1.04	1.1	2.1	1.4
0.25	0.25	3.8	$1.3 * 10^{-3}$	1.16	1.2	2.3	1.5
0.50	0.05	1.5	$6.5 * 10^{-2}$	0.77	0.80	1.6	1.1
0.50	0.10	3.0	$1.6 * 10^{-2}$	1.1	1.1	2.1	1.4
0.50	0.15	4.6	$7.3 * 10^{-3}$	1.4	1.2	2.5	1.6
0.50	0.20	6.1	$4.1 * 10^{-3}$	1.6	1.4	2.8	1.8
0.50	0.25	7.6	$2.6 * 10^{-3}$	1.7	1.5	3.1	2.0

$\Delta T = 10^oC$ for all cases listed above.
Correlation #1; $Nu_D = 0.68 \cdot Re_d^{0.4}$ [Zukauskas 1972]
Correlation #2; $Nu_D = 0.35 + Re_D^{1/2}$ [Zukauskas 1972]
Correlation #3; $Nu_D = 0.3 + 0.63 \cdot Re_D^{1/2}[1 + (3.5 * 10^{-6} \cdot Re_D)^{5/8}]^{4/5}$ [Churchill & Bernstein 1977]

It can be seen in Figure 4.6 that the results of the numerical simulations differ somewhat from those predicted by the correlations at lower values of Re_D. These values occurred at lower velocities and with the $0.1mm$ diameter cylinders. These lower results are likely the result of interference from adjacent cylinders reducing the heat transfer rate. If the boundary layers around the cylinder are larger as a fraction of the diameter for smaller diameters, then it is expected that interference would be most significant for the smallest diameter and most closely spaced cylinders simulated.

4.2.2 Forced Convection Normal to a Screen, 3D Model

The results obtained using three-dimensional models of forced convection normal to a vertical insect screen are given below. Models for $D = 0.1mm$ and $D = 0.25mm$ were created and run for velocities of $V = 0.05, 0.10, 0.15, 0.20, 0.25\ m/s$. All cases used a simulated temperature difference between the screen surface and bulk fluid of $\Delta T = 10^oC$. The results of these models are given numerically in Table 4.5 and graphically in Figure 4.7.

Table 4.5: Results for Forced Convection Normal to Screen, 3D Models

D mm	V m/s	γ	Re_D	Gr_D/Re_D^2	h_c W/m^2	Nu_D
0.1	0.05	20%	0.306	$1.31 * 10^{-2}$	82	0.32
0.1	0.10	20%	0.611	$3.27 * 10^{-3}$	136	0.53
0.1	0.15	20%	0.917	$1.45 * 10^{-3}$	173	0.68
0.1	0.20	20%	1.22	$8.17 * 10^{-4}$	200	0.78
0.1	0.25	20%	1.53	$5.23 * 10^{-4}$	223	0.87
0.1	0.05	75%	0.306	$1.31 * 10^{-2}$	26	0.10
0.1	0.10	75%	0.611	$3.27 * 10^{-3}$	53	0.21
0.1	0.15	75%	0.917	$1.45 * 10^{-3}$	81	0.32
0.1	0.20	75%	1.22	$8.17 * 10^{-4}$	106	0.42
0.1	0.25	75%	1.53	$5.23 * 10^{-4}$	132	0.52
0.25	0.05	20%	0.764	$3.27 * 10^{-2}$	62	0.609
0.25	0.10	20%	1.53	$8.17 * 10^{-3}$	89	0.870
0.25	0.15	20%	2.29	$3.63 * 10^{-3}$	107	1.05
0.25	0.20	20%	3.06	$2.04 * 10^{-3}$	122	1.19
0.25	0.25	20%	3.82	$1.31 * 10^{-3}$	135	1.32
0.25	0.05	75%	0.764	$3.27 * 10^{-2}$	27	0.26
0.25	0.10	75%	1.53	$8.17 * 10^{-3}$	54	0.52
0.25	0.15	75%	2.29	$3.63 * 10^{-3}$	78	0.76
0.25	0.20	75%	3.06	$2.04 * 10^{-3}$	101	0.99
0.25	0.25	75%	3.82	$1.31 * 10^{-3}$	122	1.19

γ = Screen Density

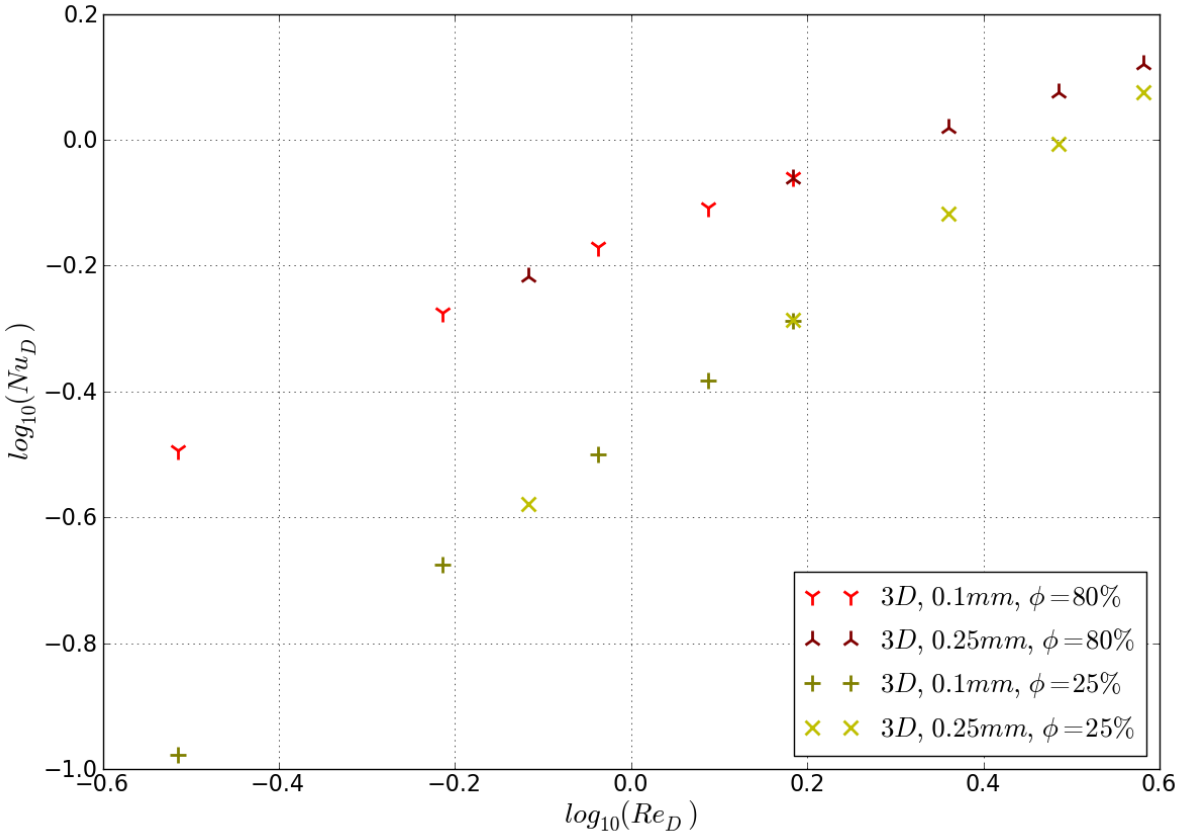

Figure 4.7: Nu_D vs. Re_D for Forced Convection Normal to 3D Screen

4.2.3 Convection Inline With an Array of Cylinders

Results obtained for forced convection inline with the array of cylinders is described below. The cylinder diameters used in the models were $0.1mm$ and $0.25mm$. For the $0.1mm$ cylinder arrays, cylinder centre-centre spacings of $10 * D$ and $2 * D$ were simulated. For the $0.25mm$ cylinder arrays, only a single cylinder spacing of $10 * D$ was simulated. Forced velocities ranging from $0.05m/s$ to $0.25m/s$ were simulated for all of the arrays investigated. All cases used a temperature difference of $\Delta T = 10^oC$ between the cylinders' surfaces and the ambient fluid. The results for the arrays with spacings of $10 * D$ are given in Table 4.6 and Figure 4.8 while those for the arrays with $2 * D$ spacings are given in Table 4.7 and Figure 4.9. Figures 4.8 and 4.9 include correlations for vertical flat plates along with the data for comparison. The correlations shown are described in the Background chapter.

Table 4.6: Results for Forced Convection Inline With Cylinder Array, $\gamma = 10\%$

D mm	V m/s	Re_D	Gr_D/Re_D^2	Nu_D				
				h_c W/m^2				
				Cyl. #1	Cyl. #2	Cyl. #3	Cyl. #4	Cyl. #5
0.10	0.05	0.306	$1.31 * 10^{-2}$	70.7	42.3	33.7	32.1	42.0
0.10	0.10	0.611	$3.27 * 10^{-3}$	116	68.4	51.2	43.9	49.3
0.10	0.15	0.917	$1.45 * 10^{-3}$	182	114	88.5	74.8	72.6
0.10	0.20	1.22	$8.17 * 10^{-4}$	206	132	104	87.9	82.6
0.10	0.25	1.53	$5.23 * 10^{-4}$	225	147	116	99.0	91.4
0.25	0.05	0.764	$3.27 * 10^{-2}$	36.5	21.5	16.4	14.6	17.8
0.25	0.10	1.53	$8.17 * 10^{-3}$	88.5	57.0	44.9	38.0	35.0
0.25	0.15	2.29	$3.63 * 10^{-3}$	102	66.8	53.6	46.1	42.1
0.25	0.20	3.06	$2.04 * 10^{-3}$	118	80.0	65.4	57.0	52.0
0.25	0.25	3.82	$1.31 * 10^{-3}$	129	87.7	71.9	62.9	57.3

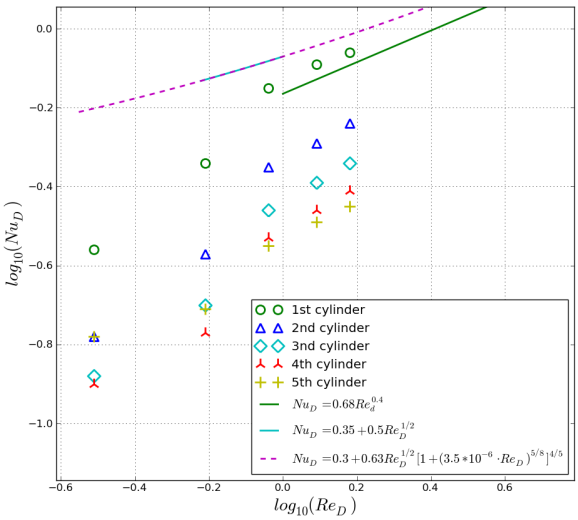

(a) 0.1mm Cylinder Array

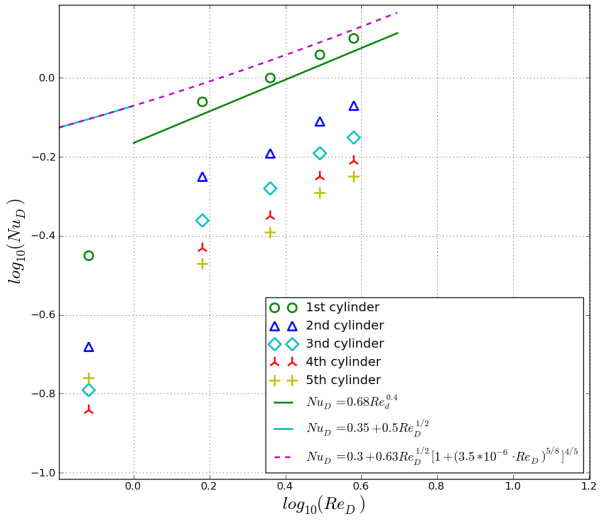

(b) 0.25mm Cylinder Array

Figure 4.8: Nu_D vs. Re_D for Forced Convection Inline With Cylinder Array, $\gamma = 10\%$

Table 4.7: Results for Forced Convection Inline With Cylinder Array, $\gamma = 50\%$

D mm	V m/s	Re_D	Gr_D/Re_D^2	Nu_D				
				h_c W/m^2				
				Cyl. #1	Cyl. #5	Cyl. #10	Cyl. #15	Cyl. #20
0.10	0.05	0.306	$1.31 * 10^{-2}$	47.4	10.8	8.4	8.4	28.6
0.10	0.10	0.611	$3.27 * 10^{-3}$	77.7	16.7	12.4	11.4	33.4
0.10	0.15	0.917	$1.45 * 10^{-3}$	95.2	19.8	14.4	12.8	35.6
0.10	0.20	1.22	$8.17 * 10^{-4}$	112	22.7	16.3	14.2	37.2
0.10	0.25	1.53	$5.23 * 10^{-4}$	166	36.0	25.9	21.9	40.7

The results were also formulated using a length dimension of L for the dimensionless parameters Re and Nu where L is the vertical centre-centre distance from the bottom cylinder to the cylinder in question. Figures 4.10 and 4.11 graphically depict the results using this formulation.

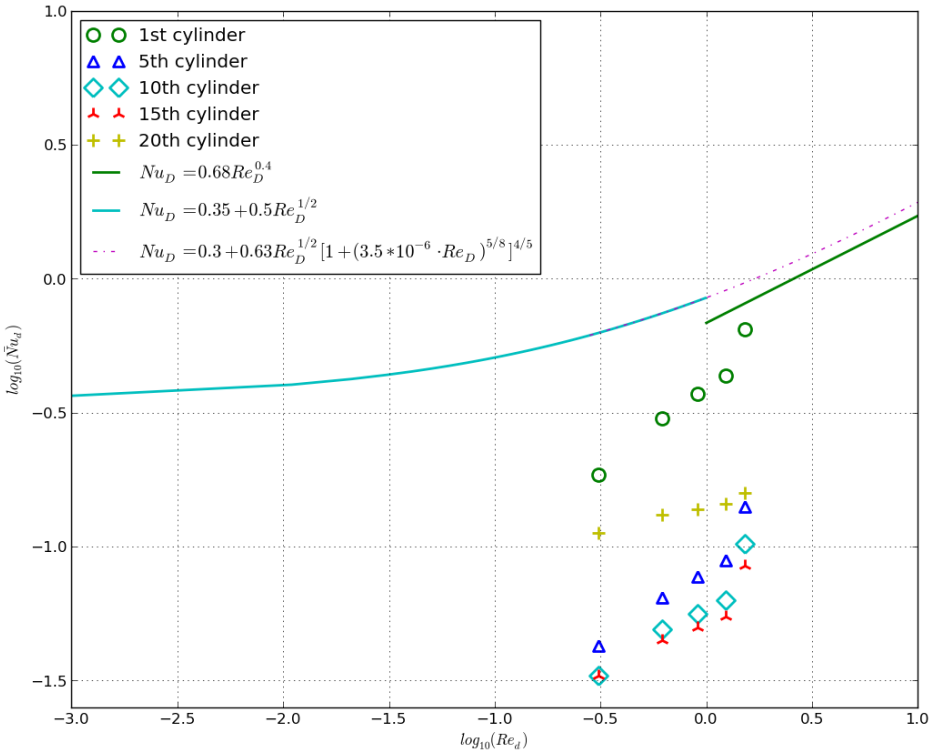

Figure 4.9: Nu_D vs. Re_D for Forced Convection Inline With Cylinder Array, $\gamma = 50\%$

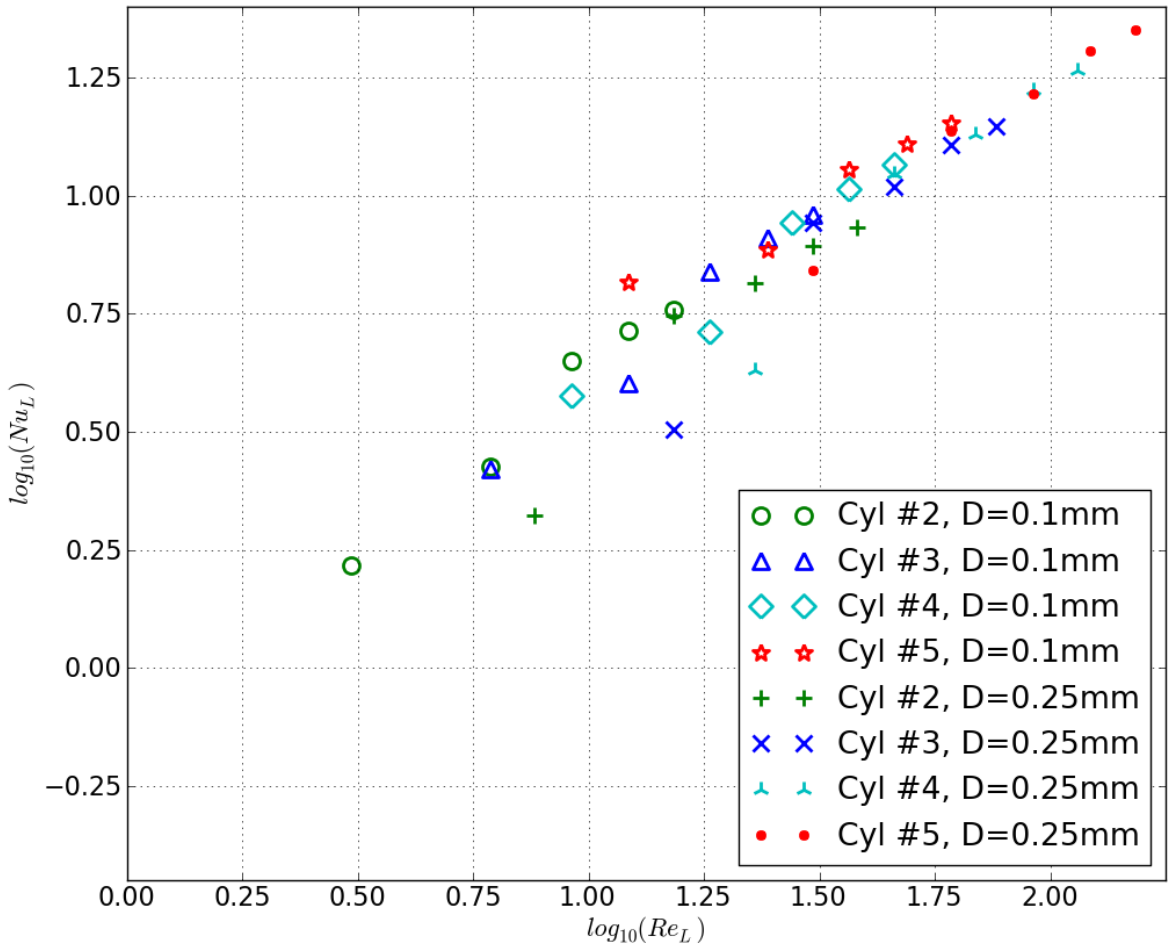

Figure 4.10: Nu_L vs. Re_L for Forced Convection Inline With Cylinder Array, $\gamma = 10\%$

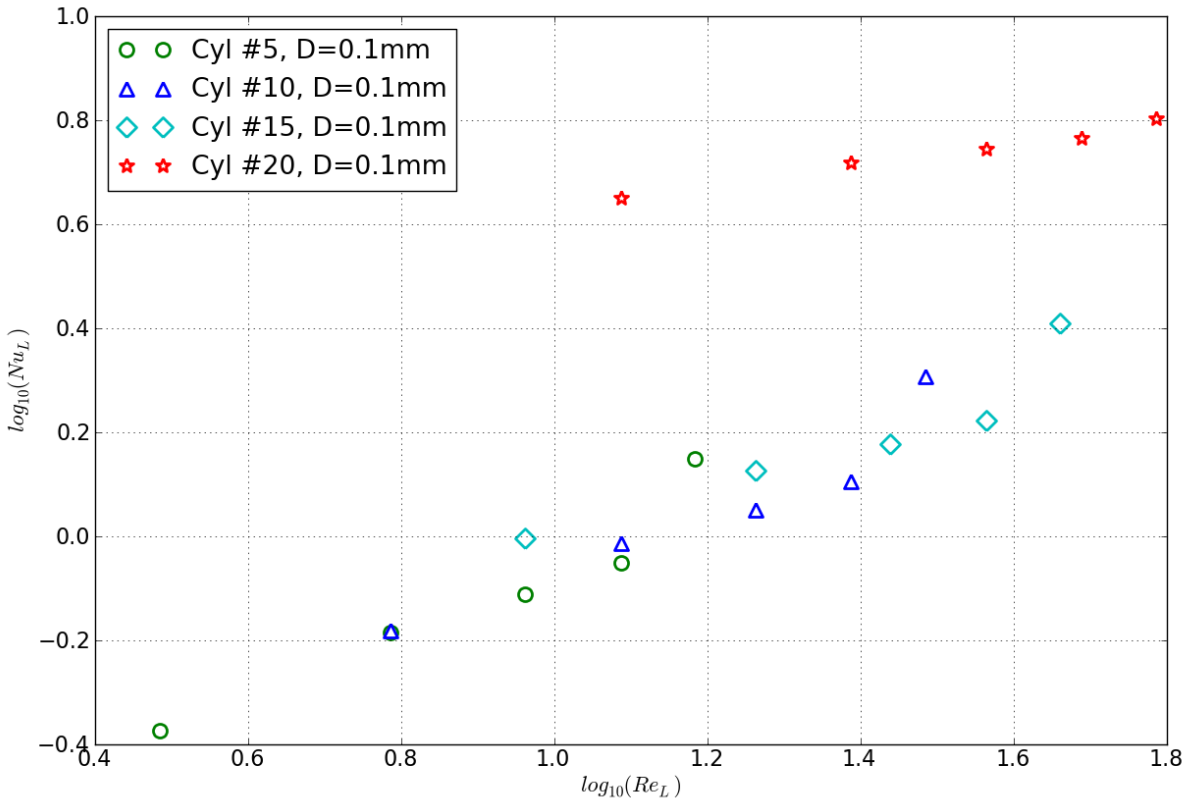

Figure 4.11: Nu_L vs. Re_L for Forced Convection Inline With Cylinder Array, $\gamma = 50\%$

4.2.4 Forced Convection Parallel to a Screen, 3D Model

The results obtained from three-dimension models for forced convection parallel to a vertical insect screen are given here. The results are tabulated in Table 4.8. As can be seen in Table 4.8, the results are given separately for different parts of the screen. Since the screen was considered to be a cartesian array of intersecting cylinders, the screen is separated into vertical and horizontal segments.

Table 4.8: Results for Forced Convection Inline With Screen, 3D Model

Horizontal Sections

D mm	V m/s	Re_D	Gr_D/Re_D^2	$\bar{h}_c$ W/m^2				
				Sec#1	Sec#2	Sec#3	Sec#4	Sec#5
0.10	0.05	0.306	$1.31 * 10^{-2}$	75.8	44.0	34.8	31.2	35.8
0.10	0.10	0.611	$3.27 * 10^{-3}$	102.7	58.8	45.4	39.3	41.7
0.10	0.15	0.917	$1.45 * 10^{-3}$	124.5	71.3	54.7	46.8	47.2
0.10	0.20	1.22	$8.17 * 10^{-4}$	142.6	81.7	62.6	53.2	52.0
0.10	0.25	1.53	$5.23 * 10^{-4}$	158.5	90.7	69.3	58.8	56.3

Vertical Sections

D mm	V m/s	Re_D	Gr_D/Re_D^2	$\bar{h}_c$ W/m^2					
				Sec#1	Sec#2	Sec#3	Sec#4	Sec#5	Sec#6
0.10	0.05	0.306	$1.31 * 10^{-2}$	128	53.6	38.3	32.5	31.5	53.1
0.10	0.10	0.611	$3.27 * 10^{-3}$	169	71.8	50.5	41.7	38.4	59.3
0.10	0.15	0.917	$1.45 * 10^{-3}$	200	86.4	60.8	50.0	45.0	64.5
0.10	0.20	1.22	$8.17 * 10^{-4}$	223	98.1	69.4	56.9	50.6	68.7
0.10	0.25	1.53	$5.23 * 10^{-4}$	241	107.8	76.6	62.8	55.5	72.3

Horizontal and Vertical sections are counted from the bottom up

The results given in Table 4.8 are illustrated in Figures 4.12 and 4.13. Figure 4.12 gives the results formulated using $Nu_D = h_c * D/k$ and $Re_D = V * D/\nu$. Using this formulation, different screen segments will have identical Re_D values for a given model case. The variation in heat transfer over the screen is indicated by the vertical spacing of

data-points for a given Re_D value. In contrast, the formulation of $Nu_L = h_c * L/k$ and $Re_L = V * L/\nu$ is used in Figure 4.13. Using the Nu_L versus Re_L formulation, the variation of heat transfer across the screen is imbued by the use of the height L in the definitions of Nu_L and Re_L. The dimension L is measured as the height above the bottom of the screen. The bottom of the screen is considered to be the bottom of the first vertical segment (i.e. the junction between the lower frustum and the first vertical section; see Figure 3.39 for an illustration of the model geometry). For the horizontal screen segments, L is measured to the cylinder axis. For the vertical segments, L is measured to midway between the top and bottom of the segment. Note that for the lowest and highest vertical segments this is not quite the geometric centre of the segments' surface due to vertical asymmetry.

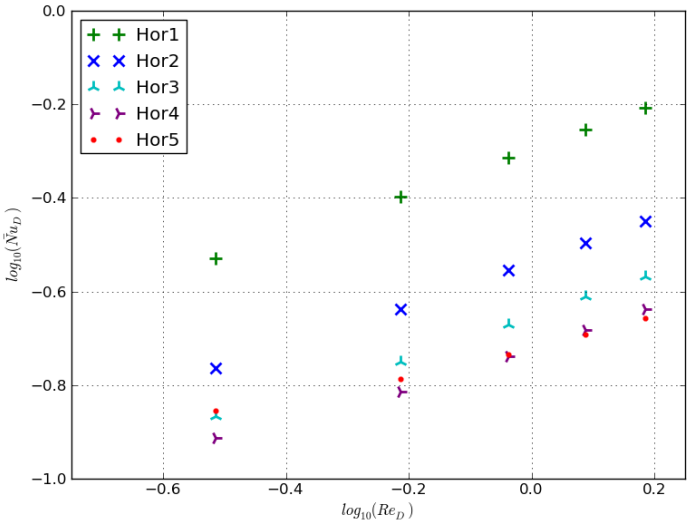

(a) Horizontal Screen Segments

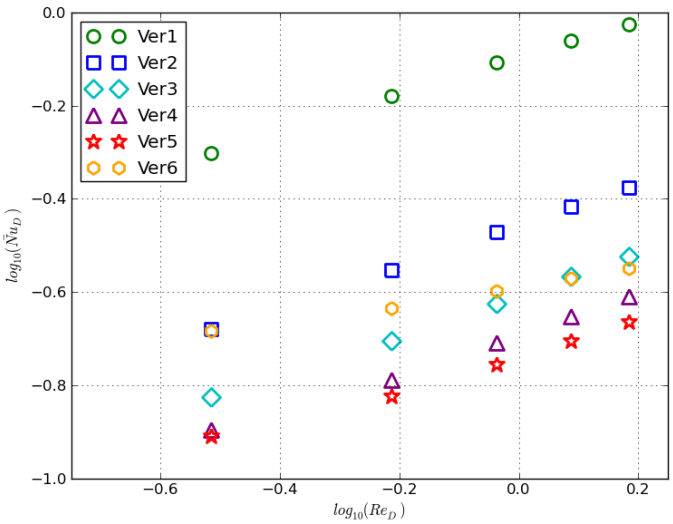

(b) Vertical Screen Segments

Figure 4.12: Nu_D vs. Re_D Plot For Forced Convection Inline With Screen, 3D Model

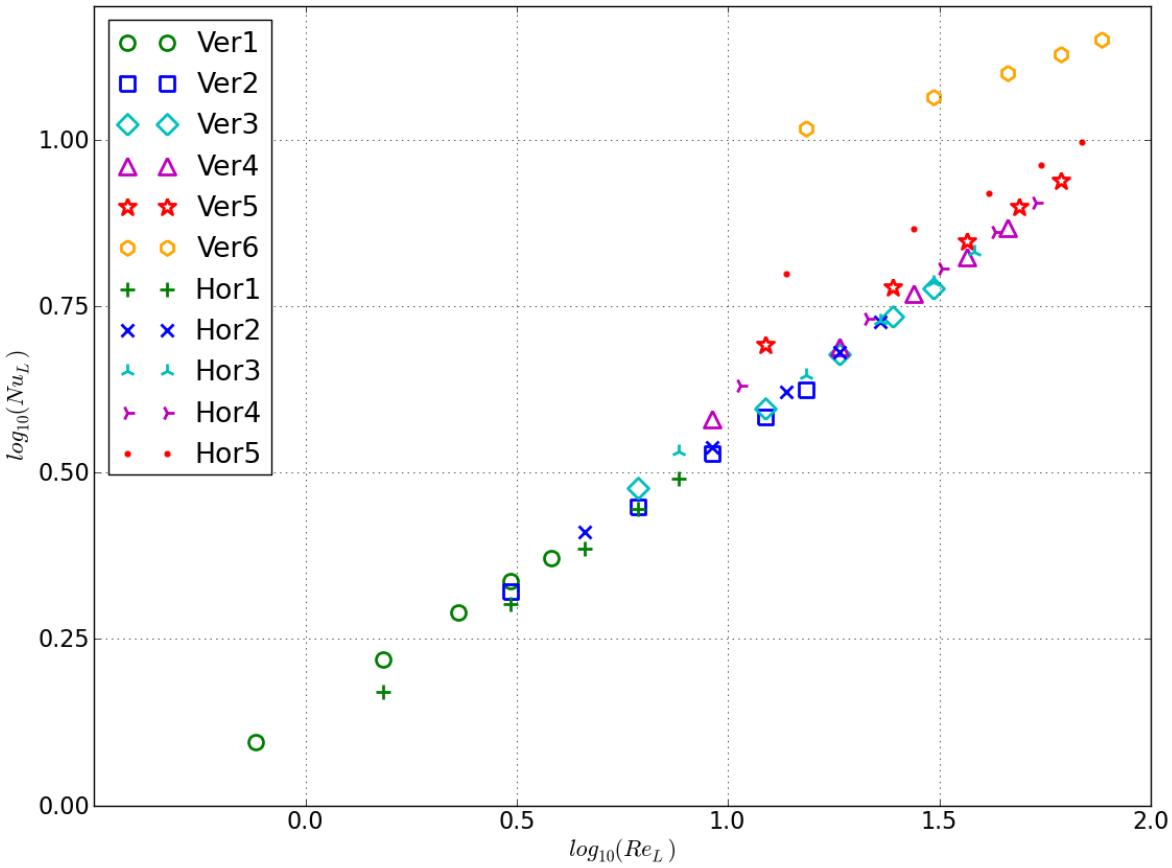

Figure 4.13: Nu_L vs. Re_D For Convection Inline With Screen, 3D Model

Chapter 5

Discussion

The original impetus for this research was to develop a greater understanding of the heat transfer processes taking place at the surface of a heated insect screen. The results obtained thus far can be used in two ways depending on both the information available and desired.

To develop an estimate for convective heat transfer from the insect screen to the surrounding air, the results developed in the natural convection simulations can be used directly. These results will not take into account effects from the geometry of the screen's installation such as window sill size etc. However, only the geometry of the screen and its temperature need to be known in order to use this method.

Alternatively, the results of the forced convection simulations can be used as inputs into more detailed models of window assemblies that include insect screens. The results of the forced convection simulations can be used as inputs into CFD models of the window assemblies. Using this method, the velocity and temperature profiles will be determined

during the course of the numerical simulation. The simulation will require an input function that gives a relation between the heat transfer at the screen surface and the local temperature and velocity profiles. The results of this work can be used to determine the relation between the surface heat transfer and the local conditions.

5.1 Natural Convection

An initial estimate for the heat transfer co-efficient of the insect screen can be obtained using the Ostrach solution [Ostrach 1953]. The Ostrach solution for a vertical flat plate is given by Equation 5.1 for air:

$$Nu_L = 0.38 \cdot Ra_L^{1/4} \quad \text{[Ostrach 1953]} \tag{5.1}$$

One way to use Equation 5.1 to estimate the value of h_c for an insect screen is to assume that the insect screen has the same amount of heat transfer per unit surface area as a flat plate. For a flat plate, the surface used is clearly $A = length \cdot width$. While it is convenient to still use the same area for calculations using the screen, clearly the actual surface area of the screen filaments will differ. The surface area of a screen is calculated below using the geometry shown in Figure 5.1.

$$A_{screen} = 2\pi(s - 1/2)\left(\frac{l \cdot w}{s^2}\right) \tag{5.2}$$

$$\frac{A_{screen}}{A_{flat\ plate}} = \frac{2\pi(s - 1/2)}{s^2} = \pi \cdot \gamma \tag{5.3}$$

Where: l & w are the screen's outside dimensions

γ = Screen density

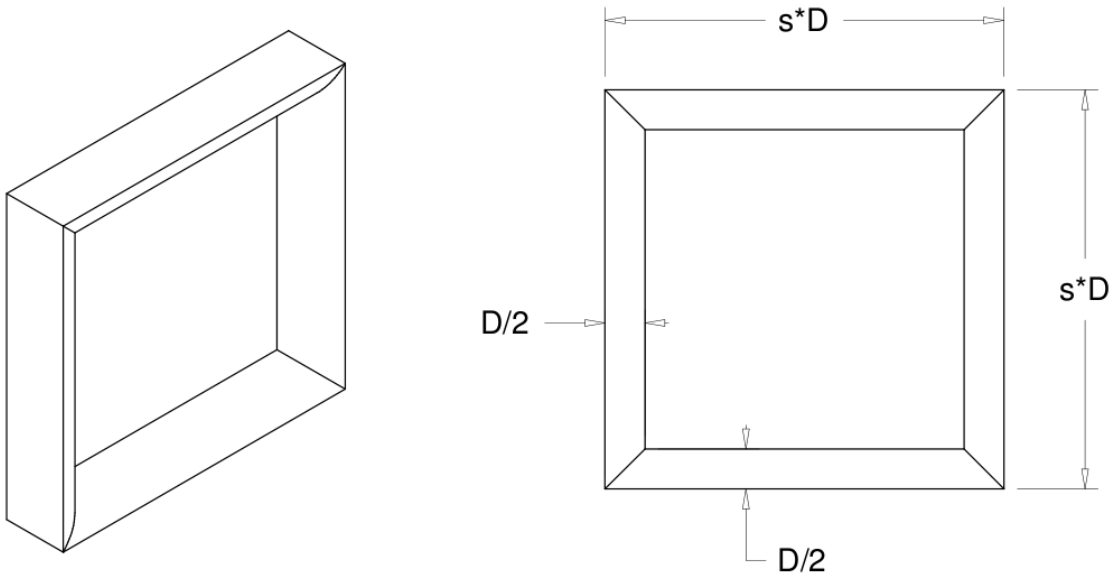

Figure 5.1: Screen Segment Dimensions

Heat transfer co-efficients for a screen can be defined as follows:

$$h_{c_{screen}} = \frac{Q_{screen}}{\text{Screen filament area} \cdot \Delta T} \tag{5.4}$$

$$h^*_{c_{screen}} = \frac{Q_{screen}}{\text{Length} \cdot \text{Width} \cdot \Delta T} \tag{5.5}$$

$$= \left(\frac{\text{Screen filament area}}{\text{length} \cdot \text{width}} \right) \cdot h_{c_{screen}} \tag{5.6}$$

$$= h_{c_{screen}} \cdot (\pi \cdot \gamma) \tag{5.7}$$

As defined above, h_c can be considered to be the 'true' coefficient that uses the real surface area of the screen whereas h^*_c can be considered to be the 'engineering' coefficient that uses the convenient value of $A = (length \cdot width)$ found using the outside dimensions of the screen. Using these definitions of heat transfer coefficients for the screen:

$$Nu^*_{L_{screen}} = \frac{h^*_{c_{screen}} L}{k} \tag{5.8}$$

$$= Nu_{L_{flat\ plate}} (\pi \cdot \gamma) \tag{5.9}$$

Equation 5.9 can be used as a rudimentary method to determine the heat transfer from an insect screen. This analysis assumes that $h_c(L)$ is identical for a screen as for a flat plate. However, the dependence of the heat transfer coefficient on the vertical position L as predicted by the Ostrach solution (Equation 5.1) indicates that this may not be a valid assumption. This dependence on vertical position suggests that the presence of lower sections of the plate do affect heat transfer characteristics higher up the plate. As such, a

differing amount of heat transfer at lower portions of the screen can be expected to alter the heat transfer for higher sections of the screen.

Another approach is to assume that the heat transfer varies similarly with height for a given surface area below a given height. Using this approach, a parameter L' is defined as the height on a vertical flat plate that would have the same surface area below it as a screen with height L. The definition of L' and the modified version of the Ostrach equation that uses it are given in Equations 5.10 and 5.11. This approach assumes that the heat transfer from the screen varies with surface area similarly to a vertical flat plate.

$$L' = L \cdot (\pi \cdot \gamma) \tag{5.10}$$

$$Nu_{L'} = 0.38 \cdot Ra_{L'}^{1/4} \tag{5.11}$$

A third approach that can be used is to define a parameter that is a function of the height along the screen. This function is labelled $\xi = f(L)$ and can be found by comparing the Ostrach solution (Equation 5.1) to functions fit to data obtained from the numerical simulations. To facilitate this, functions of the form $Nu_L = a \cdot Ra_L^b$ were fit to the numerical simulations' results and are discussed along with the results from the numerical simulations below.

5.1.1 Single Cylinders

The Nu_D versus Ra_D results obtained for single cylinders closely matched those predicted by Morgan [Morgan 1975]. As such the models of natural convection from single horizontal cylinders were considered to be validated. No further analysis was done on them.

5.1.2 Multiple Cylinders

Vertical arrays of cylinders with spacings of ten times the cylinder diameter were investigated. The Nu_D versus Ra_D results for the lowest cylinders in five cylinder arrays closely matched those predicted by Morgan [Morgan 1975] for single cylinders with $Ra_D > 0.01$. For $Ra_D < 0.01$, the predicted values for Nu_D are higher than those found. In addition, the spread between different cylinders in the array increased at higher Ra_D.

A least-squares method was used to fit functions of the form $Nu_L = a \cdot Ra_L^b$ to the data. The resulting functions are shown in Figure 5.2. The best-fit function for data from all of the diameters and temperatures simulated was found to be:

$$Nu_L = 2.4 \cdot Ra_L^{0.23} \tag{5.12}$$

Functions of the form $Nu_L = a \cdot Ra_L^b$ were also fit to the results for each diameter simulated. As can be seen in Figure 5.2, the resulting functions indicated that Nu_L as a function of Ra_L was lower for larger diameter cylinders. Due to the apparent dependence of the $Nu_L = f(Ra_L)$ relationship on D, a function of the form $Nu_L = a \cdot (D/D_o)^b \cdot Ra_L^c$

was fit to the data. The resulting correlation, given below as Equation 5.13, is also shown in Figure 5.2 by the dotted lines. The dotted lines for each diameter are of the same colour as the corresponding solid lines used for the individual diameter-specific fit functions.

$$Nu_L = 1.5 \cdot \left(\frac{D}{1mm}\right)^{-0.21} \cdot Ra_L^{0.26} \tag{5.13}$$

As can be seen by the data and fit functions in Figure 5.2, the data is closely fit by functions of the form $Nu_L \propto Ra_L^a$ where $a \approx 0.25$. This close resemblance to the form of the Ostrach solution is considered to be confirmation of the laminar nature of the flow since the Ostrach equation is valid for laminar flows only. Due to the theoretical importance of the 1/4 power in the Ostrach equation, functions of the form $Nu_L = a \cdot Ra_L^{0.25}$ were fit to the data. The resulting functions are given in Figure 5.3.

Equation 5.14 shows the fit function of the chosen form $Nu_L = a \cdot Ra_L^{0.25}$. Likewise, the fit function of the form $Nu_L = a(D/D_o)^b Ra_L^c$ is given in 5.15.

$$Nu_L = 1.9 \cdot Ra_L^{0.25} \tag{5.14}$$

$$Nu_L = 1.8 \cdot \left(\frac{D}{1mm}\right)^{-0.17} \cdot Ra_L^{0.25} \tag{5.15}$$

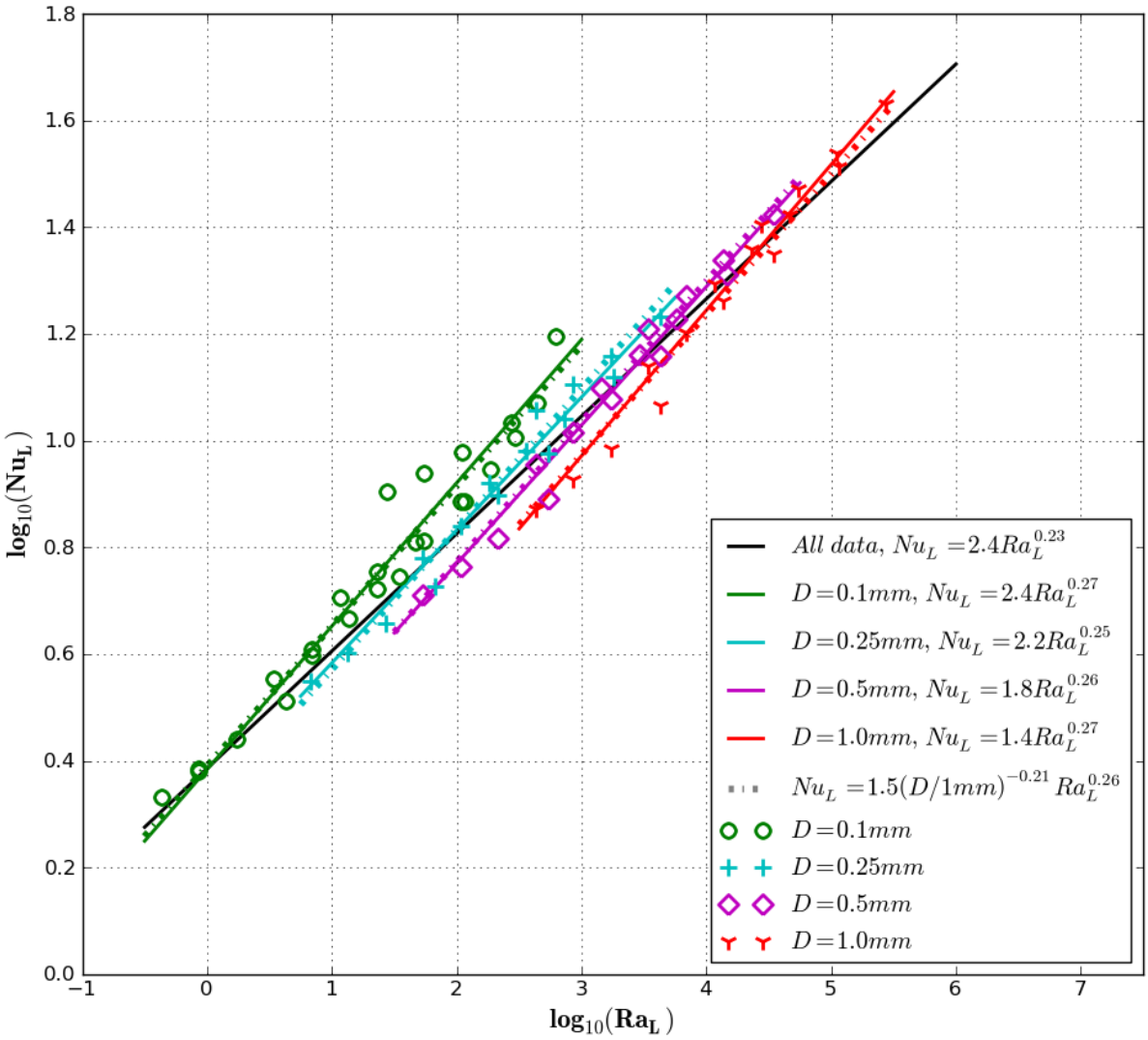

Figure 5.2: Nu_L vs Ra_L Plot Including Best Fit Lines of the Form $Nu_L = a \cdot Ra_L^b$ for Data From 2D Simulations of Natural Convection

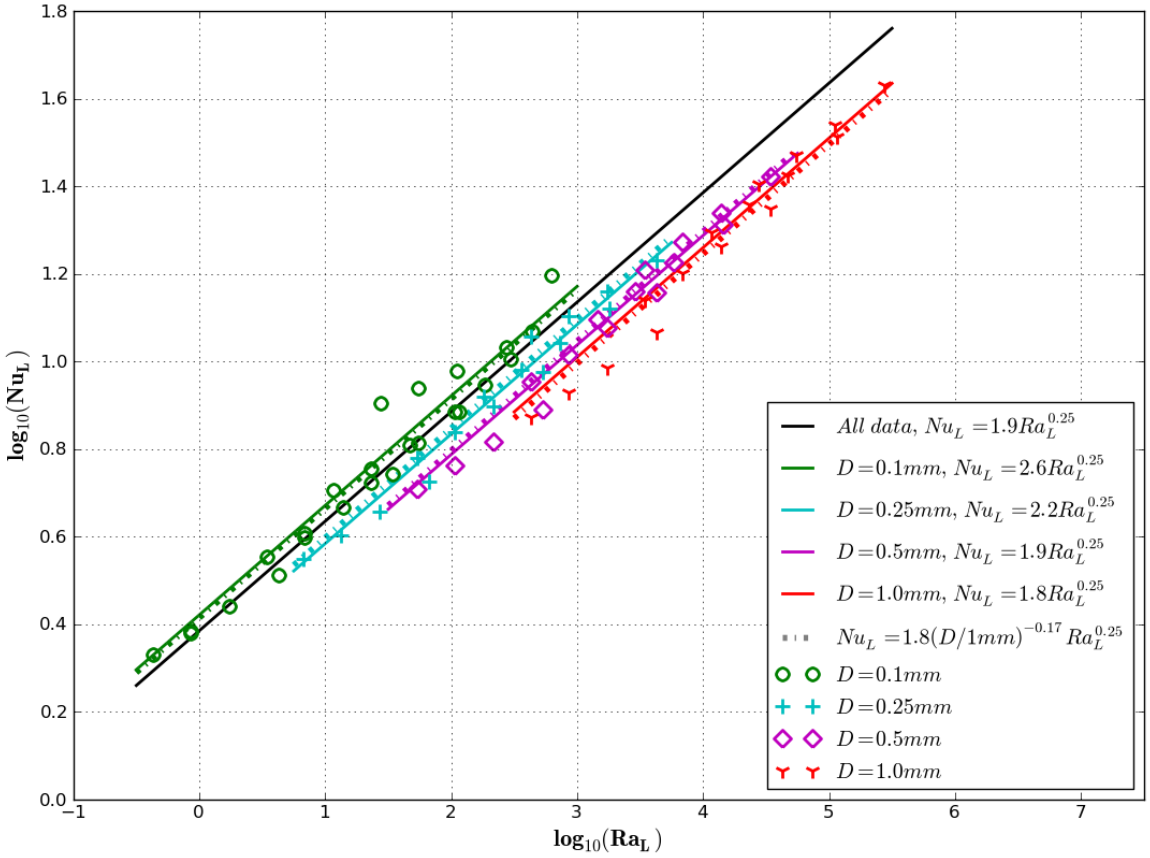

Figure 5.3: Nu_L vs Ra_L Plot Including Best Fit Lines of the Form $Nu_L = a \cdot Ra_L^{0.25}$ for Data From 2D Simulations of Natural Convection

A comparison of the heat transfer between the screen and a vertical flat plate can be made based on Equations 5.1 and 5.14 as follows:

$$\frac{Nu_{L_{screen}}}{Nu_{L_{plate}}} = \frac{h_{c_{screen}}}{h_{c_{plate}}} = \frac{1.9 \cdot Ra_L^{0.25}}{0.38 \cdot Ra_L^{0.25}} \tag{5.16}$$

$$h_{c_{screen}} = 5.0 \cdot h_{c_{plate}} \tag{5.17}$$

$$\frac{h^*_{c_{screen}}}{h_{c_{plate}}} = \frac{(\pi \cdot \gamma) \cdot 1.9 \cdot Ra_L^{0.25}}{0.38 \cdot Ra_L^{0.25}} = \frac{(\pi \cdot 0.1) \cdot 1.9 \cdot Ra_L^{0.25}}{0.38 \cdot Ra_L^{0.25}} \tag{5.18}$$

$$h_{c^*_{screen}} = 1.6 \cdot h_{c_{plate}} \tag{5.19}$$

It can be seen in Equation 5.16 that on a per area basis, the insect screen has a larger heat transfer coefficient than a vertical flat plate. When outer dimensions are used, as with h_c^* in Equation 5.18, the heat transfer coefficient of insect screen is reduced but it is still larger than that of the flat plate.

It is interesting to note that Equation 5.19 indicates that for a insect screen with $\gamma = 0.1$, that heat transfer from the screen is a simple multiple (1.6x) that of a flat plate.

As was discussed in Section 5.1, the variable ξ is defined as $\xi = f(L)$ where f is a function chosen so that if ξ is substituted for L in Equation 5.1, the resulting equation $Nu_\xi = 0.38 \cdot Ra_\xi^{0.25}$ will describe the heat transfer from the cylinder array. In this case, that would mean $Nu_\xi = 0.38 \cdot Ra_\xi^{0.25}$ being equivalent to Equation 5.14.

Equation 5.14 can be rewritten using ξ as:

$$Nu_{\xi} = 0.38 \cdot Ra_{\xi}^{0.25} \tag{5.20}$$

where:

$$Nu_{\xi} = \frac{h_{c_{screen}} \cdot \xi}{k} \tag{5.21}$$

$$\xi = 1.6 * 10^{-3} \cdot L \tag{5.22}$$

As can be seen in Equation 5.15, Nu_L appears to vary with D as $Nu_L \propto (1/D)^{0.17}$ for the range of diameters and Ra investigated ($0.1mm < D < 1.0mm,\ 10^{-3} < Ra_D < 4,\ 1 < Ra_L < 10^5$). A comparison of the resulting values of the predicted heat transfer coefficients and the Ostrach solution is given in Equations 5.23 and 5.25.

$$\frac{h_{c_{screen}}}{h_{c_{plate}}} = \frac{1.8\left(\frac{D}{1mm}\right)^{-0.17} Ra_L^{0.25}}{0.38 \cdot Ra_L^{0.25}} \tag{5.23}$$

$$h_{c_{screen}} = 4.7 \cdot h_{c_{plate}} \left(\frac{D}{1mm}\right) \tag{5.24}$$

$$\frac{h^*_{c_{screen}}}{h_{c_{plate}}} = \frac{0.57\left(\frac{D}{1mm}\right)^{-0.17} Ra_L^{0.25}}{0.38 \cdot Ra_L^{0.25}} \tag{5.25}$$

$$h_{c^*_{screen}} = 1.5 \cdot h_{c_{plate}} \left(\frac{D}{1mm}\right)^{-0.17} \tag{5.26}$$

As was done with the non-diameter-dependent correlation, Equation 5.15 can be written in terms of ξ. This was done as is shown in Equations 5.27 through 5.28.

$$Nu_\xi = 0.28 \cdot Ra_\xi^{0.25} \tag{5.27}$$

where:

$$\xi = 2.0 * 10^{-3} \left(\frac{D}{0.1mm} \right)^{0.68} L \tag{5.28}$$

5.1.3 3D Screen

A single three-dimensional case was simulated and compared to the two-dimensional models. Cylinder spacings of $10 * D$ were used, the same as with the the two-dimensional arrays. However for a given filament-mesh spacing, the three-dimensional screen will cover a larger fraction of the cross-sectional area. In the case of $10 * D$ spacing, the screen density will be $\gamma = 0.19$, about double that of the two-dimensional model with identical spacing.

The results of the three-dimensional simulations along with numerically-fit functions are given in Figure 5.4. A least-squares method was used to separately fit functions of the form $Nu_L = a \cdot Ra_L^{0.25}$ to the numerical data-points for the horizontal as well as the vertical segments of the screen mesh. As can be seen in Figure 5.4, the least-squares' fit functions were determined to be:

$$Horizontal\ Cylinders;\ \ Nu_L = 1.4 \cdot Ra_L^{0.25} \tag{5.29}$$

$$Vertical\ Cylinders;\ \ Nu_L = 1.6 \cdot Ra_L^{0.25} \tag{5.30}$$

Only a single diameter of cylindrical screen filaments ($D = 0.1mm$) was simulated in three-dimensions. As was described in the modelling section, the intended modelling methodology was to run a greater number of cases using the simpler two-dimensional models. The results of the more numerous 2D simulations could then be compared to the results of a few three-dimensional simulations. In doing so, an estimate of the error

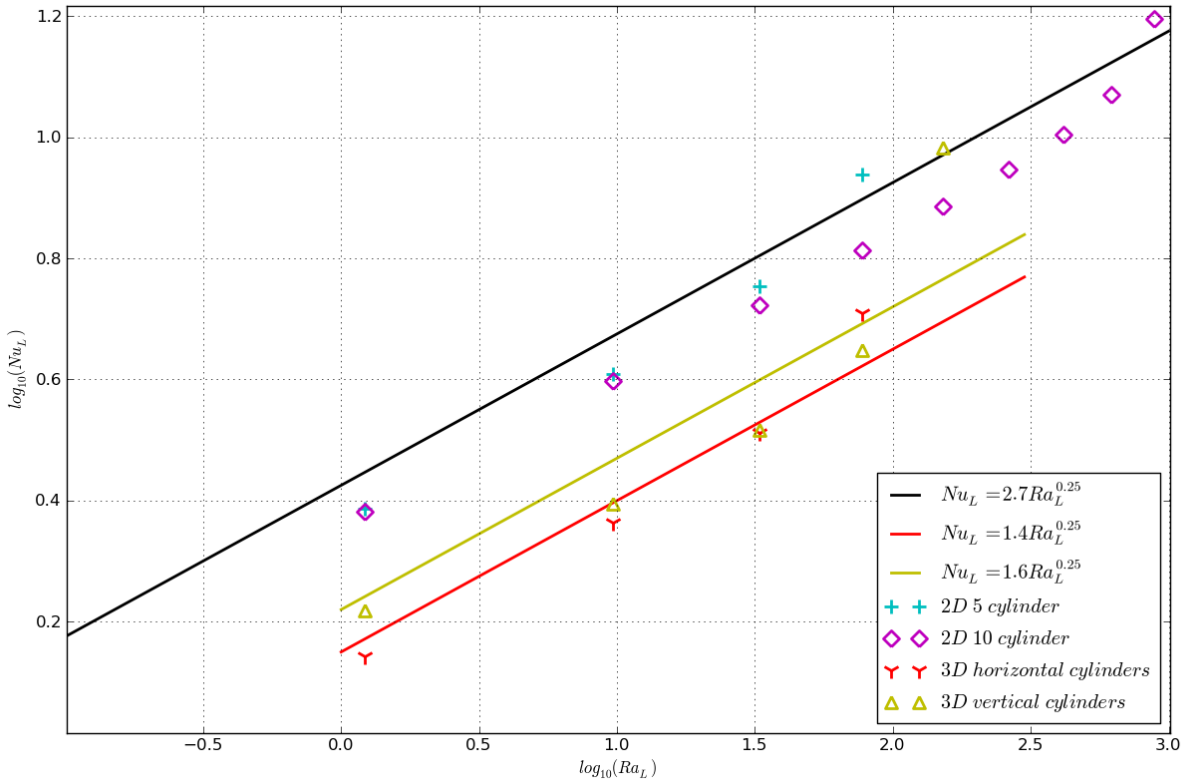

Figure 5.4: Nu_L vs Ra_L Plot Including Best Fit Lines of the Form $Nu_L = a \cdot Ra_L^{0.25}$ for Data From 3D Simulations of Natural Convection

inherent in the two-dimensional geometrical simplification would be found. This estimate can then be used to apply a compensating correction factor to generate estimates for the heat-transfer from real three-dimensional screens. For the $0.1mm$ diameter case tested, the two-dimensional correlation is given as follows:

$$Nu_L = 1.8 \cdot \left(\frac{D}{1mm}\right)^{-0.17} \cdot Ra_L^{0.25} \tag{5.13}$$

For $D = 0.1mm$:

$$Nu_L = 2.7 \cdot Ra_L^{0.25} \tag{5.31}$$

Since the horizontal and vertical components of the screen have equal area, Nu_L for the three-dimensional case is taken to be the average of Nu_L for the vertical and horizontal components and is given in Equation 5.33.

$$Nu_L = 0.5 \cdot \left(1.4 \cdot Ra_L^{0.25} + 1.6 \cdot Ra_L^{0.25}\right) \tag{5.32}$$

$$Nu_L = 1.5 \cdot Ra_L^{0.25} \tag{5.33}$$

Equation 5.33 can be rewritten in the same form as Equation 5.13, that is, $Nu_L = a \cdot (D/D_o)^b \cdot Ra_L^{0.25}$. Since only a single diameter was modelled in three dimensions, the dependence of Nu_L with diameter is assumed to be the same as for the two-dimensional case. Using $(D/1mm)^{-0.17}$ as the diameter factor, Equation 5.33 becomes:

$$Nu_L = 1.0 \left(\frac{D}{1mm}\right)^{-0.17} Ra^{0.25} \tag{5.34}$$

Equation 5.34 can be used to compare the heat transfer to that of a vertical plate as follows:

$$\frac{h_{c_{screen}}}{h_{c_{plate}}} = \frac{1.0\left(\frac{D}{1mm}\right)^{-0.17} Ra_L^{0.25}}{0.38 Ra_L^{0.25}} \tag{5.35}$$

$$h_{c_{screen}} = h_{c_{plate}} \cdot 2.6\left(\frac{D}{1mm}\right)^{-0.17} \tag{5.36}$$

$$\frac{h^*_{c_{screen}}}{h_{c_{plate}}} = \frac{(\gamma \cdot \pi) h_{c_{screen}}}{0.38 Ra_L^{0.25}} \tag{5.37}$$

$$h_{c^*_{screen}} = h_{c_{plate}} \cdot \frac{(\gamma \cdot \pi)\left(\frac{D}{1mm}\right)^{-0.17} Ra_L^{0.25}}{0.38 Ra_L^{0.25}} \tag{5.38}$$

$$h_{c^*_{screen}} = h_{c_{plate}} \cdot 1.5\left(\frac{D}{1mm}\right)^{-0.17} \tag{5.39}$$

As is shown in Equations 5.36 & 5.39, the heat transfer coefficient for a screen is predicted to be higher than that of a vertical flat plate regardless of whether h_c or h_c^* is used. However it is also important to note that values of ratios of h_c^* for the screen and h_c for a flat plate were found to be within a factor of two for the screens simulated.

Similar to what was done with the two-dimensional case, Equation 5.34 can be rewritten in terms of the variable ξ as follows:

$$For\ Nu_\xi = 0.38 \cdot Ra_\xi^{0.25}, \tag{5.40}$$

$$\xi = 2.0 * 10^{-2} \cdot \left(\frac{D}{1mm}\right)^{0.68} \cdot L \tag{5.41}$$

5.2 Forced Convection

Unlike natural convection which will only be generated in a vertical direction, forced convection can be either inline with the insect screen or normal to it. The results of these two different scenarios are discussed separately below.

5.2.1 Forced Convection Normal to Screen

The simplest geometry that forced convection normal to an insect screen can be compared to is flow past a cylinder. Correlations for forced convection past a heated cylinder are readily available and are discussed in the Background Chapter. Flow past a single cylinder is not analysed further here.

For more complex models, correlations of the form $Nu_D = a \cdot Re_D^b$ were fit using a least-squares method to the data found in the numerical simulations. Separate correlations were found for the data from the two-dimensional simulations as well as each of the different screen densities tested in three-dimensions. These correlations are shown in Figure 5.5 along with the data from which they were found. The correlations found are as follows:

For 2D, $\gamma = 10\%$;

$$Nu_D = 0.57 \cdot Re_D^{0.6} \tag{5.42}$$

For 3D, $\gamma = 20\%$;

$$Nu_D = 0.70 \cdot Re_D^{0.5} \tag{5.43}$$

For 3D, $\gamma = 75\%$;

$$Nu_D = 0.35 \cdot Re_D^{0.9} \tag{5.44}$$

It can be seen in Figure 5.5 that the results indicate that the dependence of Nu_D closely follows the form $Nu_D \propto Re_D^{constant}$. In the case of the two-dimensional data, there was a greater variance of the data from this type of fit. Finding individual correlations for each diameter tested in two-dimensions could be done. However looking at the data in Figure 5.5 it is clear that this is unlikely to be illuminating for the limited amount of data available (three diameters with five data-points each). In contrast, the three-dimensional data shows a low variance with the separate correlations generated for each of the screen porosities modelled. It is desirable to generate a general correlation for an arbitrary screen density with a form as follows:

$$Nu_D = f(\gamma, Re_D) \tag{5.45}$$

or preferably if possible;

$$Nu_D = f_{gamma}(\gamma) \cdot f_{Re_d}(Re_D) \tag{5.46}$$

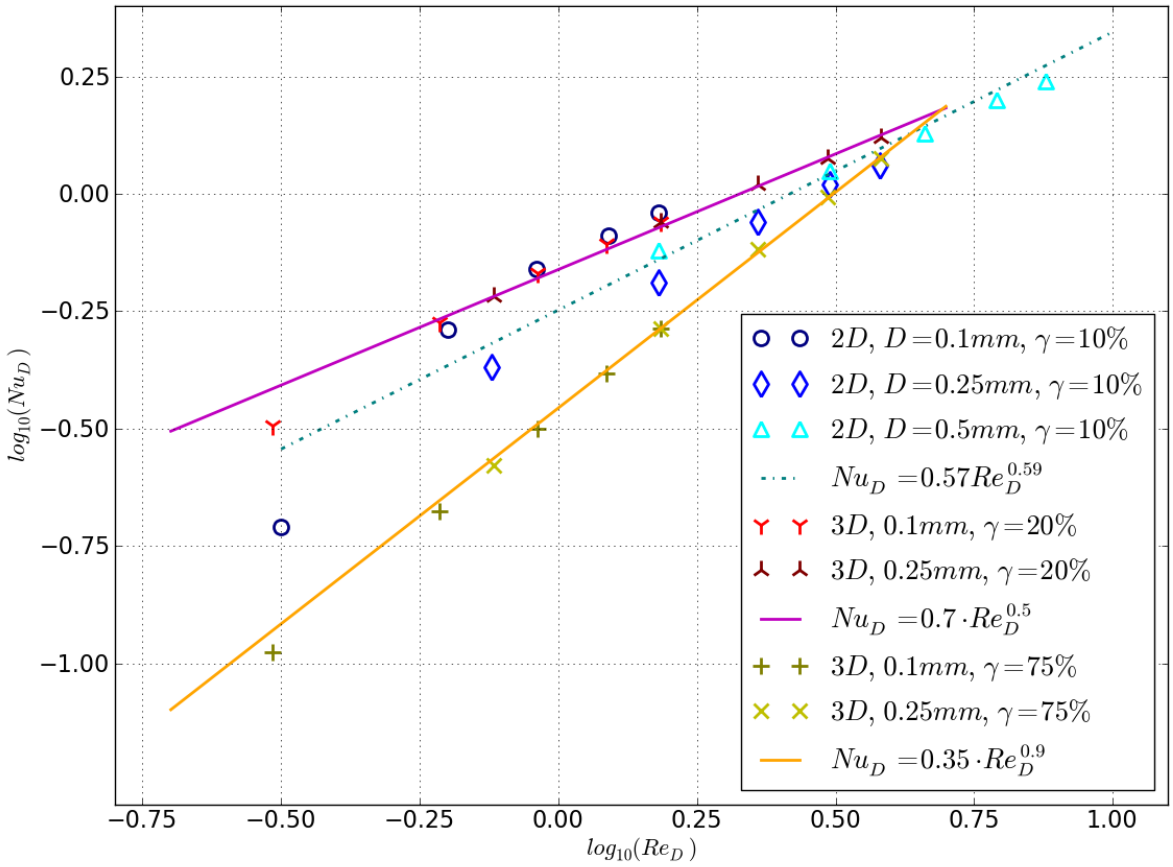

Figure 5.5: Nu_D vs. Re_D Plot for Forced Convection Normal to 3D Screen

Based on the best-fit lines shown in Figure 5.5, it appears that the function $f(\gamma, Re_D)$ is not separable into $f_\gamma(\gamma)$ and $f_{Re_d}(Re_D)$. If $f(\gamma, Re_D)$ was separable, the fit lines for the screens of different densities would be parallel lines on the $log_{10}(Nu_D)$ vs. $log_{10}(Re_D)$ plot.

In addition to the two screen densities modelled, there are the extremum cases. The low-density extremum would be expected to perform similarly to a single cylinder. For the single cylinder case the correlation given as Equation 5.48 is used. While the correlation is

given for values of Re larger than some of those used in this investigation ($1 < Re_D < 40$), other available correlations were of forms other than $a \cdot Re^b$ and were not used.

$$Nu_D = 0.75 Pr^{0.27} \cdot Re_D^{0.4} \qquad \text{[Zukauskas 1972]} \tag{5.47}$$

$$Nu_D = 0.68 Re_D^{0.4}, \quad for\ Pr = 0.71\ \&\ 1 < Re_D < 40 \tag{5.48}$$

The high-density extremum of $\gamma \to 1$ can be considered as an ill-defined case. A screen with $\gamma = 1$ is effectively a flat plate and thus flow perpendicular to it is akin to impinging flow against a flat plate. In such a case, Re_D where D is the diameter of the screen filaments has little meaning. The values of screen density that were used to generate a function $f(\gamma, Re_D) = Nu_D$ are given in Table 5.1.

Table 5.1: Data Fit Functions for Given Values of γ for Forced Convection Normal to Screen

γ	f(γ,Re_D)
$\gamma = 0$	$0.68 Re_D^{0.4}$
$\gamma = 20\%$	$0.7 Re_D^{0.5}$
$\gamma = 75\%$	$0.35 Re_D^{0.9}$

Since the Nu_D vs. Re_D data was fit to functions of the form $Nu_D = a \cdot Re_D^b$ for different values of γ, the following form of $f(\gamma, Re_D)$ was used:

$$Nu_D = a(\gamma) \cdot Re_D^{b(\gamma)} \tag{5.49}$$

Given that three values of γ have fit functions associated with them, second order polynomials were used to represent $a(\gamma)$ and $b(\gamma)$. The resulting correlation is given below:

$$Nu_D = a(\gamma) \cdot Re_D^{b(\gamma)} \tag{5.50}$$

$$Where:$$

$$a = 0.68 + 0.30 \cdot \gamma - 0.98 \cdot \gamma^2 \tag{5.51}$$

$$b = 0.40 + 0.44 \cdot \gamma + 0.30 \cdot \gamma^2 \tag{5.52}$$

$$\tag{5.53}$$

5.2.2 Forced Convection Inline with Screen

As was done with the natural convection case, a comparison with convection from a flat plate is helpful in understanding convective processes along an insect screen. Correlations for forced convection past a flat plate are readily available and described in the Background section. One simple correlation is given here:

$$Nu_L = 0.30 \cdot Re_L^{1/2} \qquad \text{[Schlichting 2000]} \tag{5.54}$$

Using Equations 5.54 & 5.9 Nu_L^* for the insect screen can be written as:

$$Nu^*_{L_{screen}} = (\pi \cdot \gamma) \cdot Nu_{L_{flat-plate}} \tag{5.55}$$

$$= (\pi \cdot \gamma) \cdot 0.30 \cdot Re_L^{0.5} \tag{5.56}$$

Equation 5.56 provides an initial estimate for the heat transfer from the screen. As can be seen in its derivation, this estimate assumes that the value of h_c for the screen is the same as that of a flat plate and that h_c^* (and thus Nu_L^*) differ from that of a flat plate only due to the reduced area available for heat transfer.

A second simplification of the heat-transfer of the screen is to assume that the heat transfer varies in similitude to that of a flat plate with the same amount of surface area for heat transfer below a given height. To make use of this simplification the dimension L' is used. Using this method, $Nu_{L'}$ will be given as follows:

$$L' = L \cdot (\pi \cdot \gamma) \tag{5.57}$$

$$Nu_{L'} = 0.3 \cdot Re_{L'}^{0.5} \tag{5.58}$$

A third approach that can be used is to define a parameter that is a function of the height along the screen. This function is labelled $\xi = f(L)$ and can be found by comparing the flat-plate solution (Equation 5.54) to functions fit to data obtained from the numerical simulations. To facilitate this, functions of the form $Nu_L = a \cdot Ra_L^b$ were fit to the numerical simulations' results and are discussed along with the results from the numerical simulations below.

2D Cylinder Arrays

The results obtained for two-dimensional arrays of cylinders are shown in Figure 5.6 along with lines of best-fit (least squares fits) for the data. A correlation for forced convection over a flat plate is also shown for reference (correlation from [Schlichting 2000]).

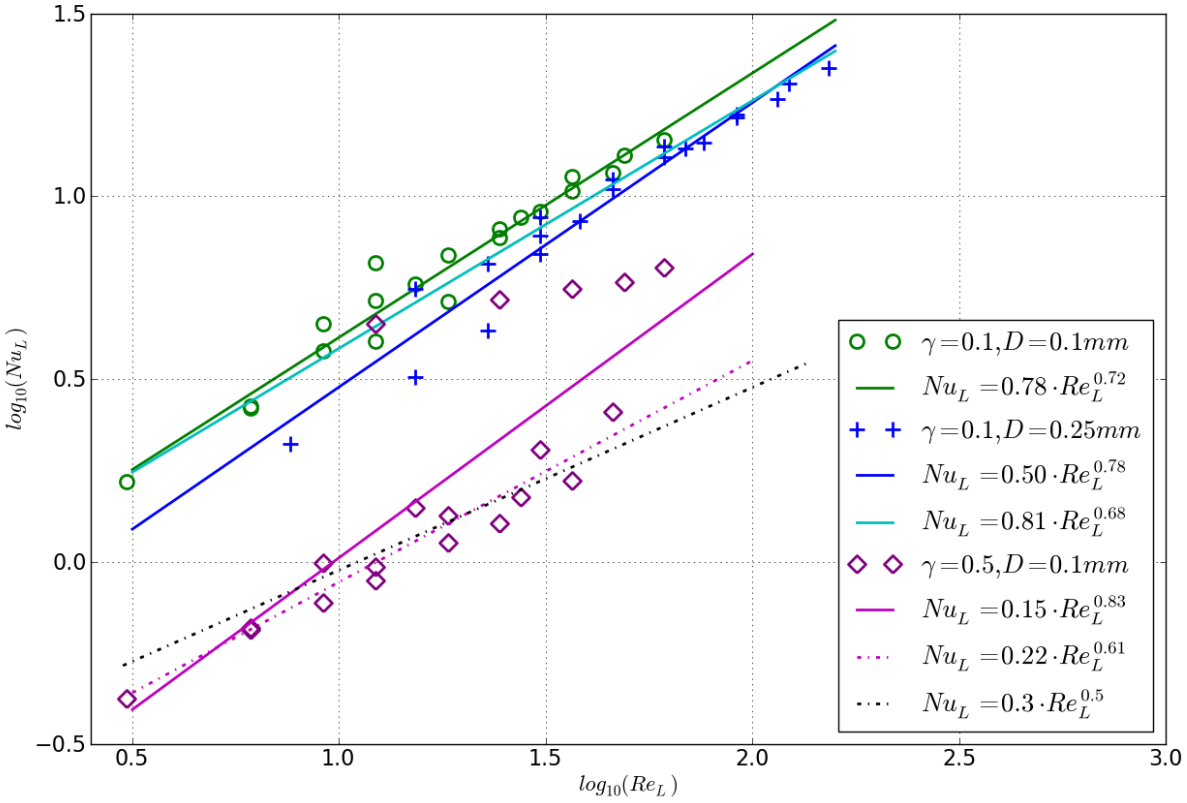

Figure 5.6: Nu_L vs. Re_L Plot for Forced Convection Inline With 2D Cylinder Array

Figure 5.6 shows results and corresponding fit lines for cylinder arrays with $s = (10 * D)$ and $s = (2 * D)$ cylinder spacings. For the $s = (10 * D)$ cylinder spacing ($\gamma = 10\%$), results for two diameters, $D = 0.1$ & $0.5\ mm$, are available and shown. It can be seen that there

is some dependence of Nu_L on the cylinder diameter. As such, separate fit lines are shown for each of the two diameters. These are as follows:

$$For \;\; \gamma = 10\% :$$

$$D = 0.1mm, \quad Nu_L = 0.78 \cdot Re_L^{0.72} \tag{5.59}$$

$$D = 0.25mm, \quad Nu_L = 0.50 \cdot Re_L^{0.78} \tag{5.60}$$

In addition to the unique fit lines for the data for each diameter, a general fit line for all of the data is shown. It is also given here as:

$$Nu_L = 0.81 \cdot Re_L^{0.68}, \quad for \; \gamma = 10\% \tag{5.61}$$

Data for only a single diameter of $D = 0.1mm$ was available for the case of $\gamma = 50\%$ (cylinder spacing $= 2{*}D$). A least-squares fit for this data produced the following correlation:

$$Nu_L = 0.15 \cdot Re_L^{0.83}, \quad for \; \gamma = 50\% \tag{5.62}$$

It can be seen in Figure 5.6 that four data-points are at a large variance from this fit and thus the rest of the data available. These data points correspond to the uppermost cylinders in an array (this is clearly indicated in Figure 4.11). This finding is not surprising, the topmost cylinder in an array is to be expected to have a larger value of h_c due to the absence of an downstream cylinder hindering flow. This effect is predictably stronger with tighter cylinder spacings and hence is more distinct in the $S = 2 * D$ cylinder arrays than

those with $S = 10 * D$. Since this effect is not of particular importance, a second correlation was fit to the data excluding the top cylinders. This correlation, seen in Figure 5.6, is as follows;

$$Nu_L = 0.22 \cdot Re_L^{0.61}, \quad for\ \gamma = 50\% \tag{5.63}$$

Combining Equations 5.61 and 5.63 using the form of $Nu_L = (a_1 + b_1 \cdot \gamma) \cdot Re_L^{(a_2 + b_2 \cdot \gamma)}$, the following correlation was found;

$$Nu_L = (0.96 - 1.5 \cdot \gamma) \cdot Re_L^{(0.70 - 0.18 \cdot \gamma)} \tag{5.64}$$

Equation 5.64 can also be rewritten in terms of ξ as given below.

$$Nu_\xi = 0.3 \cdot Re_\xi^{0.5} \tag{5.65}$$

$$where:$$

$$\xi = (3.2 - 5.0 \cdot \gamma)^{-2} \cdot \left(\frac{V}{\nu}\right)^{(0.36 \cdot \gamma - 0.4)} L^{(0.36 \cdot \gamma + 0.6)} \tag{5.66}$$

3D Screen Models

Only a single diameter and porosity of screen was simulated in three dimensions. This screen had a screen density of $\gamma = 20\%$ and 0.1mm diameter filaments. Functions were fit to the results of the simulations for this screen and are shown in Figure 5.7.

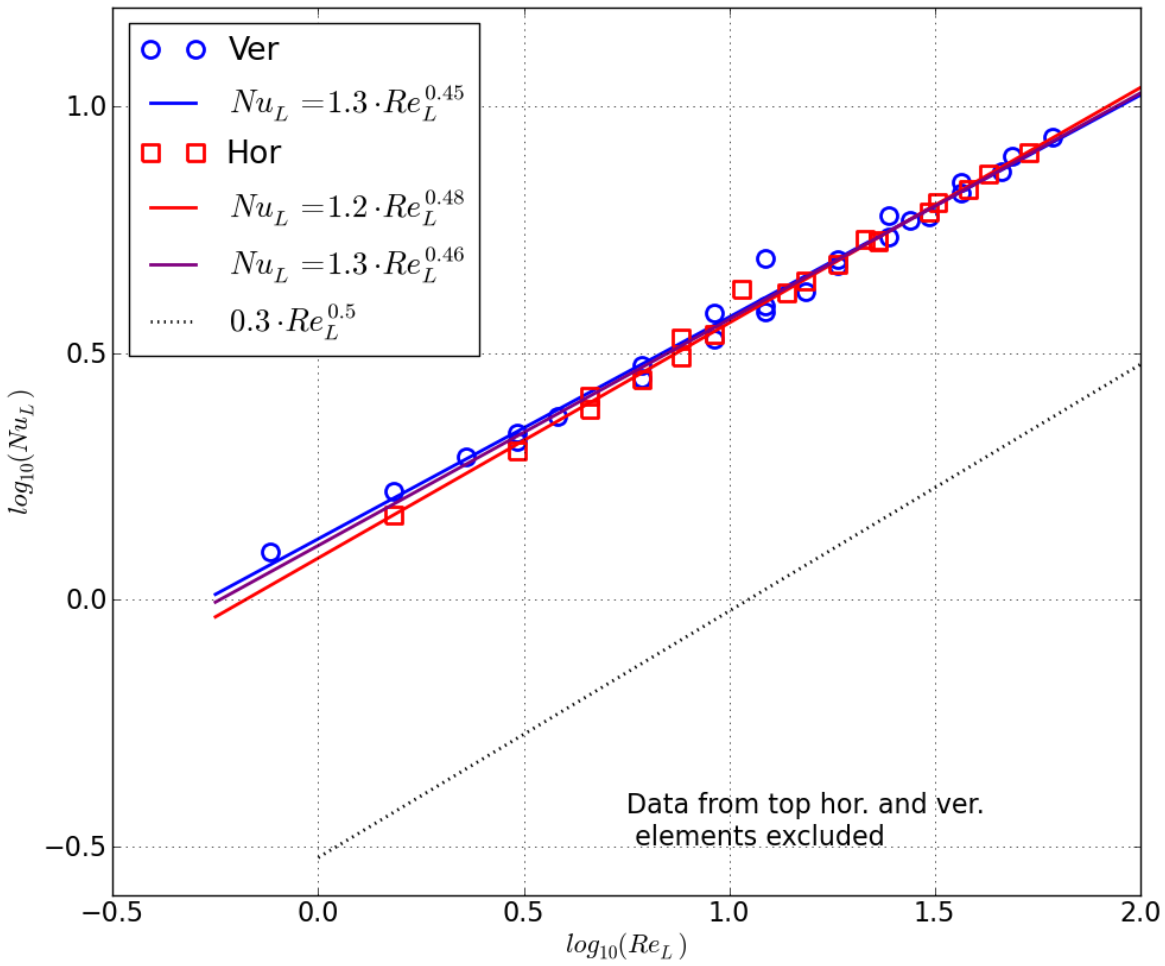

Figure 5.7: Nu_L vs. Re_L Plot for Forced Convection Inline With 3D Screen

As can be seen in Figure 5.7, numerically fit correlations for the vertical and horizontal segments of the screen are very similar. The data-points for the horizontal screen segments can be interpolated using the function $Nu_L = 1.3 \cdot Re_L^{0.45}$ while $Nu_L = 1.2 \cdot Re_L^{0.48}$ can be used for the horizontal ones. Due to similarity of these functions the average of them can

be considered to be useful in representing all of them. The correlation for the average is given by:

$$Nu_L = 1.3 \cdot Re_L^{0.46} \tag{5.67}$$

Equation 5.67 can be rewritten in terms of ξ. The result is given by Equation 5.69.

$$Nu_\xi = 0.3 \cdot Re_\xi^{0.5} \tag{5.68}$$

$$\text{Where: } \xi = 0.053 \cdot \left(\frac{V}{\nu}\right)^{0.08} L^{1.08} \tag{5.69}$$

Chapter 6

Conclusions and Recommendations

Naturally any research investigation is limited in its scope and its results must be treated as such. The uses and limitations of the present work as well as possible directions of future research are described below.

6.1 Use of Results

As was discussed in the Modelling chapter, the heat transfer from a heated or cooled insect screen can be expected to be a function of seven variables;

$$h_c = F(D, \phi, \Delta T, V, \theta, y, \text{position effects})$$

Because of this dependence on a large number of variables, it was not possible to rigorously investigate all possible scenarios. Instead, a select number of scenarios were modelled and

analyzed. Several correlations were developed from these models which can be helpful in increasing understanding of the process of convective heat transfer from an insect screen.

As described in the Discussion chapter, there are two main ways in which the correlations developed in this work can be used. The first method uses the results of the natural convection models. Using this method, the natural convection from a screen can be estimated. The correlations developed in this manner would represent the heat transfer from a screen in a large stagnant volume of air. Effects of the adjacent window glazing and sills will not be accounted for by this method. It was found that an insect screen behaves similarly to a vertical plate plate. For the screens investigated, the heat transfer was found to be within a factor of two relative to a similarly sized flat plate.

The results of the forced convection models can be used in a more involved method for estimating the heat transfer from the insect screen. The forced convection results can be used to give estimates for the value of h_c at a given location based on the local fluid velocity. These estimates can be used as applied surface functions in a CFD model that simulates the fluid flow and heat transfer adjacent to a window/screen assembly.

6.2 Limitations

A major limitation resulting from the large number of variables is that only a limited number of values for any given variable could be simulated. The maximum number of values simulated for any given variable were:

Screen filament diameters; 4	$D =:$	$0.1mm, 0.25mm.0.5mm, 1mm$
Screen porosity; 2	$\phi =:$	$2D : 0.1, 0.5 \quad 3D : 0.25, 0.8$
ΔT; 5	$\Delta T =:$	$1, 5, 10, 20, 50K$
Forced velocity; 5	$V =:$	$0.05m/s, 0.10m/s, 0.15m/s, 0.20m/s, 0.25m/s$
Forced convection direction; 2	$=:$	aligned and perpendicular
Height of screen; $10 * (D \cdot s)$	$=$	maximum screen height of 10 screen filaments

The limited number of cases simulated necessarily reduces accuracy and confidence for the developed correlations. The quality of the correlations could be improved in the future with the use of a greater number of models. Experimental results could be obtained and incorporated for the same reason.

Another limitation of this work is that relatively small sections of screens have been used in the models. Due to the fine spacing of screen filaments, a typical screen will have more filaments than are possible to model. In cases such as forced convection normal to the screen, this large number of filaments can be reduced by symmetry so that a simple model geometry can be used. In other cases, such as convection inline with the screen, it is not possible to model all of the filaments necessary to represent an entire typical screen,

Furthermore, as this work has found that the heat transfer varies over the height of the screen, simulating the whole height of the screen is desirable. One recommended method to overcome this hurdle is to model the screen in varying levels of detail.

Results from a detailed model of a small section of a screen can be used to generate simplifications that can be used on less detailed models of larger-scale sections of the screen. This method uses a strategy similar to that recommended for the use of the forced convection results in screen-assembly CFD models.

6.3 Alternative Approaches

This investigation used a range of numerical simulations to gain an understanding of the convective heat transfer from an insect screen with arbitrary properties. Other approaches are also possible.

Individual Screen Models

If a high degree of accuracy is required for a given application, the ambiguity inherent with the large number of variables could be reduced by modelling the actual screen in question. This could be done numerically or experimentally.

Analytical Methods

This work was based primarily on numerical simulations. An alternative is to use some of the analytical techniques that have been previously used to analyze convective heat transfer

and customize and extend them to the case of an insect screen. Boundary layer methods for analysis of convection have been used for the case of a flat plate [Ostrach 1953]. These methods could be further investigated and modified to account for the peculiarities of an insect screen.

Another possible approach is the use of Colborne analogy which takes advantage of similarities seen between heat and momentum transfer [Middleman 1997].

Bibliography

[Blasius 1908] Blasius, H., 1908, The Boundary Layers in Fluids With Little Friction. English Translation: NACA Technical Memo 1256, 1950.

[Bruneau 2006] Bruneau, A., et al, The Report of the National Advisory Panel on Sustainable Energy Science and Technology, Natural Resources Canada 2006.

[Brunger 1999] Brunger, A. b. and Dubrous, F. M., 1999, Measurement of the Solar Heat Gain Coefficient and U Value of Windows with Insect Screens. ASHRAE Transactions 105:1038-1044.

[CAGBC 2010] LEED ® Canada For New Construction and Major Renovations, Canadian Green Building Council, Ottawa, ON CA, 2010.

[Cengel 2007] Cengal, Yunas A, Heat and Mass Transfer, McGraw-Hill 2007.

[Churchill & Usagi 1972] Churchill, S. W. and Usagi, R., 1972, A general expression for the correlation of rates of transfer and other phenomena. AIChE Journal 18:1121-1128.

[Churchill & Chu 1975(1)] Churchill, S. W. and Chu, H. H. S., 1975, Correlating Equations for Laminar and Turbulent Free Convection From a Horizontal Cylinder. International Journal of Heat and Mass Transfer 18:1049-1053.

[Churchill & Chu 1975(2)] Churchill, S. W. and Chu, H. H. S., 1975, Correlating Equations for Laminar and Turbulent Free Convection From a Vertical Plate. International Journal of Heat and Mass Transfer 18:1323-1329.

[Churchill & Bernstein 1977] Churchill, S. W. and Bernstein, M., 1977, A Correlating equation for forced convection from gases and liquids to a circular cylinder in crossflow. Journal of Heat Transfer 99:2:300-306.

[Collis & Williams 1959] Collis, D. C. and Williams, M. J., 1959, Two-dimensional convection from heated wires at low Reynolds numbers. Journal of Fluid Mechanics 6:357-384.

[Corcione 2005] Corcione, M., 2005, Correlating equations for free convection heat transfer from isothermal cylinders set in a vertical array. International Journal of Heat and Mass transfer 48:3660-3673.

[Daly 2002] Daly, Allan, 2002, Operable Windows and HVAC Systems, Heating/Piping/Air-Conditioning, 2002:Dec:22-30.

[Eckert 1963] Eckert. E. R. G., 1963, Introduction to Heat and Mass Transfer, New York US: McGraw Hill.

[Farouk & Guceri 1981] Farouk, B., Guceri, S. I., 1981, Natural convection from a horizontal cylinder-laminar regime. Transactions of the ASME v103.

[Fluent 2005] Fluent,2005,Fluent 6.3 Manual.

[Fowler 1994] Fowler, A.J. and Bejan, A., 1994. Forced Convection in banks of inclined cylinders at low Reynolds numbers. International Journal of Heat and Fluid Flow 15:2:90-99.

[Fox 2004] Fox, R.W., McDonald, A.T. and Pritchard, P.J., 2004, Introduction to Fluid Mechanics, New Jersey US: John Wiley and Sons.

[Gambit 2005] Gambit,2005,Gambit 2.3 Manual.

[Gebhart 1988] Gebhart, B., Jaluria, Mahajan, R.L., Sammakia, B., 1988, Bouyancy Induced Flows and Transport, Washington DC US: Hemisphere Publishing.

[Hedge 1989] Hedge, A., Burge, P.S., Wilson, A.S., and Harris-Bass, J., 1989, Work-related illness in office workers: a pro-posed modelof the sick building syndrome. Environment International, 15, 143-158.

[Heerwagen 1998] Heerwagen, J. and Wise, J.,1998, Green building benefits: differences in perceptions and experiences across manufacturing shifts. Heating/Piping/Air-Conditioning, 1998:Feb:57-63.

[Incropera 2002] Incropera, F.P., DeWitt D.P., 2002, Fundamentals of Heat and Mass Transfer, 5^{th} Ed., NY, US: John Wiley and Sons Inc.

[Jaluria 1980] Jaluria, Y., 1980, Natural Convection Heat and Mass Transfer 1^{st} Ed., Oxford Uk: Pergamon Press.

[Kakac 1987] Kakac, S., Shah, R., and Aung, W., 1987, Handbook of Single-Phase Convective Heat Transfer, NY, US, John Wiley and Sons.

[Kittel 1997] Kittel, C., Kroemer, H., 1997, Thermal Physics 2^{nd} Ed., NY US: W.H. Freeman and Company.

[Kreith 1997] Kreith, F., Bohn, M. S., 1997, Principles of Heat Transfer 5^{th} Ed., Boston, MA, US: PWS Publishing Company.

[Lieberman & Gebhart 1969] Lieberman, J. and Gebhart, B., 1969, Interactions in Natural Convection From An Array of Heated Elements, Experimental. International Journal of Heat and Mass Transfer 12:1385-1396.

[Lomanowski 2008] Lomanowski, B. A., 2008, Implementation of Window Shading Models into Dynamic Whole-Building Simulation, M.A.Sc. thesis, University of Waterloo.

[Lorenz 1881] Lorenz, L., 1881. Ann. Phys. Chem. 31:582.

[Middleman 1997] Middleman, Stanly, 1997, An Introduction to Mass and Heat Transfer, NY, US: John Wiley and Sons.

[Miguel 1997] Miguel, A. F., van de Braak, N. J. and Bot, G. P. A., 1997, Analysis of the airflow characteristics of greenhouse screening materials. Journal of Agricultural Engineering Research 67:105-112.

[Miguel 1998] Miguel, A. F., 1998, Airflow through porous screens: from theory to practical considerations. Energy and Buildings 28:63-69.

[Morgan 1975] Morgan, V. T., 1975, The Overall Convective Heat Transfer From Smooth Circular Cylinders. Advances in Heat Transfer 11:199-264.

[Norford 1994] Norford, L.K. et al, Two-to-one discrepency between measured and predicted performance of a 'low-energy' office building: insights from a reconciliation based on the DOE-2 model. Energy and Buildings 21:121-131.

[Norris 2009] Norris, Neil, 2009, Numerical Analysis of Natural Convection Heat Transfer for Windows with Porous Screening Material, M.A.Sc. thesis, University of Waterloo.

[Ohman 1970] Ohman, G. A., 1970, A note on the experimental determination of convective heat transfer from wires at extremely small reynolds and grashof numbers. Acta Academiae Aboensis Ser. B 30:1.

[D'Orazio & Fontana 2010] D'Orazio, A. and Fontana, L, 2010, Experimental study of free convection from a pair of vertical arrays of horizontal cylinders at very low Rayleigh numbers. International Journal of Heat and Mass Transfer 53:3131-3142.

[Ostrach 1953] Ostrach, S., 1953, An analysis of laminar free convection flow and heat transfer about a flat plate parallel to the direction of the generating body force. NACA TR 1111.

[Pikulev 2003] Pikulev, A. A., 2003, Heat-Transfer Coefficient of a Fine Heated Wire in a Gas Flow. Technical Physics, 48:6:693-696.

[Saville & Churchill 1967] Saville, D. A. and Churchill, S. W., 1967, Laminar free convection in boundary layers near horizontal cylinders and vertical axisymmetric bodies. Journal of Fluid Mechanics, 29:2:391-399.

[Schlichting 2000] Schlichting, H., 2000, Boundary Layer Theory, NY, US: Springer.

[Turner 2008] Turner, C. and Frankel, M., Energy Performance for LEED New Construction Buildings, Washington DC, US: U.S. Green Building Council.

[White 2006] White, Frank M., 2006, Viscous Fluid Flow 3^{rd} Ed., NY, US: McGraw-Hill.

[Zukauskas 1972] Zukauskas, A.A., 1972, Heat Transfer from Tubes in Cross Flow. Advances in Heat Transfer 8:93-106.

[Zumdahl 1992] Zumdahl, S. S., 2002, Chemical Principles, MA, US: D.C. Heath.